Advances in Polymer Technology

Engineered Nanoreinforcements and High-Performance Polymeric Nanocomposites

Lead Guest Editor: Wei Hong
Guest Editors: Li Zibiao, Wenxin Fu, Wei Yang, and Ming Wang

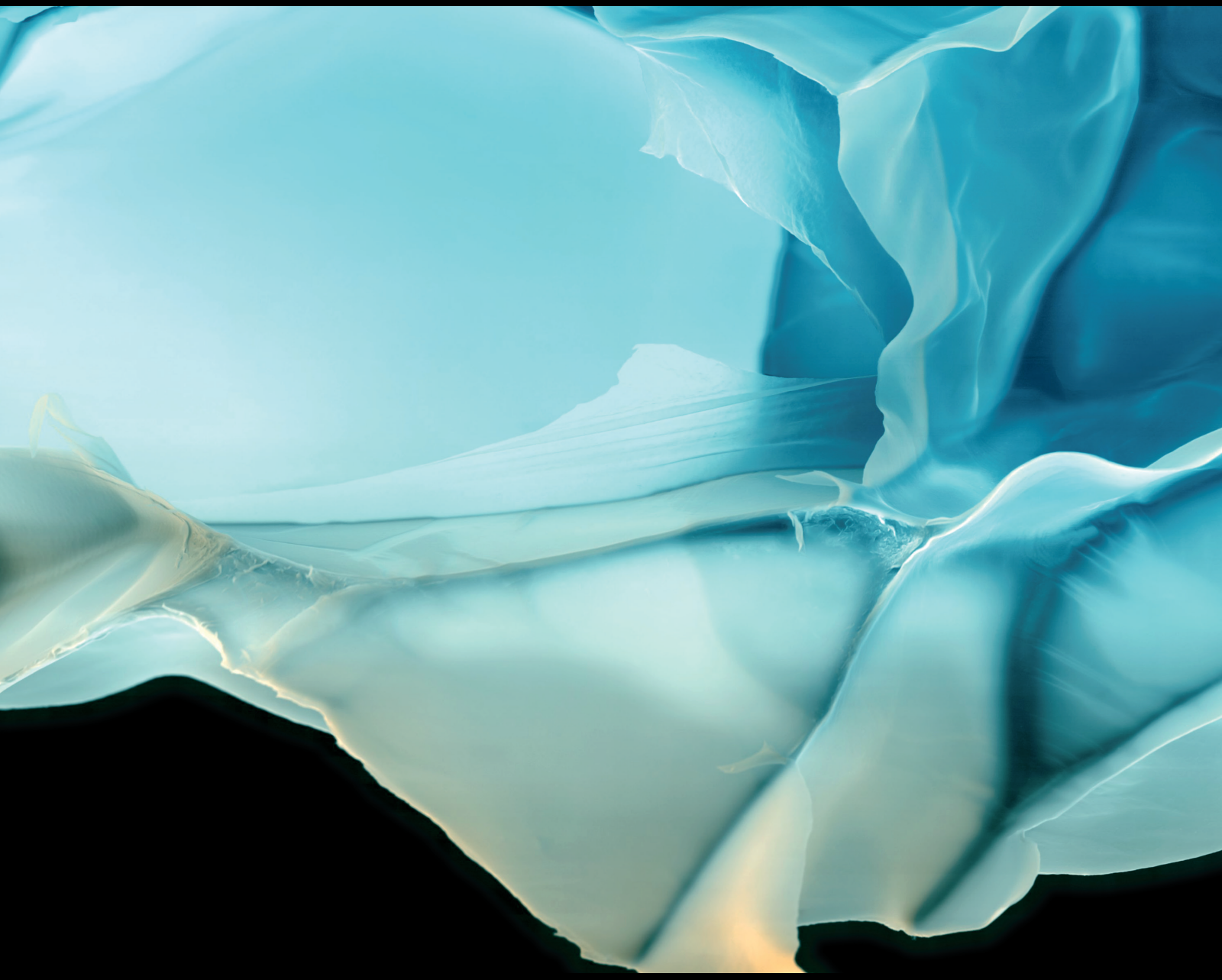

Engineered Nanoreinforcements and High-Performance Polymeric Nanocomposites

Advances in Polymer Technology

Engineered Nanoreinforcements and High-Performance Polymeric Nanocomposites

Lead Guest Editor: Wei Hong
Guest Editors: Li Zibiao, Wenxin Fu, Wei Yang, and Ming Wang

Contents

Hindawi
Advances in Polymer Technology
Volume 2019, Article ID 8687450, 11 pages
https://doi.org/10.1155/2019/8687450

Research Article

Thermal Performances of UHMWPE/BN Composites Obtained from Different Blending Methods

Yiyou Guo,[1] Changlin Cao,[1,2] Huibin Cheng,[1] Qinghua Chen,[1,3] Baoquan Huang,[1] Fubin Luo,[1] and Qingrong Qian,[1]

[1]*Engineering Research Center of Polymer Green Recycling of Ministry Education and Fujian Key Laboratory of Pollution Control & Resource Reuse, College of Environmental Science and Engineering, Fujian Normal University, Fuzhou 350007, China*
[2]*Key Laboratory for Polymeric Composite and Functional Materials of Ministry of Education and Key Laboratory of High Performance Polymer-Based Composites of Guangdong Province, School of Chemistry, Sun Yat-Sen University, Guangzhou 510275, China*
[3]*Fujian Normal University Fuqing Branch, Fuzhou 350300, China*

Correspondence should be addressed to Baoquan Huang; qbh811@sina.com and Qingrong Qian; qrqian@fjnu.edu.cn

Received 29 May 2019; Accepted 14 August 2019; Published 20 December 2019

Guest Editor: Ming Wang

UHMWPE/BN composites were prepared by solvent mixing (SM) in this work, then were characterized by scanning electron microscope (SEM), Raman mapping, differential scanning calorimeter (DSC), thermogravimetric analysis (TG), and thermal conductivity meter to study the morphology, filler distribution, segregated structure, and thermal stability as well as thermal conductivity. Compared to the traditional melt mixing (MM), SM followed by molding contributes to the construction of segregated structures in UHMWPE composite. This segregated structure can greatly improve the thermal conductivity of the composites. The segregated structure of composites prepared by MM is destroyed by shearing. Moreover, the thermal stability of composites by SM is improved with the increment of BN content, which is better than that of samples by MM, probably resulting from the barrier function of the segregated structure.

1. Introduction

Ultra high molecular weight polyethylene (UHMWPE) is an engineering plastic that is widely used in aerospace, defense military, biological joints, pipeline transportation, etc., due to its outstanding wear resistance, excellent impact resistance, as well as good biocompatibility [1]. A crucial issue currently remaining unresolved is low heat distortion temperature and poor thermal conductivity of UHMWPE, causing UHMWPE to be locally susceptible to thermal deformation, resulting in limited application areas. At present, some researchers manipulate the polymer chain alignment to form orientations [2–4] and the high crystallinity [5, 6] in the matrix to get high thermal conductivity of UHMWPE. There is such a problem that this method requires high production equipment and leads to limited application. In addition to adjust the alignment of polymer chains, UHMWPE doped with the thermally conductive fillers has also gained significant attention. The improved thermal conductivity of UHMWPE composites have been obtained through doping of fillers, such as aluminium nitride (AlN) [7, 8], boron nitride (BN) [9], silicon nitride (Si_3N_4) [10], silicon carbide (SiC) [11], and aluminium oxide [12].

However, UHMWPE cannot be extruded and injection molded like other thermoplastic materials at temperatures above its melting temperature due to its extremely high melt viscosity. Nowadays, the processing of this material is basically limited to compression molding [13–15] and ram extrusion. Therefore, the distribution of thermally conductive fillers in the matrix of UHMWPE has become a key factor affecting the thermal conductivity of composites. In order to allow the thermally conductive particles to be well distributed in the UHMWPE matrix, scholars are currently mixing them: (1) by dispersing the filler and UHMWPE particles in an organic solvent, then volatilizing the organic solvent to dry; (2) by stirring the filler with UHMWPE pellets at high speed in a high speed mixer for a period of time [16]; (3) by mixing the filler and UHMWPE pellets at a certain temperature [17]. For the first type of dispersion, the organic solvents commonly used by research scholars are acetone [18], ethanol [19–22], 1,2 dicholorobenzene [23], etc. Whether dispersed in a solvent

or stirred in a high-mixer, the composite has a segregated structure with a good thermal path, since compression molding is a static flow field. When the filler and the UHMWPE matrix are mixed in a molten state, the segregated structure is damaged to some extent. It has been reported [24] that the order of increase in thermal conductivity is melt mixing, twin roll mixing, solution mixing, and powder mixing. Then, the influence of mixing methods on morphological structure and thermal conductivity, and the relationship between them remains to be further understood.

In this work, the UHMWPE/BN composites were pretreated by MM and SM, and then was performed compression molding. We investigated the effects of microstructure of composites prepared by these two mixing methods on thermal conductivity. Furthermore we focus on the relationship between morphological structure and thermal stability of the composite.

2. Materials and Methods

2.1. Materials. UHMWPE particles with an average diameter of ~150 μm (Mv = 2.5×10^6 g/mol) was purchased from LianLe Chemical Co., Ltd., (Shanghai, China). Hexagonal Boron Nitride platelets with an average diameter of 3 μm and density of 2.25 g/cm^3 were supplied by Yingkou Tianyuan Chemical Research Institute Co. Ltd., (Liaoning, China).

2.2. Preparation of the UHMWPE/BN Composites

2.2.1. Preparation of the UHMWPE/BN Composites by Solvent Mixing. A specified amount (0, 10, 20, 30, 40 wt%) of BN microsheets was fed into ethanol to form a suspension under magnetic stirring for 1 h. Then UHMWPE particles were added into the suspension followed by magnetic stirring at 60°C for another several hours to ensure ethanol completely evaporated. Subsequently, the mixtures were compression-molded at 220°C and 17.6 MPa for 5 min after preheating for 20 min. The resulting UHMWPE/BN composites were cooled to room temperature by cold compression molding for 40 min.

2.2.2. Preparation of the UHMWPE/BN Composites by Melt Mixing. BN microsheets were first dried in an oven at 80°C for 12 h. UHMWPE powder was then mixed with 0, 10, 20, 30, 40wt% of BN microsheets in Harper torque rheometer at 190°C and 30 rpm for 10 min. Then, the mixtures were immediately transferred to a mold for hot pressing at 220°C and 17.6 MPa for another 10 min followed by cold compression molding for 40 min.

2.3. Characterization. The morphology of the samples was obtained with a scanning electron microscope (SEM, JSM-7500F, JEOL, Japan). It was performed at an acceleration voltage of 5 kV. The fractured surfaces of samples were sprayed with Au before SEM examination.

Raman mapping was performed by a micro-laser confocal Raman spectrometer (Thermo Scientific DXR2xi, America). For each sample, a total of 3721 spectra were collected in 70 min on a sample area of 300 × 300 μm with a spatial resolution of 5 μm between spectra. The test condition was that the laser power is 10 mW, and the total exposure is 20 times with 0.025 s exposure time for each spectrum. Peak area of Raman characteristic peak of BN at 1365 cm^{-1} in Raman mapping data was processed by OMMIC analysis software, which can represent the content of BN. In addition, the color in the mapping from dark blue to red indicates the distribution of the BN characteristic peak area from small to large.

Crystalline properties were measured by differential scanning calorimeter (DSC, Q20, TA). The samples were first heated up to 200°C and held isotherm at 200°C for 3 min to remove heat history and then cooled to 40°C. The samples were reheated from 40 to 200°C at 10°C/min. The crystallinity (X_c) was counted according to the following equation:

$$X_c = \frac{\Delta H_m}{\Delta H_{m0} * (1 - \phi)} \times 100\%, \quad (1)$$

where ΔH_m is the melting enthalpy of samples, ΔH_{m0} is the standard enthalpy of PE (290 J/g) [25], and φ is the mass fraction of h-BN platelets.

The weight loss of samples was evaluated by thermal gravimetric analyzer (TGA, Q50, TA) with range from 40 to 600°C at a heating rate of 10°C/min under nitrogen atmosphere.

The thermal conductivity was investigated by a hot–wire thermal conductivity instrument (Xiatech TC3000E, China) according to ASTM D5930. Before thermal conductivity measurement, the hot wire was placed between two same samples of 1 mm thickness with a specific weight on top of the stacked samples to make good contact with samples due to its mechanical flexibility.

3. Results and Discussion

3.1. Morphology of UHMWPE/BN Composites. Figures 1(a) and 1(c) depicts the surface morphologies of UHMWPE nascent powder before and after SM. UHMWPE nascent powder is composed of a plurality of secondary particles connected by fibers. There is no significant changes in morphology of UHMWPE particles after SM. In contrast, the fibers on the surface of UHMWPE particles by MM are melted due to the high temperature. The morphologies of the core-shell UHMWPE/BN particles with 40 wt% BN through two mixing methods are shown in Figures 1(d) and 1(f). It can be seen that BN is uniformly attached to the surface of UHMWPE particles by SM due to smooth surface, less defects, and higher aspect ratio of BN (Figure 1(b)). However, BN tightly adheres to the surface of UHMWPE particles by MM.

Figure 2 depicts the SEM observation of the cryo-fracture surface of the UHMWPE/BN composites, giving more details about microstructure differences of composites prepared via two mixing methods. As shown in Figure 2(a), cryo-fracture surface of pure UHMWPE prepared by SM is porous. There are obvious weld marks between UHMWPE particles. This is because UHMWPE particles are only subjected to the vertical direction by hot pressing without force in the horizontal direction, so that molecular chain motion is limited, resulting in obvious weld lines between the particles and the porous brittle

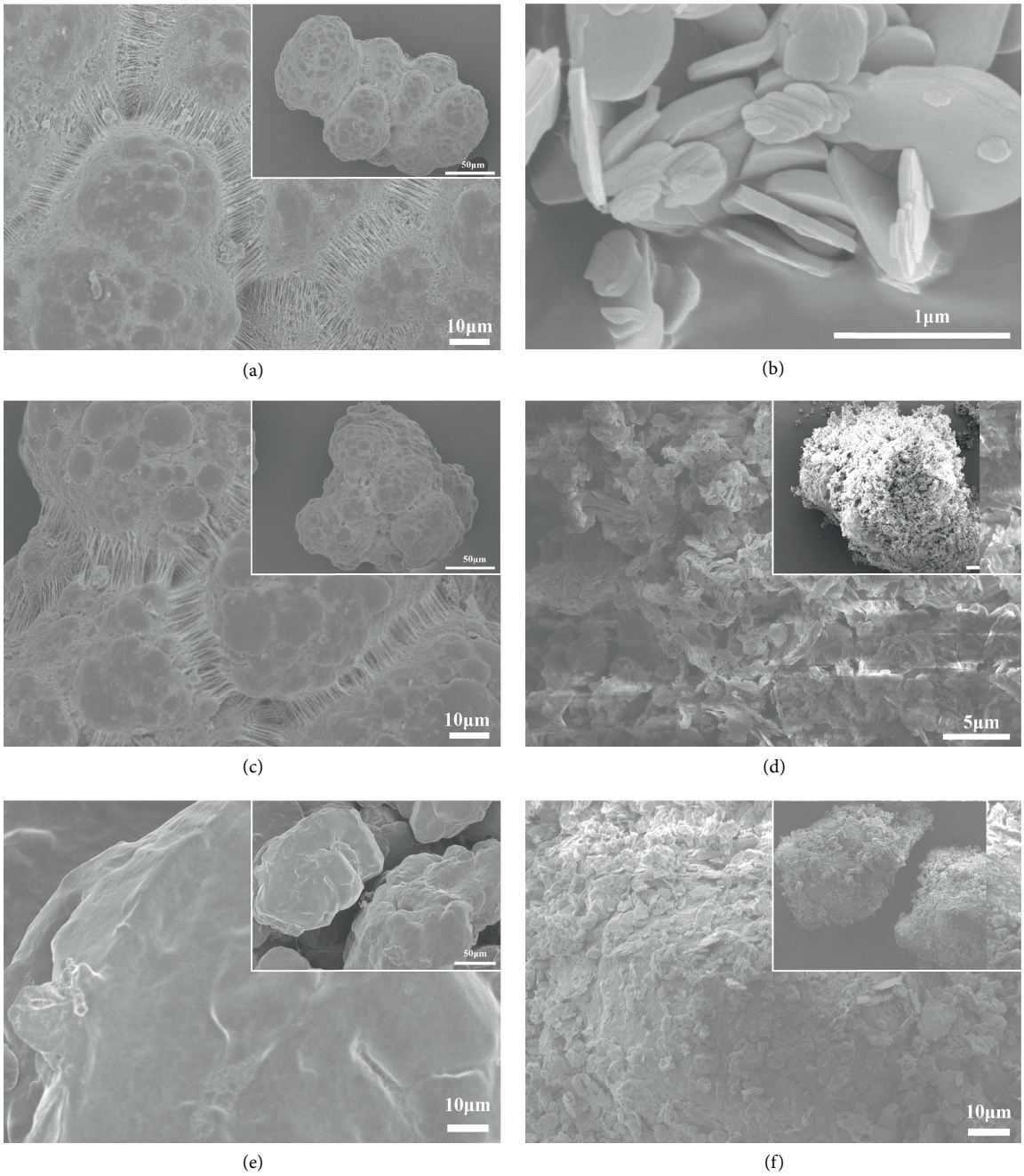

Figure 1: SEM of (a) UMMWPE nascent powder; (b) BN; (c) 0 wt% and (d) 40 wt% BN coated on UHMWPE particles by solvent mixing before hot pressing, (e) 0 wt% and BN (f) 40 wt% BN coated on UHMWPE particles by melt mixing before hot pressing.

profile, while there is no porous brittle profile in cryo-fracture surface of the samples via MM resulting from shear mixing at high temperatures promoting the diffusion of UHMWPE molecular chains inside and between particles. As shown in Figure 4(b), with addition of BN up to 40 wt%, BN adheres to the surface of the UHMWPE particles, and forms BN pathways, which can improve the decomposition hindering effect of the 2D thermal conductivity filler and thermal conductivity of UHMWPE/BN composites. However, it can be seen in Figure 2(d) that part of BN is embedded in UHMWPE particles due to shear at high temperature resulting in damage in segregated structure, which might be the reason why the thermal conductivity and thermal stability of the composite by MM is lower than that of samples via SM.

3.2. Raman Mapping. Raman mapping of UHMWPE/BN composites by SM and MM with various addition of BN is shown in Figure 3. As depicted in Figure 3, Figure a-1, b-1, c-1, d-1, is Raman mapping of test area (Figure a-2, b-2, c-2, d-2) of composites with various addition of BN, respectively. The color in the image from blue to red represents the peak area of Raman characteristic peak of the boron nitride at $1365\,cm^{-1}$ in the composite material from small to large, which can indicate the distribution of BN in the composite matrix.

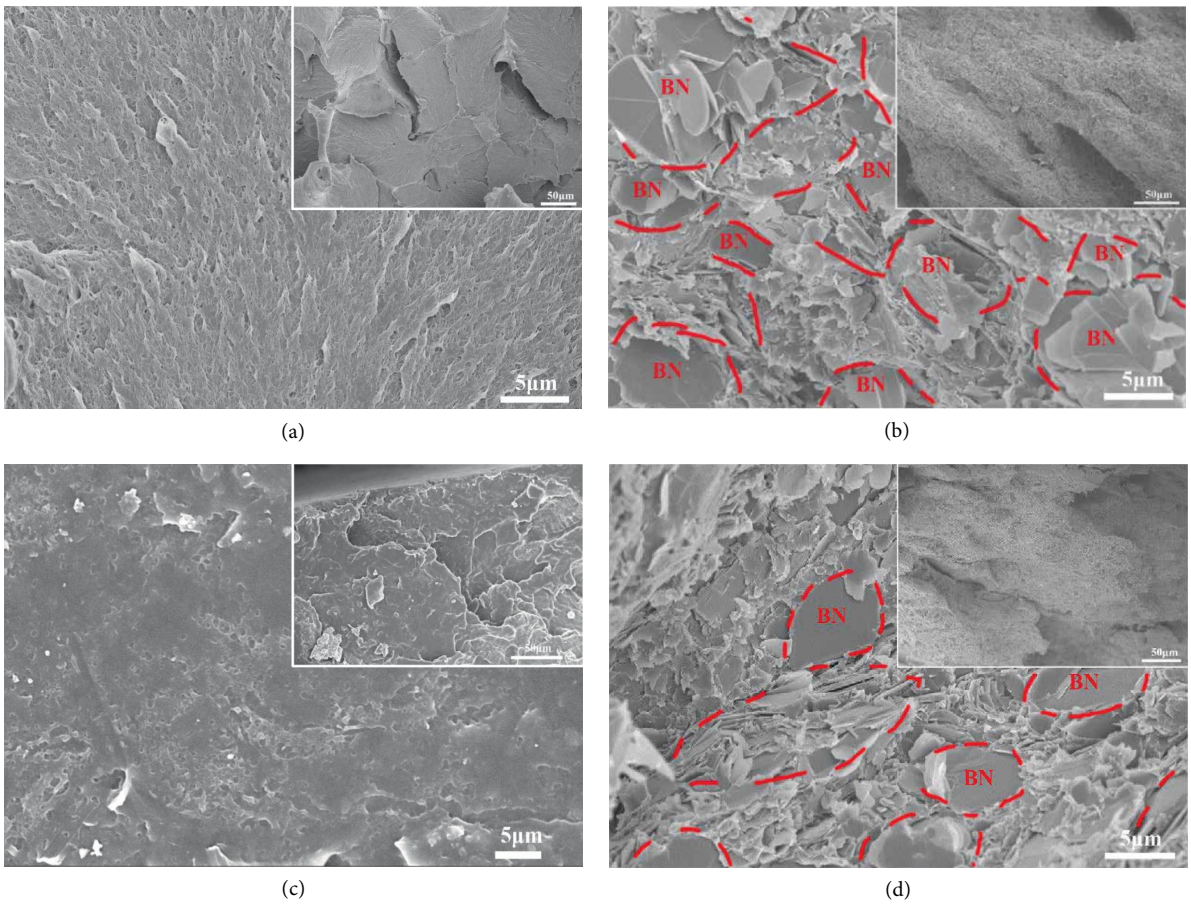

Figure 2: SEM of UHMPWE/BN composites by solvent mixing (a) 0 wt% BN; (b) 40 wt% BN; and melt mixing. (c) 0 wt% BN; (d) 40 wt% BN.

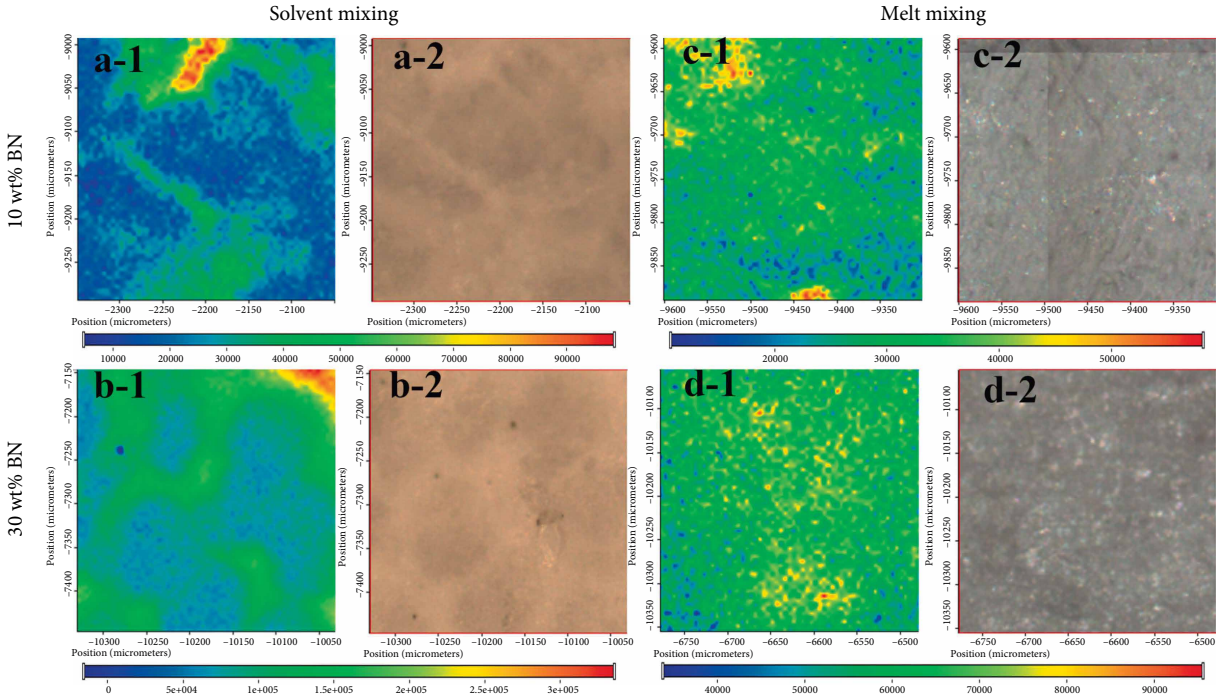

Figure 3: Raman Mapping of UHMWPE/BN composites by solvent mixing and melt mixing.

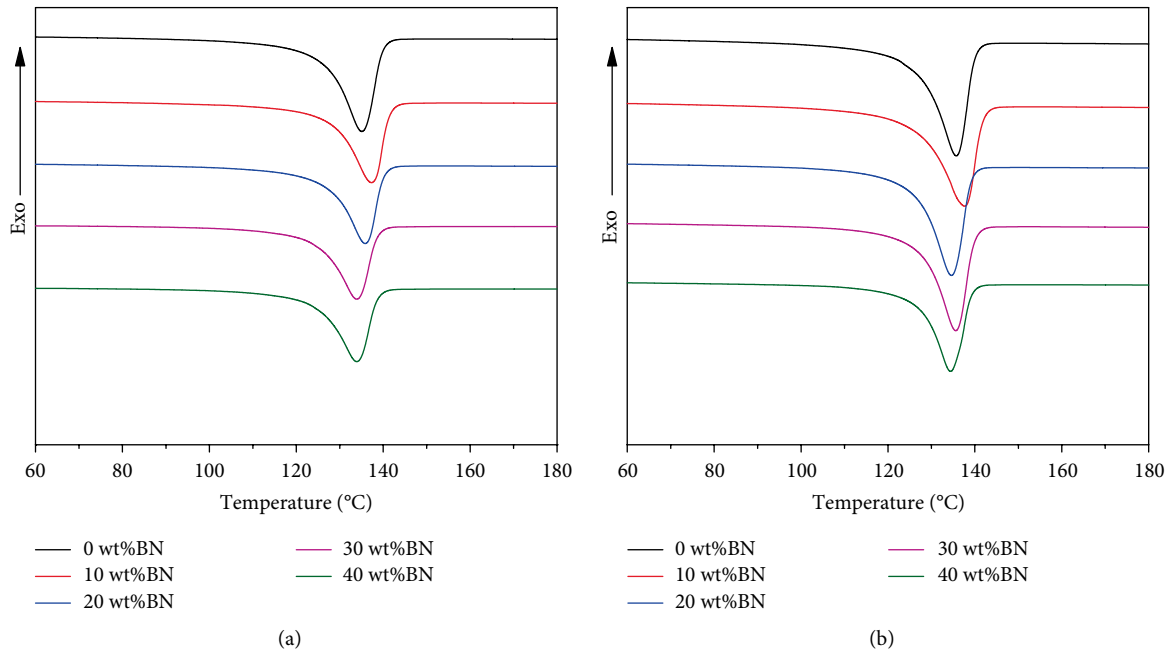

Figure 4: Heating melting function curve of UHMWPE composites by solvent mixing (a) and melt mixing (b), respectively.

Table 1: DSC thermal parameters of UHMWPE/BN composites by solvent mixing and melt mixing.

Mixing method	BN content (wt%)	T_m(°C)	ΔH_m (J/g)	T_c(°C)	ΔH_c (J/g)	X_c(%)
SM	0	135.1	144.3	116.2	148.1	49.8
	10	137.3	131.8	117.4	124.2	50.5
	20	135.9	121.8	117.0	114.4	52.5
	30	133.9	114.0	115.7	107.9	56.2
	40	132.3	106.1	114.4	106.1	61.0
MM	0	135.7	148.6	118.3	145.9	51.2
	10	137.7	145.7	116.6	139.5	55.8
	20	134.6	137.6	117.4	127.7	59.3
	30	135.6	127.1	117.3	119.0	62.6
	40	136.0	108.5	116.9	108.2	62.4

With the increment of BN content, BN coated on the surface of UHMWPE particles forms a continuous thermal conduction path inside the solvent-mixed composite, while the BN signal distribution is relatively uniform in the Raman mapping of composites by MM, indicating that the segregated structure of the composites is damaged due to shearing.

3.3. Crystallization Behavior of UHMWPE/BN Composites. Figure 4 depicts the on-heating DSC curves of UHMWPE composites by different mixing methods and DSC thermal parameters are shown in Table 1. As shown in Table 1, the crystallinity of pure UHMWPE pre-treated by SM and MM is 49.8 and 51.2%, respectively. With the content of BN up to 40 wt%, the crystallinity of the composites via SM and MM increases to 61.0 and 61.4% respectively, due to BN as heterogeneous nucleating agent. However the crystallinity of the composites by MM is higher than that of the samples through SM, resulting from shear promoting better dispersion of BN in the matrix, leading to better heterogeneous nucleation.

3.4. Thermal Stability of UHMWPE/BN Composites. Thermogravimetric analysis (TGA) is carried out to characterize the thermal stability of the composites by different mixing methods under nitrogen atmosphere. The TGA curves and DTA curves are shown in Figure 5 and relevant thermal data are summarized in Table 2. Figure 5 shows that there is only a single stage from the temperature of 400 to 500°C during the thermal decomposition of UHMWPE/BN composites. It illustrates that the addition of BN and different mixing methods does not affect the thermal decomposition behavior. The temperatures at 5%, 30%, and 50% weight loss (T_5, T_{30}, and T_{50}) are shown in Table 2. As Table 2 shows, T_5 of samples by MM decreases with addition of BN and T_{30} and T_{50} has not changed significantly, while T_5, T_{30}, T_{50} of composites by SM both increase. In addition, heat resistance index (HRI) [26] calculated by T_5 and T_{30} of composites by MM decreases slightly from 299.1 to 226°C, while HRI of samples via SM increases from 225 to 230.5°C.

To obtain a better understanding of the thermal stability of the composites by different mixing methods, integral procedural decomposition temperature (IPDT) based on Doyle's proposition [27] and activation energy (E_a) can be used to assess material's thermal stability. The IPDT is determined from TGA curves and reckoned by following equations [28–30]:

$$IPDT(^{\circ}C) = AK \cdot \left(T_f - T_i\right) + T_i, \tag{2}$$

$$A = \frac{S_1 + S_2}{S_1 + S_2 + S_3}, \tag{3}$$

Table 2: Thermal data of UHMWPE/BN composites from TG analyses.

Mixing method	BN content (wt%)	Weight loss temperature(°C)			Heat-resistance index*(°C)	Residual weight/%	
		T_5	T_{30}	T_{50}		Theory	Actual
MM	0	456.5	474.9	480.1	229.1	0	0.20
	10	455.1	475.5	482.3	229.0	10	10.02
	20	451.4	474.3	482.0	227.9	20	20.29
	30	448.8	473.6	482.7	227.2	30	30.23
	40	444.3	472.5	482.7	226.0	40	39.79
SM	0	443.6	469.6	477.0	225.0	0	0.31
	10	436.7	465.3	474.4	222.4	10	10.04
	20	450.6	475.0	482.9	228.0	20	20.67
	30	453.7	476.6	484.7	229.0	30	28.45
	40	457.4	480.1	489.7	230.8	40	40.96

*$T_{\text{Heat-resistance index}} = 0.49 * [T_5 + 0.6(T_{30} - T_5)]$. T_5 and T_{30} is corresponding decomposition temperature of 5 and 30% weight loss, repectively.

$$K = \frac{S_1 + S_2}{S_1}, \tag{4}$$

where A is the area ratio of total experimental curve divided by total TGA curve; K is the coefficient of A (Figure S2); T_i is the onset experimental temperature (50°C, in this work) and T_f is the terminal experimental temperature(550°C). The results of composites by different mixing methods are present in Table 3. The IPDT can be usually attributed to the unstable parts in composites, indicating that the higher IPDT is, the better the thermal stability of composites is.

The E_a required for thermal decomposition of the UHMWPE/BN composites can be reckoned by the Horowitz–Metzger integral kinetic method according to Equation (5) [31–33].

$$\ln\left(\ln(1-\alpha)^{-1}\right) = \frac{E_a}{RT_{\max}^2}\theta, \tag{5}$$

where α is the mass fraction of sample decomposed; the E_a values of the UHMWPE/BN composites can be calculated from the slope of the plot of $\ln\left(\ln(1-\alpha)^{-1}\right)$ versus θ as shown in Figure 6 (kJ/mol); R is the real gas constant (8.314 J/(mol·K)); $T_{\max}$ is decomposition temperature at the maximum weight loss rate (°C); θ is the difference between decomposition temperature T and $T_{\max}(K)$.

E_a is a parameter used to evaluate the thermal stability of materials. The higher E_a value the polymer composites have, the more thermally stable it is. Generally, relatively large crosslinking density results in high decomposition temperature [29]. It can be seen in Figures S1, S3, and Table S1 that both IPDT and the E_a rise with the increase of relative molecular weight of UHMWPE, indicating that the higher relative molecular mass UHMWPE has, the higher the internal physical entanglement density is and the better thermal stability UHMWPE has [34, 35]. The IPDT and E_a of UHMWPE with the same relative molecular mass prepared by MM is 499.7°C and 530.27 kJ/mol, respectively higher than the IPDT and the E_a of UHMWPE prepared by SM, which is 475.5°C and 478.65 kJ/mol. During the MM process, the shearing action leads to a certain decrease in the relative molecular mass of UHMWPE, but also promotes the increase in physical entanglement density, resulting in better thermal stability.

As shown in Table 3, with addition of BN, the IPDT of the composites increases gradually and the IPDT of the melt-mixed samples is higher than that of the solvent-mixed samples, indicating that MM increases the inherent thermal stability of the composites. In addition, with the increment of BN content, the E_a values of composites via MM or SM are reduced compared to pure UHMWPE resulting from the introduction of high thermal conductivity filler BN causing heat to pass faster in the composites. And the E_a values of composites by MM decrease more than those of samples via SM. This is because that the segregated structure of the composites through SM makes the 2D material BN hinder the diffusion of the volatile decomposition part [36], while the segregated structure of samples via MM is damaged to some extent due to shear at high temperature. Thereby, the contribution of both IPDT and E_a induces differences in thermal stability between samples prepared by MM and SM [37].

3.5. Thermal Conductivities of the UHMWPE/BN Composites. Figure 7 illustrates the thermal conductivity and enhancement ratio of the UHMWPE/BN composites by different mixing methods. The thermal conductivity enhancement ratio is defined as:

$$X = \frac{\lambda_c - \lambda_p}{\lambda_p} * 100\%, \tag{6}$$

where X is the thermal conductivity enhancement ratio; λ_c is the thermal conductivity of the composite; λ_p is the thermal conductivity of pure UHMWPE. As shown in Figure 7(a), it can be seen that the thermal conductivity of two mixing methods is increasing with the increment of BN content. The thermal conductivity of composites prepared through MM increases from 0.38 to 1.50 $\text{Wm}^{-1}\text{K}^{-1}$, increased by 294.74% with addition of BN up to 40 wt%, while the thermal conductivity of composites prepared by SM is up to 1.76 $\text{Wm}^{-1}\text{K}^{-1}$, increased by 363.16% at the same filler content. It is obviously seen that the thermal conductivity of composites prepared by

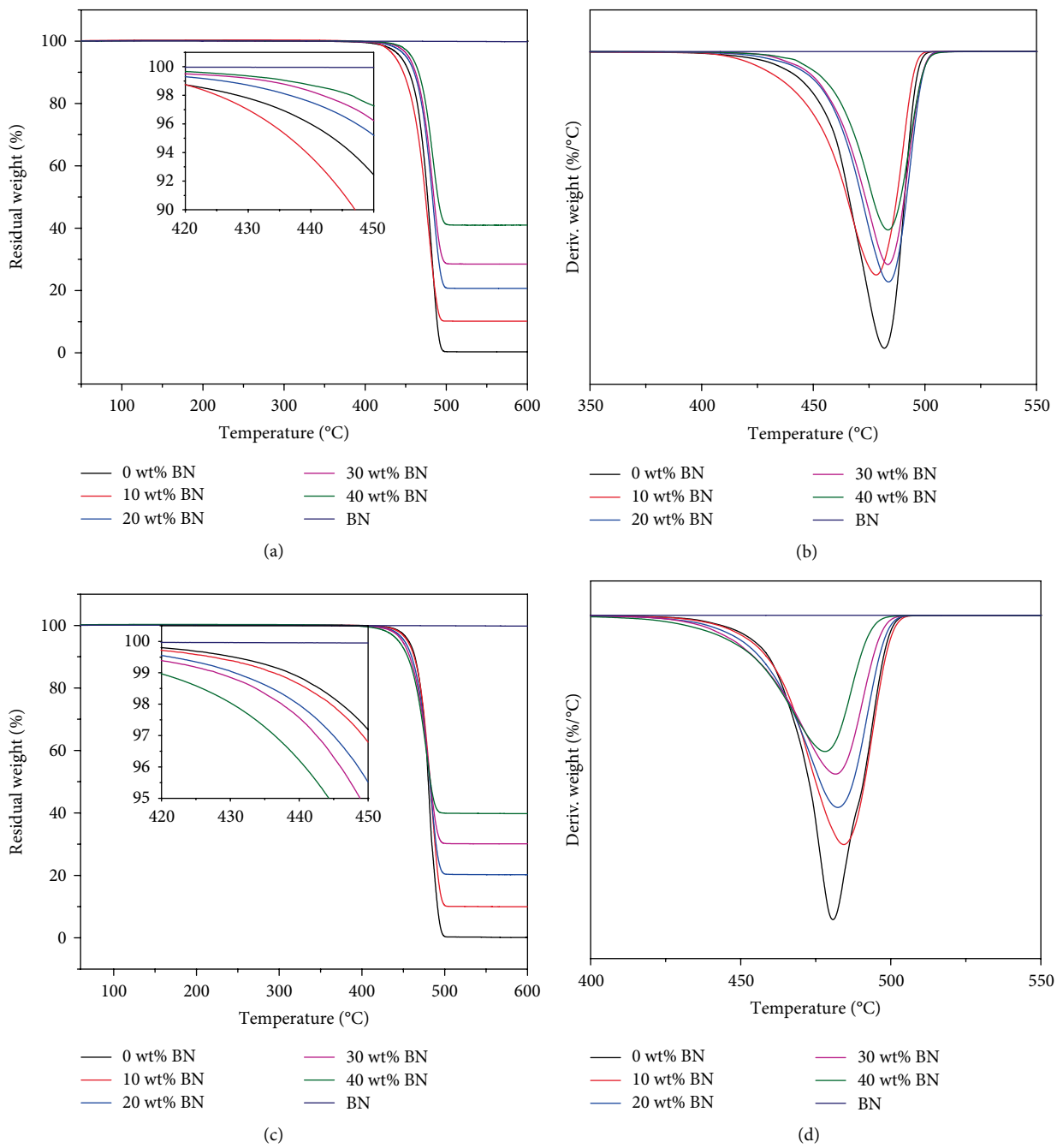

Figure 5: TGA and DTA curves of UHMWPE/BN composites by solvent mixing (a) (b) and melt mixing (c) (d).

Table 3: Thermal stabilities of the composites by different mixing obtained from TGA curves.

BN content (wt%)	T_{max} [a] (°C)		IPDT (°C)		E_a [b] (kJ/mol)	R^2	E_a [b] (kJ/mol)	R^2
	SM	MM	SM	MM	SM		MM	
0	481.8	480.8	475.5	499.7	478.65	0.997	530.27	0.997
10	478.2	484.4	534.8	566.7	335.62	0.999	430.27	0.995
20	483.7	482.4	535.7	649.6	356.59	0.991	356.34	0.991
30	483.4	481.6	626.4	742.9	342.05	0.986	305.78	0.986
40	483.5	478.1	705.9	875.2	333.03	0.979	281.07	0.982

[a]The decomposition temperature at the maximum rate of the weight loss. [b]The activation energy calculate by Horowitz–Metzger integral kinetic method.

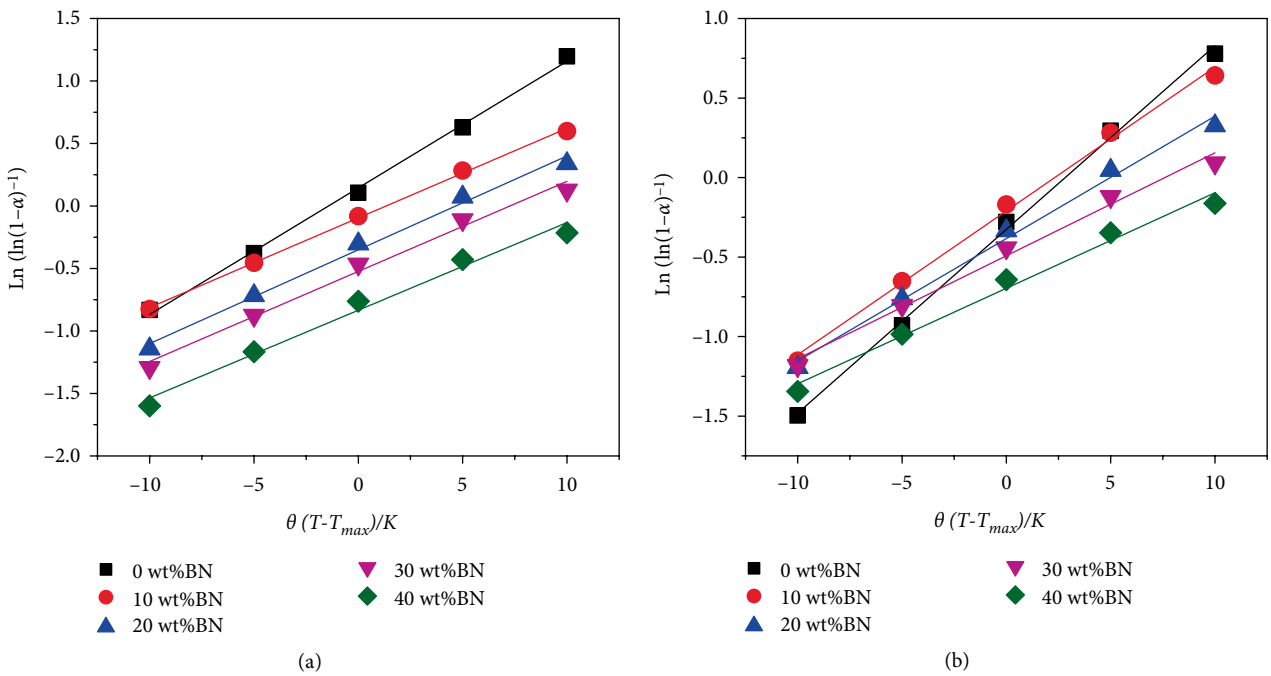

FIGURE 6: The plots of $\ln\left(\ln(1-\alpha)^{-1}\right)$ versus θ as shown for the UHMWPE/BN composites by solvent mixing (a) and melt mixing (b).

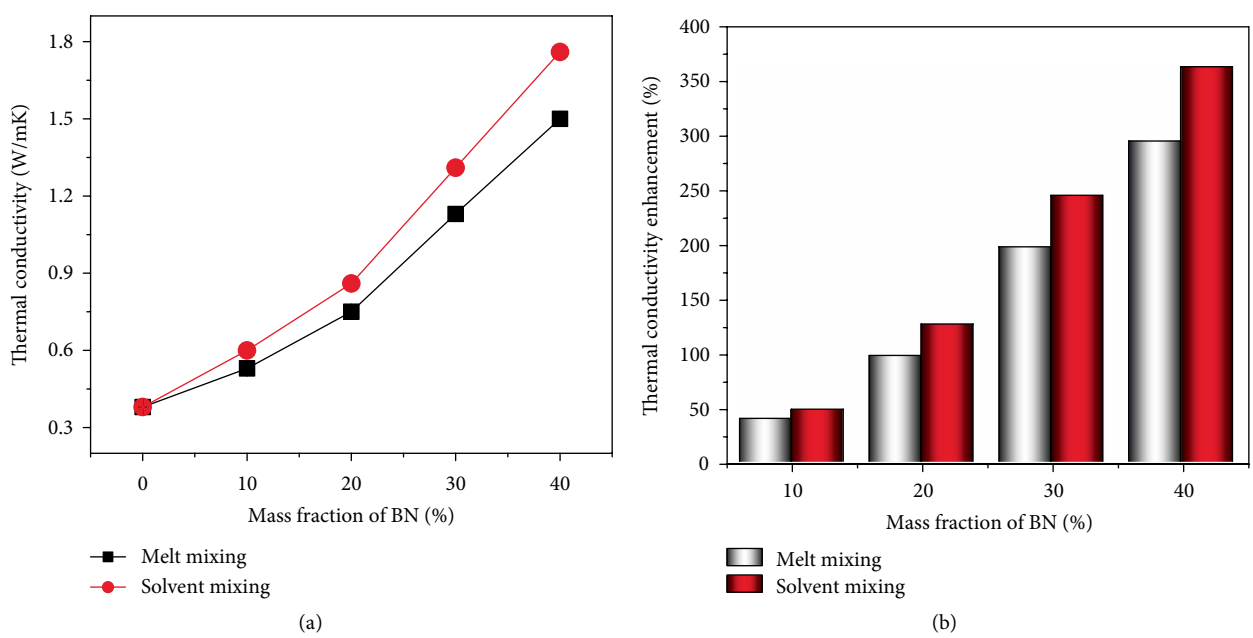

FIGURE 7: Thermal conductivity and enhencement of the UHMWPE/BN composites by melt mixing and solvent mixing.

SM is superior to that of composites prepared by MM, which is consistent with the results of some researchers [38–40]. SM helps BN to physically adhere to the surface of UHMWPE particles, and composite materials with isolated structure can be prepared by molding, which results in improvement of thermal conductivity of UHMWPE/BN composites. However, the isolated structure of the composite is destroyed after the MM, which causes the thermal path inside the UHMWPE to be destroyed, resulting in lower thermal conductivity than that of composites by SM.

The effective thermal conductivities of two-phase polymeric composites have been predicted by many researchers via proposing theoretical and empirical models. Hereon, Agari's semi-empirical model [41–45] can fit better results than other models. The logarithmic equation of Agari is shown as follows:

$$\log\lambda = VC_2\log\lambda_2 + (1-v)\log(\lambda_1 C_1), \quad (7)$$

where C_1 denotes the effect of doping BN on the UHMWPE structure; C_2 denotes the contribution of BN to construction

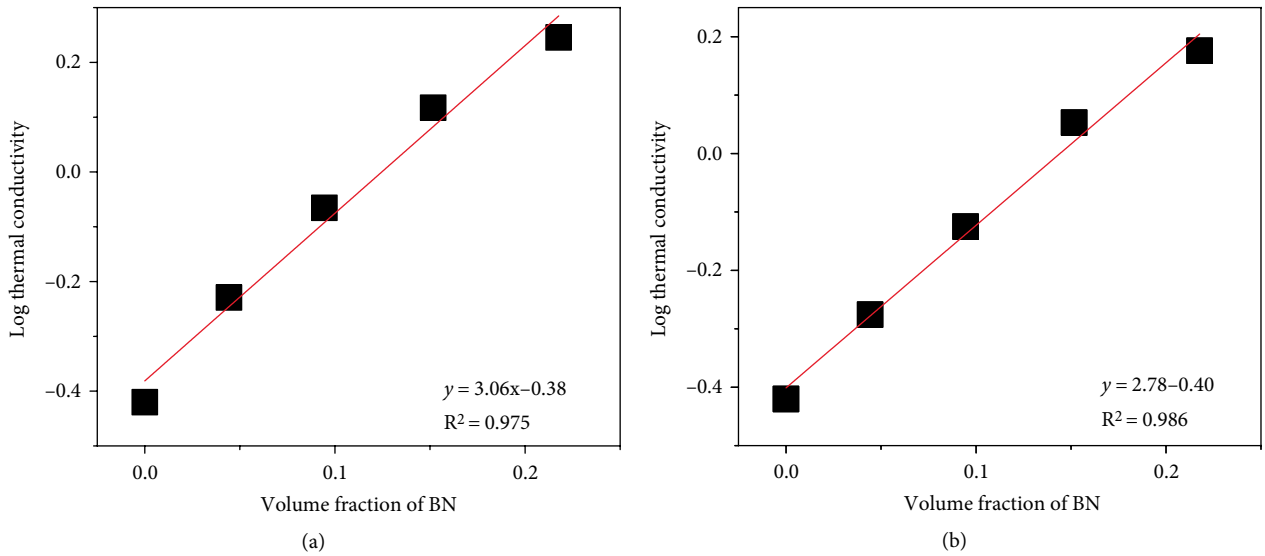

Figure 8: Logarithmic thermal conductivities of the UHMWPE composites as a function of the BN volume fraction by solvent mixing (a) and melt mixing (b).

of continuous thermally conductive chains & networks, $0 < C_2 < 1$, the easier formation of thermal conduction paths of fillers, the more the C_2 close to 1; V denotes the volume fraction of fillers; λ, λ_2, and λ_1 denote the thermal conductivity of composites, fillers and polymeric matrix, respectively.

Figure 8 shows the logarithmic values of thermal conductivities as a function of the BN volume fraction by MM and SM. Herein, λ_2 is $290\,\mathrm{Wm^{-1}K^{-1}}$ and λ_1 is $0.38\,\mathrm{Wm^{-1}K^{-1}}$, According to Equation (7), the results are calculated in Table S2. It can be seen that the parameters of C_2 of composites by SM is higher than that of samples by MM, revealing that SM makes it easier for BN to form continuous thermally conductive networks in the UHMWPE matrix than MM, resulting in better thermal conductivity of the composite.

4. Conclusions

UHMWPE/BN composites, which were prepared by SM and MM, were characterized through SEM, Raman mapping, TG, DSC, and thermal conductivity meter. It aims to mainly discuss the effect of different mixing methods on the thermal conductivity and thermal stability of the composites. The samples by SM have a better segregated structure than the samples by MM whose segregated structure is destroyed due to high temperature shearing. Although the crystallinity of samples via MM is larger than that of the SM, the thermal conductivity of composites by SM is better than that of samples by MM, resulting from structural differences caused by the difference between the two mixing methods. The reason is explained by calculated IPDT and activation energy of the composites that the thermal stability of the composite by SM increases with continuous addition of BN due to the decomposition hindering effect of the 2D thermal conductivity filler, while the thermal stability of the composite by MM decreases.

Data Availability

The data used to support the findings of this study are available from the corresponding author upon request.

Conflicts of Interest

The authors declare that they have no conflicts of interest.

Funding

Financial supports from the National Key Research and Development Program of China (2016YFB0302300).

Acknowledgments

This research was supported by the Engineering Research Center of Polymer Green Recycling of Ministry Education and Fujian Key Laboratory of Pollution Control & Resource Reuse, College of Environmental Science and Engineering Fujian Normal University. The authors are grateful to Xianning Wang for the guidance and maintenance of the polymer processing equipment.

Supplementary Materials

Figure S1: TGA curves of UHMWPE particles with various relative molecular weight. Table S1: thermal data of UHMWPE nascent powder with different relative molecular weight. Figure S2: Schematic representation of S1, S2, and S3 for A and K. Figure S3: the plots of $\ln\left(\ln(1-\alpha)^{-1}\right)$ versus θ as shown for the UHMWPE with various relative molecular weights. Table S2: thermal data of UHMWPE nascent powder with different relative molecular weight. (*Supplementary Materials*)

References

[1] S. M. Kurtz, *The UHMWPE Handbook: Ultra-high Molecular Weight Polyethylene in Total Joint Replacement*, Elsevier, Amsterdam, The Netherlands, 2004.

[2] W. Zhou, C. Wang, T. Ai, K. Wu, F. Zhao, and H. Gu, "A novel fiber-reinforced polyethylene composite with added silicon nitride particles for enhanced thermal conductivity," *Composites Part A: Applied Science and Manufacturing*, vol. 40, no. 6–7, pp. 830–836, 2009.

[3] C. L. Choy, Y. Fei, and T. G. Xi, "Thermal conductivity of gel-spun polyethylene fibers," *Journal of Polymer Science Part B: Polymer Physics*, vol. 31, no. 3, pp. 365–370, 1993.

[4] S. Ronca, T. Igarashi, G. Forte, and S. Rastogi, "Metallic-like thermal conductivity in a lightweight insulator: solid-state processed ultra high molecular weight polyethylene tapes and films," *Polymer*, vol. 123, pp. 203–210, 2017.

[5] Y. Guo and S. N. Leung, "Strain-induced oriented crystallization of UHMWPE: enhanced thermal conductivity through molecular chain alignment," *AIP Advances*, vol. 8, no. 4, p. 045126, 2018.

[6] F. Zhong, R. Thomann, and R. Mülhaupt, "Processing–nanostructure–property relationships of all-polyethylene composites reinforced by flow-induced oriented crystallization of UHMWPE," *Macromolecular Materials and Engineering*, vol. 303, no. 5, p. 1800022, 2018.

[7] Y. Wang, X. Qiao, J. Wan, Y. Xiao, and X. Fan, "Preparation of AlN microspheres/UHMWPE composites for insulating thermal conductors," *RSC Advances*, vol. 6, no. 83, pp. 80262–80267, 2016.

[8] W. Zhou, "Thermal and dielectric properties of the AlN particles reinforced linear low-density polyethylene composites," *Thermochimica Acta*, vol. 512, no. 1–2, pp. 183–188, 2011.

[9] C. Gao, H. Lu, H. Ni, and J. Chen, "Structure, thermal conductive, dielectric and electrical insulating properties of UHMWPE/BN composites with a segregated structure," *Journal of Polymer Research*, vol. 25, no. 1, p. 6, 2018.

[10] Q. An, S. Qi, and W. Zhou, "Thermal, electrical, and mechanical properties of Si3N4 filled LLDPE composite," *Polymer Composites*, vol. 30, no. 7, pp. 866–871, 2009.

[11] J. Gu, Y. Guo, Z. Lv, W. Geng, and Q. Zhang, "Highly thermally conductive POSS-g-SiCp/UHMWPE composites with excellent dielectric properties and thermal stabilities," *Composites Part A: Applied Science and Manufacturing*, vol. 78, pp. 95–101, 2015.

[12] S. Yang, W. Li, S. Bai, and Q. Wang, "Fabrication of morphologically controlled composites with high thermal conductivity and dielectric performance from aluminum nanoflake and recycled plastic package," *ACS Applied Materials & Interfaces*, vol. 11, no. 3, pp. 3388–3399, 2018.

[13] H. Pang, Y. Y. Piao, Y. Q. Tan, G.-Y. Jiang, J.-H. Wang, and Z.-M. Li, "Thermoelectric behaviour of segregated conductive polymer composites with hybrid fillers of carbon nanotube and bismuth telluride," *Materials Letters*, vol. 107, pp. 150–153, 2013.

[14] L. C. Jia, D. X. Yan, X. Jiang et al., "Synergistic effect of graphite and carbon nanotubes on improved electromagnetic interference shielding performance in segregated composites," *Industrial & Engineering Chemistry Research*, vol. 57, no. 35, pp. 11929–11938, 2018.

[15] S. Zhao, D. Lou, P. Zhan et al., "Heating-induced negative temperature coefficient effect in conductive graphene/polymer ternary nanocomposites with a segregated and double-percolated structure," *Journal of Materials Chemistry C*, vol. 5, no. 32, pp. 8233–8242, 2017.

[16] Z. G. Wang, F. Gong, W. C. Yu et al., "Synergetic enhancement of thermal conductivity by constructing hybrid conductive network in the segregated polymer composites," *Composites Science and Technology*, vol. 162, pp. 7–13, 2018.

[17] Y. F. Huang, J. Z. Xu, J. S. Li, B.-X. He, L. Xu, and Z.-M. Li, "Mechanical properties and biocompatibility of melt processed, self-reinforced ultrahigh molecular weight polyethylene," *Biomaterials*, vol. 35, no. 25, pp. 6687–6697, 2014.

[18] K. Liu, S. Ronca, E. Andablo-Reyes, G. Forte, and S. Rastogi, "Unique rheological response of ultrahigh molecular weight polyethylenes in the presence of reduced graphene oxide," *Macromolecules*, vol. 48, no. 1, pp. 131–139, 2014.

[19] S. K. Reddy, S. Kumar, K. M. Varadarajan, P. R. Marpu, T. K. Gupta, and M. Choosri, "Strain and damage-sensing performance of biocompatible smart CNT/UHMWPE nanocomposites," *Materials Science and Engineering: C*, vol. 92, pp. 957–968, 2018.

[20] Y. Wang, J. Yang, S. Zhou, W. Zhang, and R. Chuan, "Electrical properties of graphene nanoplatelets/ultra-high molecular weight polyethylene composites," *Journal of Materials Science: Materials in Electronics*, vol. 29, no. 1, pp. 91–96, 2018.

[21] C. P. Feng, L. Chen, F. Wei, H. Y. Ni, J. Chen, and W. Yang, "Highly thermally conductive UHMWPE/graphite composites with segregated structures," *RSC Advances*, vol. 6, no. 70, pp. 65709–65713, 2016.

[22] T. K. Gupta, M. Choosri, K. M. Varadarajan, and S. Kumar, "Self-sensing and mechanical performance of CNT/GNP/UHMWPE biocompatible nanocomposites," *Journal of Materials Science*, vol. 53, no. 11, pp. 7939–7952, 2018.

[23] Z. Zhang, S. Mogurampelly, S. Percec et al., "Mechanically strong polymer sheets from aligned ultrahigh-molecular-weight polyethylene nanocomposites," *The Journal of Physical Chemistry Letters*, vol. 9, no. 10, pp. 2652–2658, 2018.

[24] Y. Agari, A. Ueda, and S. Nagai, "Thermal conductivities of composites in several types of dispersion systems," *Journal of Applied Polymer Science*, vol. 42, no. 6, pp. 1665–1669, 1991.

[25] F. J. Medel, M. J. Martínez-Morlanes, P. J. Alonso, J. Rubín, F. J. Pascual, and J. A. Puértolas, "Microstructure, thermooxidation and mechanical behavior of a novel highly linear, vitamin E stabilized, UHMWPE," *Materials Science and Engineering: C*, vol. 33, no. 1, pp. 182–188, 2013.

[26] Z. Han and A. Fina, "Thermal conductivity of carbon nanotubes and their polymer nanocomposites: a review," *Progress in Polymer Science*, vol. 36, no. 7, pp. 914–944, 2011.

[27] C. D. Doyle, "Estimating thermal stability of experimental polymers by empirical thermogravimetric analysis," *Analytical Chemistry*, vol. 33, no. 1, pp. 77–79, 1961.

[28] S. J. Park and M. S. Cho, "Thermal stability of carbon-MoSi2-carbon composites by thermogravimetric analysis," *Journal of Materials Science*, vol. 35, no. 14, pp. 3525–3527, 2000.

[29] M. S. Goyat, S. Ray, and P. K. Ghosh, "Innovative application of ultrasonic mixing to produce homogeneously mixed nanoparticulate-epoxy composite of improved physical properties," *Composites Part A: Applied Science and Manufacturing*, vol. 42, no. 10, pp. 1421–1431, 2011.

[30] C. F. Kuan, W. J. Chen, Y. L. Li, C.-H. Chen, H.-C. Kuan, and C.-L. Chiang, "Flame retardance and thermal stability of carbon nanotube epoxy composite prepared from sol–gel method," *Journal of Physics and Chemistry of Solids*, vol. 71, no. 4, pp. 539–543, 2010.

[31] S. Y. Wu, Y. L. Huang, C. C. M. Ma, S.-M. Yuen, C.-C. Teng, and S.-Y. Yang, "Mechanical, thermal and electrical properties of aluminum nitride/polyetherimide composites," *Composites Part A: Applied Science and Manufacturing*, vol. 42, no. 11, pp. 1573–1583, 2011.

[32] Y. Zhang, X. Ge, F. Deng, M.-C. Li, and U. R. Cho, "Fabrication and characterization of rice bran carbon/styrene butadiene rubber composites fabricated by latex compounding method," *Polymer Composites*, vol. 38, no. 11, pp. 2594–2602, 2017.

[33] K. E. Gonsalves, X. Chen, and M. I. Baraton, "Mechanistic investigation of the preparation of polymer/ceramic nanocomposites," *Nanostructured Materials*, vol. 9, no. 1–8, pp. 181–184, 1997.

[34] X. L. Wang, R. K. Y. Li, Y. X. Cao, and Y. Z. Meng, "Essential work of fracture analysis of poly (propylene carbonate) with varying molecular weight," *Polymer Testing*, vol. 24, no. 6, pp. 699–703, 2005.

[35] A. Mamun, S. M. M. Rahman, S. Roland, and R. Mahmood, "Impact of molecular weight on the thermal stability and the miscibility of poly (ε-caprolactone)/polystyrene binary blends," *Journal of Polymers and the Environment*, vol. 26, no. 8, pp. 3511–3519, 2018.

[36] W. Jin, L. Yuan, G. Liang, and A. Gu, "Multifunctional cyclotriphosphazene/hexagonal boron nitride hybrids and their flame retarding bismaleimide resins with high thermal conductivity and thermal stability," *ACS applied materials & interfaces*, vol. 6, no. 17, pp. 14931–14944, 2014.

[37] Z. Su, H. Wang, X. Ye et al., "Anisotropic thermally conductive flexible polymer composites filled with hexagonal born nitride (h-BN) platelets and ammine carbon nanotubes (CNT-NH2): Effects of the filler distribution and orientation," *Composites Part A: Applied Science and Manufacturing*, vol. 109, pp. 402–412, 2018.

[38] R. Xia, M. Sun, B. Yang et al., "Morphology, Thermal and Crystallization Properties of Polyamide-6/Boron Nitride (BN) Thermal Conductive," *Composites*, vol. 42, no. 2, pp. 230–241, 2018.

[39] Q. Mu and S. Feng, "Thermal conductivity of graphite/silicone rubber prepared by solution intercalation," *Thermochimica Acta*, vol. 462, no. 1–2, pp. 70–75, 2007.

[40] T. Liu, J. Li, X. Wang et al., "Preparation and properties of thermal conductive polyamide 66 composites," *Journal of Thermoplastic Composite Materials*, vol. 28, no. 1, pp. 32–45, 2015.

[41] Y. Agari, A. Ueda, and S. Nagai, "Thermal conductivity of a polymer composite," *Journal of Applied Polymer Science*, vol. 49, no. 9, pp. 1625–1634, 1993.

[42] Y. Agari, A. Ueda, and S. Nagai, "Thermal conductivity of a polyethylene filled with disoriented short-cut carbon fibers," *Journal of Applied Polymer Science*, vol. 43, no. 6, pp. 1117–1124, 1991.

[43] J. Gu, N. Li, L. Tian, Z. Lv, and Q. Zhang, "High thermal conductivity graphite nanoplatelet/UHMWPE nanocomposites," *RSC Advances*, vol. 5, no. 46, pp. 36334–36339, 2015.

[44] S. Yang, S. Bai, W. Duan, and Q. Wang, "Production of Value-Added Composites from Aluminum-Plastic Package Waste via Solid-State Shear Milling Process," *ACS Sustainable Chemistry & Engineering*, vol. 6, no. 3, pp. 4282–4293, 2018.

[45] S. Yang, W. Li, S. Bai, and Q. Wang, "High-performance thermal and electrical conductive composites from multilayer plastic packaging waste and expanded graphite," *Journal of Materials Chemistry C*, vol. 6, no. 41, pp. 11209–11218, 2018.

Hindawi
Advances in Polymer Technology
Volume 2019, Article ID 6519018, 26 pages
https://doi.org/10.1155/2019/6519018

Review Article

Functional Micro–Nano Structure with Variable Colour: Applications for Anti-Counterfeiting

Hailu Liu, Dong Xie, Huayan Shen, Fayong Li, and Junjia Chen

GuangDong Provincial Bioengineering Institute (GuangZhou Sugarcane Industry Research Institute), Guangdong Biomaterials Technology Research Center, Guangzhou 510316, China

Correspondence should be addressed to Junjia Chen; gzcsircjj@163.com

Received 19 June 2019; Accepted 7 August 2019; Published 8 December 2019

Guest Editor: Wei Hong

Colour patterns based on micro-nano structure have attracted enormous research interests due to unique optical switches and smart surface applications in photonic crystal, superhydrophobic surface modification, controlled adhesion, inkjet printing, biological detection, supramolecular self-assembly, anti-counterfeiting, optical device and other fields. In traditional methods, many patterns of micro-nano structure are derived from changes of refractive index or lattice parameters. Generally, the refractive index and lattice parameters of photonic crystals are processed by common solvents, salts or reactive monomers under specific electric, magnetic and stress conditions. This review focuses on the recent developments in the fabrication of micro-nano structures for patterns including styles, materials, methods and characteristics. It summarized the advantages and disadvantages of inkjet printing, angle-independent photonic crystal, self-assembled photonic crystals by magnetic field force, gravity, electric field, inverse opal photonic crystal, electron beam etching, ion beam etching, laser holographic lithography, imprinting technology and surface wrinkle technology, etc. This review will provide a summary on designing micro-nano patterns and details on patterns composed of photonic crystals by surface wrinkles technology and plasmonic micro-nano technology. In addition, colour patterns as switches are fabricated with good stability and reproducibility in anti-counterfeiting application. Finally, there will be a conclusion and an outlook on future perspectives.

1. Introduction

The interaction of the micro/nano structure with incident light can produce a structural colour which is mainly consequent on multi-layer thin film interference, diffraction of surface or periodic structure, and wavelength selective scattering by sub-wavelength particles [1–5]. There are many natural examples of microstructure, such as peacock tails, chameleons, butterflies, pearls, the elytra of beetles and opal native to Australia [6–10]. Peacock tail feather has a central stem of barbs array with flat barbules which disperse the incident light and cause colouration. The barbules with different diameters of more than one hundred nanometers form a two-dimensional array, which are shown in different colours by varying the lattice constant and shifting the midgap frequency of the partial photonic bandgap [11]. For pearls with a closely packed multilayer structure, the colour have been ascribed to interference and/or diffraction of light within the binding regions of the aragonite tiles, and the rainbow-like diffraction colours of pearl has been demonstrated to depend on the width of the edge-band structure of organic matrix in aragonite [12]. The golden colour of elytra of beetles results from a multilayer interference involving a homogeneous melanoprotein layer and a melanoprotein nanoparticles-with-air-vids layer. Their scales can change colour from golden to red in wet state and back to golden in dry state [13]. Meanwhile, light scattering, dispersion, grating diffraction, etc. can also produce structural colour phenomenon. The blue sky is the most prominent representation of the structural colour of light scattering. When sunlight enters the atmosphere, light of shorter wavelengths such as blue, cyan, and purple is scattered by the action of fine dust in the air. The rainbow comes from the dispersion of light under the action of fine droplets.

The animals control their colour with environmental change for camouflage, signal communication, conspecific recognition and reproductive behaviour [14, 15]. Researchers are inspired to discover new materials and structures to understand the mechanisms of stimulus response processes and

structural colour formation. The artificial structural colour is produced by the interactions of natural light with microstructures, which is different from pigmentary colour produced by selective absorption of natural light. With its high brightness and saturation but no fading, iridescent phenomenon and polarization effect, structural colour is widely used in many fields such as display and imaging technology [16], printing and painting [17], textile industry [18], fluorescence manipulation [19], energy conversion [20, 21] information storage devices [22, 23], sensors [24–27], photonic devices [28] and anti-counterfeiting technology [29–32].

In particular, fabricating micro-nano structure has become one of the most competitive and promising technologies in the world today. With different microstructures, the surface of the material can be characterized by superhydrophobicity, antireflection properties, drag reduction and light trapping in the fields of photonic crystal preparation [33], surface modification, adhesion regulation [34], chemical detection [35, 36], and optical devices [37–39]. Meanwhile, preparation of large-area micro-nano structure [40, 41], regulation of structural morphology and size [42–44], and the correlation between performance and structural parameters [45–47] have become hot topics in the research of new functional materials. At present, both the "top-down" micro-nano structure processing technology and the "bottom-up" micro-nano structure synthesis assembly technology have their own technical limitations in pattern construction [48, 49], so further research of the preparation method and mechanism of nanostructure arrays are needed, especially for security [50–52]. This review will focus on recent developments in fabrication method of micro-nano structures for patterns and summarizes the pattern construction in anti-counterfeiting by inkjet printing technology, ink responsiveness method, photomask technology, electromagnetic responsiveness method, stress responsiveness method, surface wrinkles technology, plasmonic micro-nano technology, and finally make predictions of future research.

2. Fabrication Methods of Micro–Nano Structures for Patterns

There are many methods for preparing micro-nano structures for patterns (see Table 1), such as inkjet printing [53], angle-independent photonic crystal [54], self-assembled photonic crystals by magnetic field force [55], gravity [56], electric field [57], inverse opal photonic crystal [58, 59], electron beam etching [60], ion beam etching [61], laser holographic lithography [62], imprinting technology [63] and surface wrinkle technology [64], etc. In traditional micro-nano structure preparation methods, self-assembled monodisperse colloids are driven by noncovalent bond forces such as hydrogen bonding [65–67], π–π bonding [68], Van der Waals interactions [69], and metaloordination [70]. Usually monodisperse colloids are used when preparing photonic crystals by vertical deposition method, field force induced self-assembly method and inkjet direct writing technology combined with self-assembly. The inverse opal photonic crystal structure is similar to the opal structure which is obtained by introducing a high refractive index material into the voids of the opal photonic crystal and removing the template. Its preparation method includes sol-gel method [71–73], chemical vapor deposition [74], atomic layer deposition [75, 76], electrochemical deposition [77, 78], etc. As a micromachining technology, lithography has many advantages such as highly controllable and accurate graphics, simple design and process and easy industrialization. It has become the most mature and widely used in the field of micro-nano structure construction. Photolithography is a process in which a mask of a geometric pattern is applied to a photosensitive material (photoresist) on a substrate by ultraviolet light, but the lithography resolution is limited by the wavelength of the exposed ultraviolet light [79]. After that an electron beam etching technique (EBL) has emerged using an electron beam as a radiation source. The electron-sensitive adhesive coating prepared on the substrate is scanned and exposed to the focused electron beam, and then the patterned structure is obtained by using the developing solution, and the process of constructing the micro-nano structure is more flexible [60, 80]. All optical lithography and EBL can only be effectively exposed or written on the surface of soft materials (photoresists) and affected by the diffraction limit of the wave and the scattered electrons. Relatively, ion beam etching technology directly focuses the ion beam directly against the target with a higher energy density at a relatively short wavelength, and directly realizes the micro-nano array on the surface of the hard material [81]. Laser holographic lithography technique utilizes multiple beams of coherent light to converge in space, and its refractive index is periodically changed to form an ordered structure with periodic changes due to the different degree of sensitivity of the recording medium in the interference field [82, 83]. Imprinting technology is a simple and quick technique that uses a combination of physical pressure to precisely bond a rigid template to a substrate and mechanically modify the pattern on the template to the substrate. Its base material is typically thermoplastic with ultraviolet radiation (UV) [84, 85] or heat cure [86] or other methods of morphological changes [87]. The thermoplastic material can be embossed in its liquid state, and then its surface is fixed by ultraviolet light or heat. A relatively new method is the interface self-organizing technology, which utilizes the inherent Van der Waals force, polarity, steric hindrance and electrostatic force of the polymer film to produce yield deformation to relax the internal instability of the system and spontaneously form a micro-nano structure. The means including instability factors such as dewetting [88, 89], electrohydrodynamics [90, 91], phase separation [92], temperature [93], reaction-diffusion [94], strain [95–97] and swelling induced instability [98–101].

3. Micro–Nano Structure of Photonic Crystal in Patterns Construction and Anti-Counterfeiting Application

The photonic crystal anti-counterfeiting technology is a method for intelligently adjusting the optical forbidden band structure under certain physical or chemical conditions to change the ordered structure of the reflected signal and the

Table 1: Fabrication of micro–nano structures for patterns.

Styles	Materials	Method	Characteristic
Inkjet printing	Photonic crystal latexes such as silica [102], polystyrene [103], and polymethyl methacrylate (PMMA) [104], and responsive functional monomers [105–109]	Combination of colloidal emulsion and self-assembly technology	By controlling the self-assembly conditions (substrate wettability [110, 111], substrate temperature [112], colloidal particle size [113], paper surface [114]), photonic crystal structure can be prepared simply, quickly, and at low cost
Angle-independent photonic crystal	Inorganic nanoparticles Silicon dioxide (SiO_2) [115], titanium dioxide (TiO_2) [116], copper oxide (CuO) [117], organic nanoparticles (polystyrene [118], polydopamine [119])	Spraying, atomizing, spin coating, dispensing	The self-assembly of biomimetic isotropic films are achieved with a characteristic length-scale comparable to the wavelength of visible light [120]
Self-assembled photonic crystals by magnetic field force	Magnetic particles and nanospheres (silica [121], polystyrene [122], carbon [123], polyvinylpyrrolidone [124], polyacrylamide [125])	Monodisperse microspheres self-assemble into ordered structures under the action of a magnetic field	The self-assembly process is reversible, and the band gap position can also be adjusted by controlling the strength of the magnetic field
Self-assembled photonic crystals by gravity	Monodisperse microspheres with higher density such as silica [126]	Colloidal particles are free to settle and self-assemble into an ordered structure in constant temperature, humidity and vapor pressure environment [127]	The photonic crystal obtained by the gravity is difficult to control and is prone to defects
Self-assembled photonic crystal by electric field	Charged monodisperse microspheres [128, 129]	Monodisperse microspheres are deposited on the electrode by an electric field to form an ordered structure	Colloidal sedimentation rate can be controlled by applying a positive and negative electric field
Inverse opal photonic crystal	Template agent such as silica, polystyrene or polymethyl methacrylate microspheres, precursors such as metal salts, metal alkoxides, metal oxides, inorganic salt solutions and organic substances	Filling by melt method, chemical precipitation method, monomer polymerization, etc. Removing the template by melting, heating, etc. [130]	High refractive index precursor is filled into the voids of the crystal, and the corresponding infrastructure is obtained by removing the opal template [131]
Electron beam etching	PMMA (positive rubber) and SU-8 (negative rubber) materials [132]	Polymer in the region exposed to the electron beam will undergo a soluble change, and the micro-nano structure can be obtained by the developer	There is no need to contact the surface of the material, the deformation is small under stress, and the pollution is less, and the surface of the material is not oxidized
Ion beam etching	Metals and compounds, inorganic and organic, insulators and semiconductors [67, 133]	The electrostatic beam is used to focus the ion beam emitted by the liquid metal ion source into a very small size ion beam stream, and the physical collision is used to cut and grind the base material to obtain a micro-nano structure	This method is not limited by etching materials, with good directionality and high resolution
Laser holographic lithography	SU-8, photoinitiator, photosensitive resin solution [83]	Single photon or two-photon polymerization with laser-assisted technology	The lattice symmetry, lattice period, band gap position, medium duty ratio, etc. control the structure
Imprinting technology	Photoresist resin combined with quartz (hard template), Polydimethylsiloxane (PDMS) and other imprint templates	Transfer the template pattern to the substrate by heat [86] or ultraviolet irradiation [84, 85]	The resolution is not affected by the most exposed wavelength, and is closely related to the original template resolution. It has high fidelity, high resolution, low cost and high yield
Surface wrinkle technology	PDMS [134], polystyrene [135] and shape memory materials [136–139] are used as base materials, organic polymer materials [140], metal materials [141], and inorganic materials [142] can be used as surface hard layer materials	Surface instability factors are induced by heat, force, electromagnetic field, humidity, phase separation, osmotic pressure, capillary force and polymerization shrinkage stress	The inherent Van der Waals force, polarity, steric hindrance and electrostatic force of the polymer film produce yield deformation to relax the internal instability of the system [143]

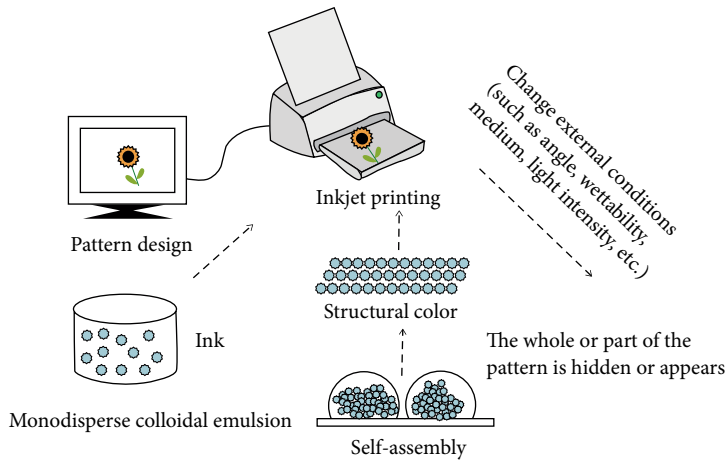

Figure 1: The inkjet printing of photonic crystals.

structural colour. The responsive photonic crystal could be combined with various substrates to prepare anti-counterfeiting materials. Conventional luminescent material has a fixed structural colour, while patterns of photonic crystals is invisible under normal conditions, and the invisible pattern can appear under certain physical or chemical effects, and the pattern can be hidden when the action is removed. Here, we introduce some pattern construction of photonic crystal by different means such as inkjet printing, ink responsiveness, photomask, electromagnetic responsiveness, stress responsiveness, and systematically summarize the application of photonic crystal patterning in the field of anti-counterfeiting.

3.1. Inkjet Printing Technology. Inkjet printing technology is a non-contact technology that developed in the 1970s. The required pattern or graphic is input into a computer through a scanner or a digital camera, then it was directly drawn by a computer, and the characteristic digital signal obtained after pattern or graphic conversion is transmitted to a printer as electronic signal, and a nozzle can control the ejection of ink droplets to create a corresponding image on a print carrier. Laser direct writing required a special high-cost device, and the traditional method of self-assembly photonic crystal is complicated, time-consuming and expensive. Direct preparation of patterned photonic crystals can be achieved by inkjet printing, which is simple and easy to operate by effectively controlling the wettability of the printing substrate and the composition of the monodisperse latex emulsion ink, efficient spread of the monodisperse latex droplets on the surface of the substrate and highly ordered three-dimensional assembly of the monodisperse latex particles ultimately. The whole or part of the pattern is hidden or displayed by changing external conditions such as angle, wettability, medium, light intensity, etc. (see Figure 1).

Park et al. [144, 145] fabricated a photonic crystal structure composed of hemispherical colloidal assemblies by inkjet printing, and they used monolayer (SAM) of octadecyltrichlorosilane (OTS) modifying the silicon wafer to get a hydrophobic surface. Based on the nucleation and growth kinetics and the magnitude of the capillary stress, they proposed interrelationship of the crystal quality of the photonic crystal, the colloidal particle size, and the pore size which in turn influenced the evaporation-induced solvent flow through the pore and the magnitude of the capillary stress. They also used microreflectance spectroscopy and studied reflectance spectrum from an individual colloidal droplet. The wet conditions of the colloidal suspension have an important influence on the size, shape and self-assembled structure of the colloidal aggregates, which is determined from the intrinsic properties of the substrate, ink composition, and evaporation conditions. It is possible to control the printing of photonic crystals and patterns on different substrates by controlling the wettability of the substrate [146], the evaporation of the solvent [147–149], and the size of the photonic crystal [150], space and delay time of neighboring droplets [151–153], composition of inks [154].

Wang et al. [155] studied response of photonic crystal microdots incorporating poly (N-isopropyl acrylamide) (PNIPAm) by inkjet printing, they designed a fastest response of 1.2 s to water vapor attributed to the hydrophobic transition of PNIPAm above its lower critical solution temperature (LCST) (see Figure 2(a_1)), and patterned a macroscopic image of a Chinese dragon with reversible response by changing wetting states/adhesion properties of adsorbed water on the polymer segments (see Figure 2(a_2)). When wet vapor approached the responsive dragon image, it resulted in a red shift from 480 to 580 nm within 6.2 s (see Figure 2(a_3)), and with distinct colour alteration from transparent to bright green, and the corresponding recovery process was reversible when the water vapor was removed. Bai et al. [156] built a method of controlling the original colour and vapor-responsive colour shift by mesoporous colloidal nanoparticle ink. By designing inks of droplets of MSNs (mesoporous silica nanoparticles) or solid silica nanoparticles (SSNs), photonic crystal patterns with multicolour shifting properties were printed on both rigid and soft substrates, and by adjusting the size, type and mesopore proportion of nanoparticles, the wavelength of the responsive pattern was well controlled by flection peak position movements. Patterns printed on PDMS substrate usually causes a problem of angle dependence of photonic crystals. It could be

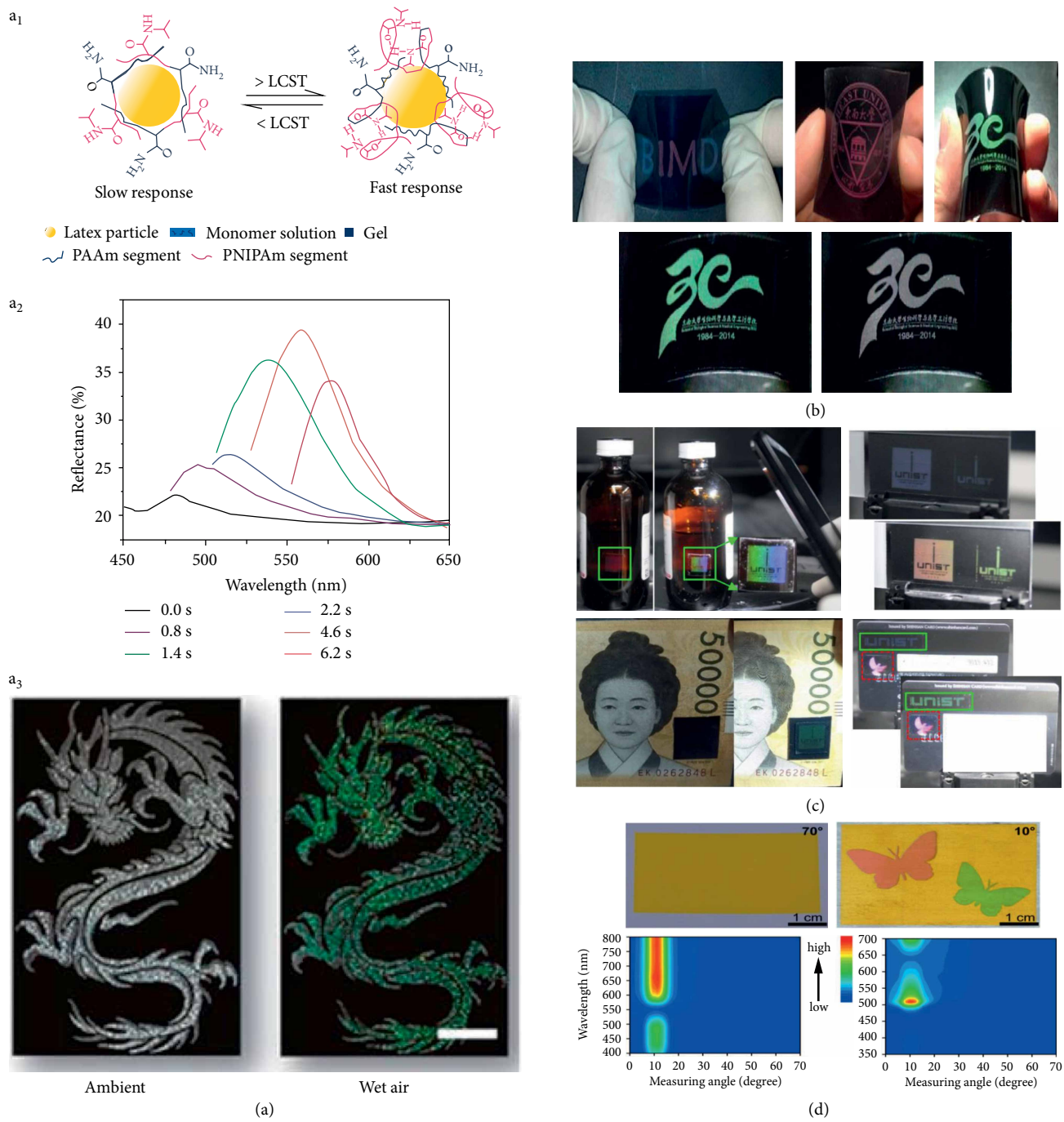

FIGURE 2: (a_1) Hydrophobic transition of the molecular conformation of PAAm-co-PNIPAm incorporated in the PC microdot above its LCST. (a_2) Changes in reflectance spectra of the PC image with time. (a_3) Colour photographs of dragon images taken at low (left) and high (right) concentration of wet air. Adapted from [155]. (b) Patterns printed on a modified PDMS film with different contact angle and vapor. Adapted from [156]. (c) Covert-overt transformation of SAPC patterns on a chemical bottle, a bare glass, a paper bill, and a credit card for anti-counterfeiting applications. Adapted from [146]. (d) Patterns were shown at viewing angle of 70° and 10° with colour-filled contour map of red and green regions. Adapted from [157].

solved by controlling the wettability of the substrate, and patterns presented angle-independent structural colour due to the high height/diameter rate of mesoporous colloidal photonic crystal (MCPC) domes. Even if the view angle was changed, the incident light reflected passed through their centers back, and the wavelengths were similar (see Figure 2(b)). This bio-inspired vapor-responsive colloidal photonic crystal pattern method was of great potential for anti-counterfeiting applications. Nam et al. [146] patterned photonic crystals (silica particles) with 500 nm diameter on various substrates with different wettabilities (glass slides, silicon wafers, polypropylene, and polydimethylsiloxane) by

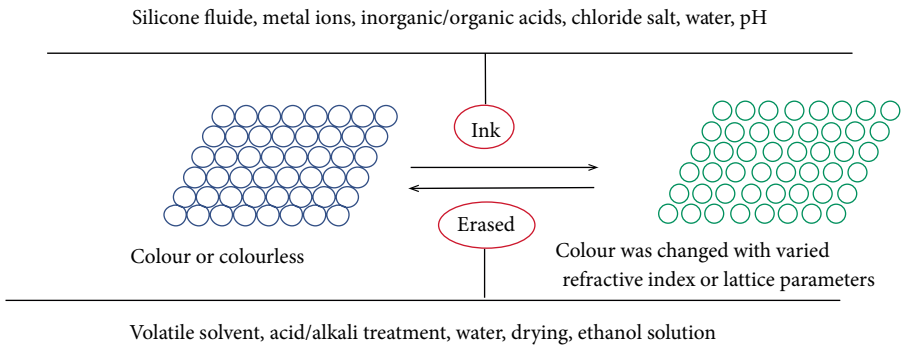

Figure 3: Photonic paper patterned by ink responsiveness.

inkjet printing. They applied the mono-layered, self-assembled photonic crystal (SAPC) patterns technology to several items. They built anti-fake label patterns on a PDMS slab with a contact angle of 10° and a thickness of 200 nm, and moved it to a chemical bottle, a bare glass, a paper bill, and a credit card respectively (see Figure 2(c)). These anti-fake label patterns could be hidden or rendered in colour by controlling the light density and background colour. This technique solved the difficulty of anti-counterfeiting application caused by the instability of photonic crystals in the construction process by constructing mono-layered, self-assembled crystal on PDMS slab. Wu et al. [157] proposed a brilliant structure colour pattern by using monodisperse cadmium sulfide (CdS) spheres with different diameters on photonic papers with contact angle >50° via a common inkjet printer. Their technique took advantage of the angle dependence of photonic crystals, used the observation angle as a switch. When the angle of observation was changed, the colour of the pattern could be selectively hidden and rendered. They designed patterns of a red butterfly and a green butterfly in a yellow background with three different diameters of CdS spheres (270 nm, 290 nm and 335 nm). Due to the angle dependence of photonic crystals, at a particular angle, the butterfly patterns were hidden, and only the yellow background could be seen. When the viewing angle matched the incident angle, the green (270 nm CdS spheres) and red butterflies (335 nm CdS spheres) appeared in the yellow background (290 nm CdS spheres). To explain the mechanism, they studied the evolution of reflection spectra of two butterflies at different viewing angles, they found that when incidence angle was fixed at 10° and viewing angle was close to specular angle at 8–10°, the patterned colour was highest (see Figure 2(d)).

3.2. Ink Responsiveness. In early times, photonic crystal paper is coated with common solvents, salts or reactive monomers to change refractive index or lattice parameters to obtain different patterns, so the durability, inks and the removing and precision of the ink are the most important parameters, A number of scientific research achievements have been accumulated. Colour or colourless photonic paper can be processed by ink of silicone fluid, metal ions, inorganic/organic acids, chloride salt, water, pH, its patterns usually are erased by volatile solvent, acid/alkali treatment, water, drying, ethanol solution (see Figure 3).

Fudouzi and Xia [158] used the swelling capacity of liquid to vary the stop bands of photonic paper which was colloidal crystal of polymer beads embedded in an elastomer matrix made of PDMS. When the lattice constant and the wavelength of Bragg-diffracted light were varied (see Figure 4(a)), the pattern of the polystyrene beads could be varied from violet to other colours. They patterned some letters with silicone fluid DMS-T05 as ink, 202 nm polystyrene in a PDMS matrix, but the pattern removal process (by immersing the paper in a volatile solvent) was inconvenient. Liu et al. [159] prepared novel poly (4-vinylpyridine) based inverse opals (PVPIO) photonic crystal, a collapse of the protonation/deprotonation processes controlled by metal ions, organic acids or inorganic acid followed by dehydration, the contacted region coated with inks could transfer from a collapsed disordered to an ordered inverse opal structure. The pattern method by controlling the structure of inverse opal from disordered to ordered was actually to use Bragg diffraction. This strategy was developed by Ge et al. [160] They fabricated photonic paper by magnetically tunable assembly techniques using Fe_3O_4@SiO_2 colloids mixed inside a poly (ethylene glycol) diacrylate (PEGDA) matrix. They used a water-ethanol solution of a chloride salt as ink (see Figure 4(b)), the letters could be patterned due to the increased interparticle space during swelling accompanied by red-shifting. The pattern could be erased by distilled water to wash the salt. The template method was also used to fabricate polymer photonic crystal paper by filling the polymer into the photonic crystal and then etching the photonic crystal. Gu et al. [161] constructed poly(ethylene glycol) diacrylate (PEGDA) photonic crystal paper, they prepared different colour papers, and patterned letters by writing saturated ethanol solution of LiCl, these papers were of vivid colours, wide viewing angle, rewritability, and flexibility. Du et al. [162] fabricated photonic crystal paper by filling chitosan into the colloidal crystals, the structural colour could be adjusted by the particle size of photonic coatings, or written with aqueous solutions of certain pH. At first, photonic crystal paper was colourless and transparent (see Figure 4(c)). When they patterned letters with water on papers, the letters were purple, green and red, respectively. Chen et al. [163] prepared clickable colloidal photonic crystal of monodispersed silica particles modified with vinyl group by rapid and controllable post-patterning approach. β-mercaptoethanol, pentanethiol, octanethiol, N-dodecyl mercaptan, 1H, 1H, 2H,

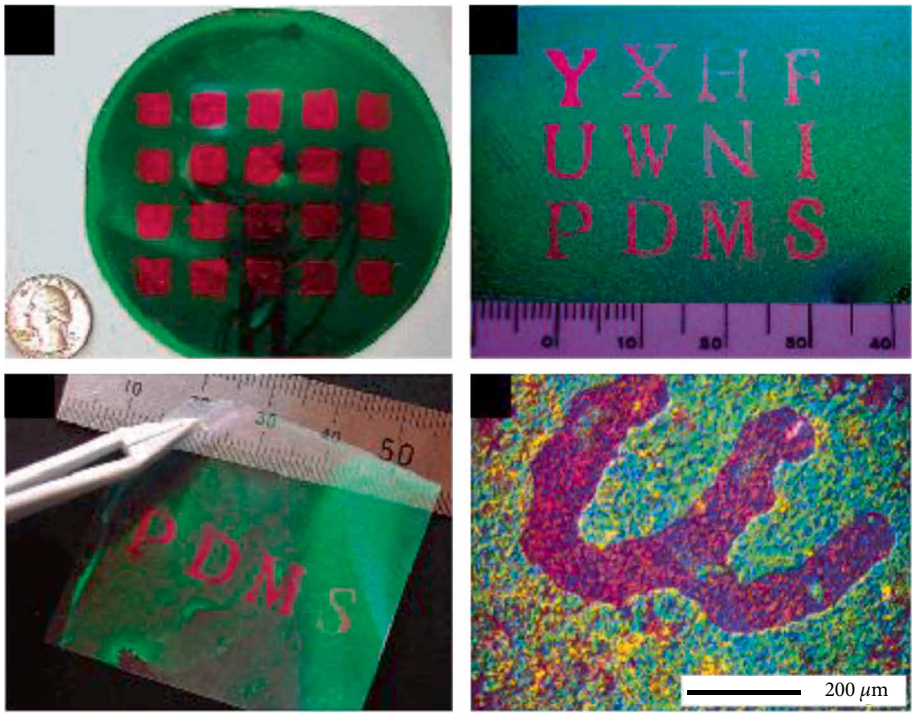

(a)

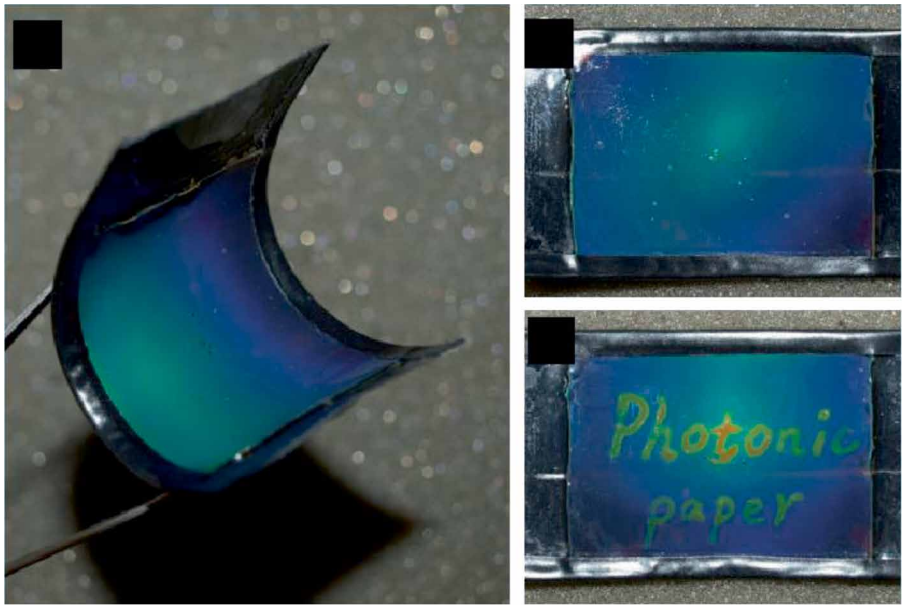

(b)

Figure 4: Continued.

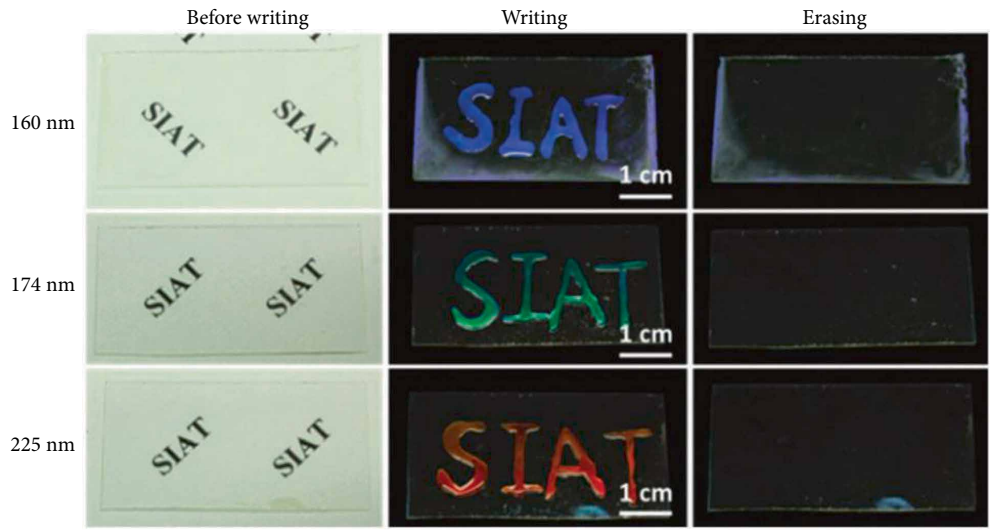

(c)

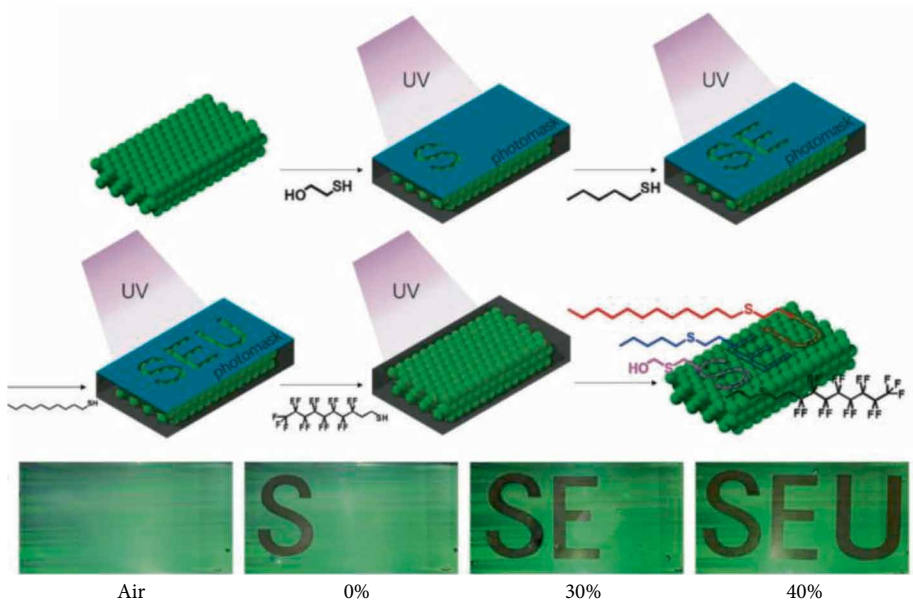

(d)

Figure 4: (a) Photonic papers were assembled from 202 nm PS beads in a PDMS matrix. Adapted from [158]. (b) Photonic papers had a uniform blue colour when observed with the naked eye and patterns were shown by the flash lamp illuminating as a point light source. Adapted from [160]. (c) Digital photo images of photonic coatings with various sizes from ca. 160 nm to ca. 225 nm on glass slides before writing (left), after writing with water (middle), and erasing by water evaporation (right). Adapted from [162]. (d) Photonic crystal film with differently patterned photomask and patterned in different concentration of ethanol aqueous solution. Adapted from [163].

2H-perfluorodecanethiol as reactive monomer were introduced to modify the vinyl modified photonic crystals. Chemical encoded photonic crystal patterns were achieved by the different ethanol concentration for full infiltration of different chemical group. The pattern letters were modified with β-mercaptoethanol ("S"), pentanethiol ("E"), N-dodecyl mercaptan ("U") by different templates (see Figure 4(d)), the rest playground region was modified by 1H, 1H, 2H, 2H-perfluorodecanethiol. The letters were gradually revealed by controlling the concentration of ethanol solution.

3.3. Photomask Technology. Photomasks are usually required when preparing patterns by means of crosslinking and modification, and the preparation process is usually divided into two steps. Firstly, the mask is used to control the degree of reaction of the ultraviolet curing system, then the Bragg diffraction is changed by flushing unreacted monomers, crosslinking treatment, hydrophobic treatment, etc. and the process is simple and controllable.

Wang et al. [164] patterned organic/inorganic one-dimensional photonic crystals (1DPCs) hybrid by photolithography of thin films of poly methyl methacrylate-co-hydroxyethyl methacrylate-co-ethylene glycol dimethacrylate (PMMA-co-PHEMA-co-PEGDMA) and titania nanoparticle sol. The 1DPCs was of uniform colour, thickness and minimal adventitious striations, cracks, and comets (see Figure 5(a)).

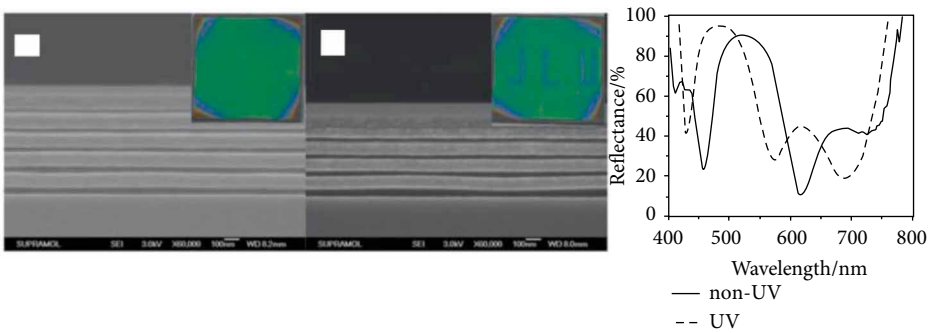

(a)

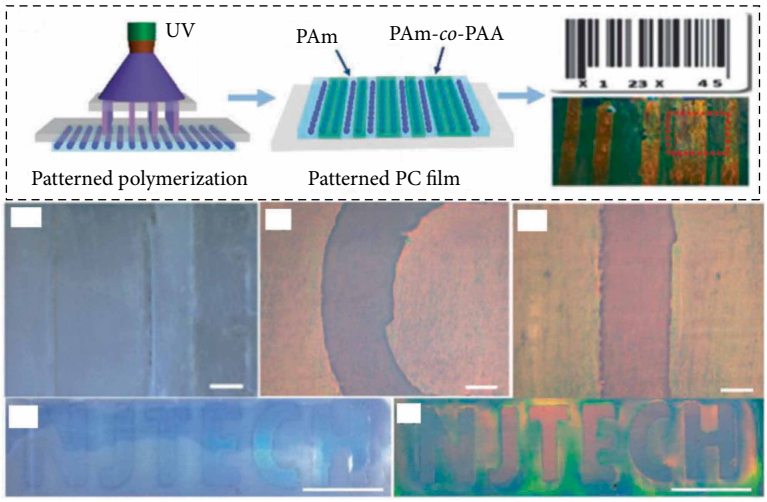

(b)

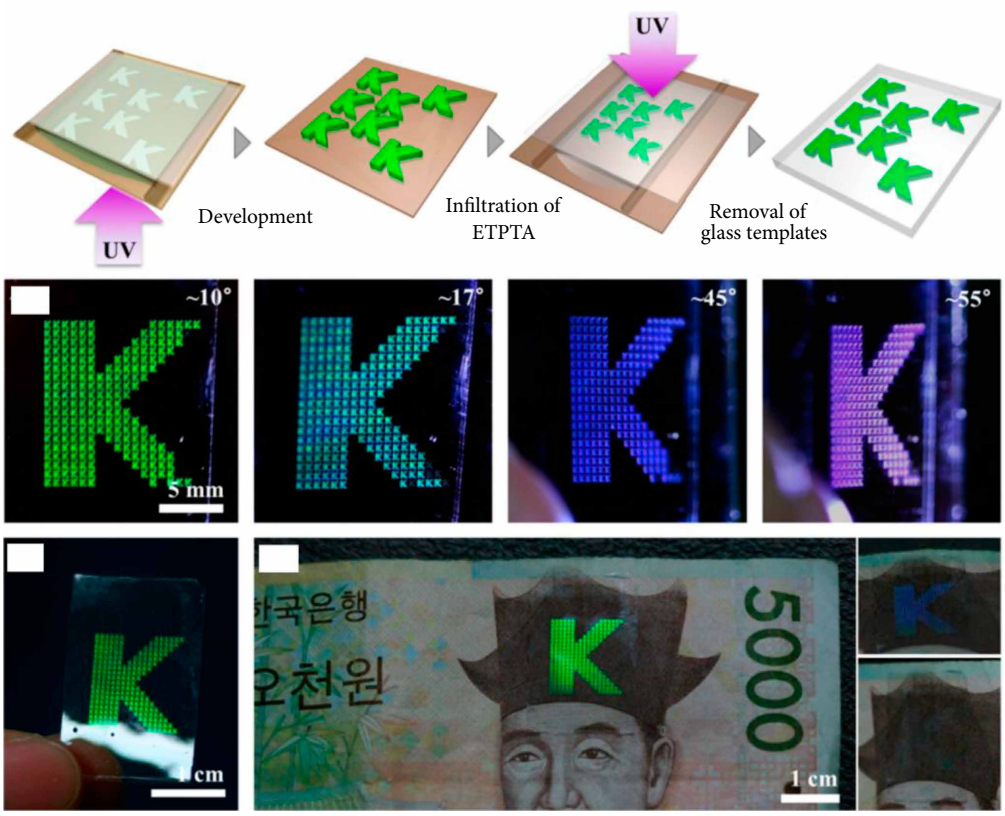

(c)

Figure 5: Continued.

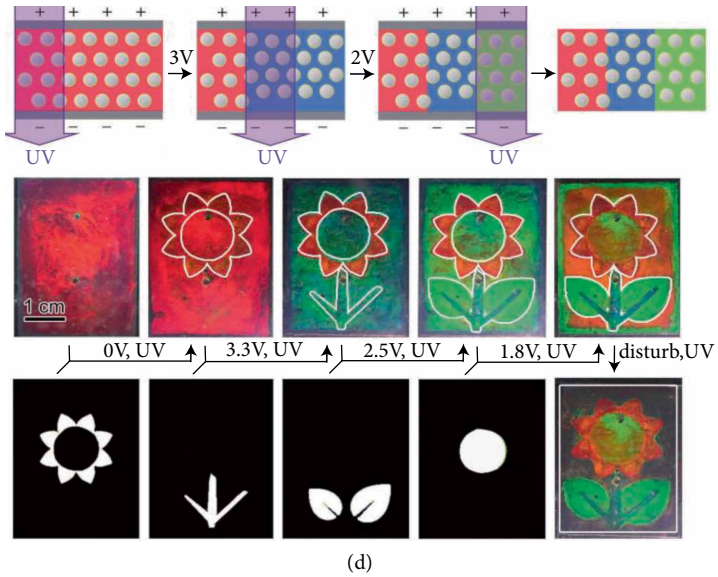

Figure 5: (a) Cross-linking SEM images, photographs, and their corresponding reflective spectra. Adapted from [164]. (b) Optical image of the RPC-based barcode film at the dried state and after smeared with deionized water. Adapted from [166]. (c) Photolithography with an amorphous silicon photomask on a glass wafer enabled the patterning of small K's with different colours by angle and its application on a Korean bank note. Adapted from [165]. (d) Lithographical printing of multicolour flower by periodically photomask covering, electric field tuning, and UV curing. Adapted from [129].

A pattern "JLU" was prepared by controlling the lighting time. Increased irradiation time decreased the thickness of the top layer, the structure became more disordered with blue shift. The patterns could be reversible by organic solvents. Lee et al. [165] structured composite photonic films with photocurable resin of ethoxylated trimethylolpropane triacrylate and silica particles. Small "K" was patterned to film by photolithography of a photomask (see Figure 5(c)). When the film was placed on a Korean bank note, the film was difficult to discern for high transparency. It could be used for anti-counterfeiting or optical identification codes taking advantage of angle-independent structural colour. Zhang et al. [166] demonstrated an easy-to-perform and efficient method to structure two dimensional responsive photonic crystals (2-D RPC), this technology combined the colloid crystallization and solid-liquid-assisted assembly processes. The close-packed colloid crystals were formed by negatively-charged polystyrene suspensions grafted the sulfopropyl methacrylate potassium salt that were transferred into the same charged hydrophilic substrate. The anti-forgery label was constructed by sulfonated polystyrene powders, acrylamide (Am), N,N-methylenebisacrylamide (MBA) and diethoxyacetophenone (DEAP), after curing by UV radiation for 5 min, then a mask was used to pattern the film for 24 h curing (further immersed into an aqueous solution containing Am, MBA, AA and DEAP), this nonsynchronous swelling technology could control the emergence of coding message by water (see Figure 5(b)). Chen et al. [129] combined multicolour control under electric field with photomask and UV curing to achieve multicolour pattern printing (see Figure 5(d)). When the pre-assembled photonic crystals were subjected to slight pressure or interference from the outside, they would be unassembled immediately, the reflection intensity would be reduced to 0, and the metastable colloidal crystals remaining stationary would be reassembled and restored to the structural colour. The strong ultraviolet light selectively cured the photonic crystal structure. SiO_2/ETPTA (trimethylolpropane ethoxylate triacrylate) liquid photonic crystal was used as E-ink for printing petals, roots, leaves and stamens at different volts by periodical photomask covering, electric field tuning, and UV curing.

3.4. Electromagnetic Responsiveness. Colloidal particles dispersed in solution are usually disordered due to Brownian motion. However, when an electric field is applied to the colloidal solution, the charged colloidal particles will rapidly move toward the electrode opposite to its surface charge due to electrostatic attraction, and this attraction is sufficient to gather and assemble the colloidal particles to form a stable colloid. Similarly, as the external magnetic field increases or decreases, the lattice structure of the photonic crystal changes as the external magnetic field changes. Therefore, the use of electromagnetic fields to regulate photonic crystals to achieve patterning and anti-counterfeiting has become a very effective way.

Ge et al. [167] constructed magnetically responsive photonic structures that could operate in nonaqueous solutions, the fundamental details of interparticle forces was very different from assembling highly charged superparamagnetic Fe_3O_4 colloidal nanocrystal clusters (CNCs) in aqueous solutions. Tunable photonic structures have been formed in alkanol solutions by assembling silica-coated surface modification Fe_3O_4-CNC colloids using magnetic fields. To further illustrate the applications of magnetic response, patterns were structured by background film and the letters using ethylene glycol (EG) /PDMS mixtures that included Fe_3O_4@SiO_2 with different core

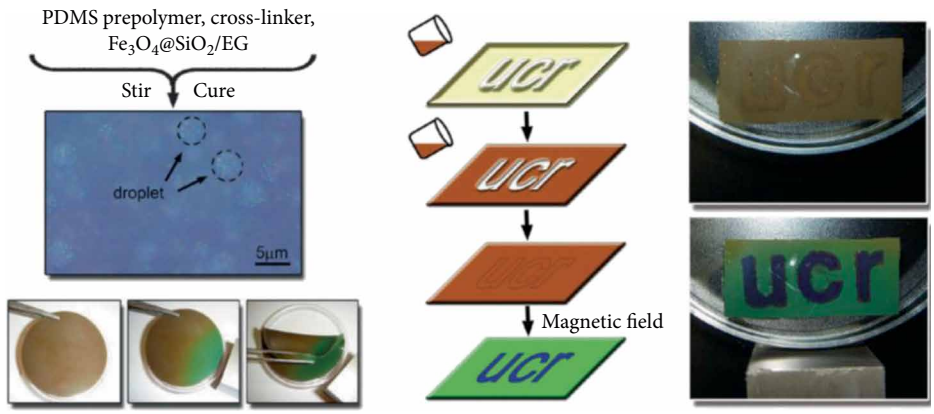

(a)

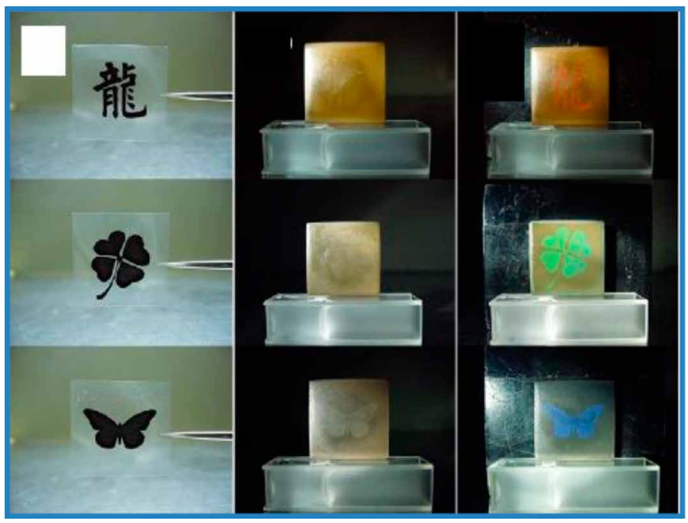

(b)

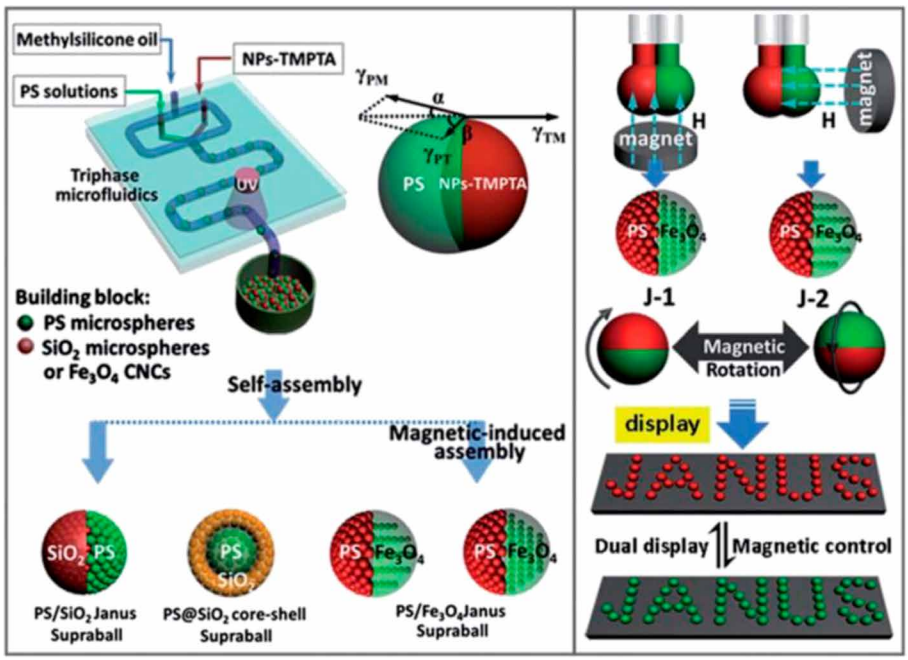

(c)

Figure 6: Continued.

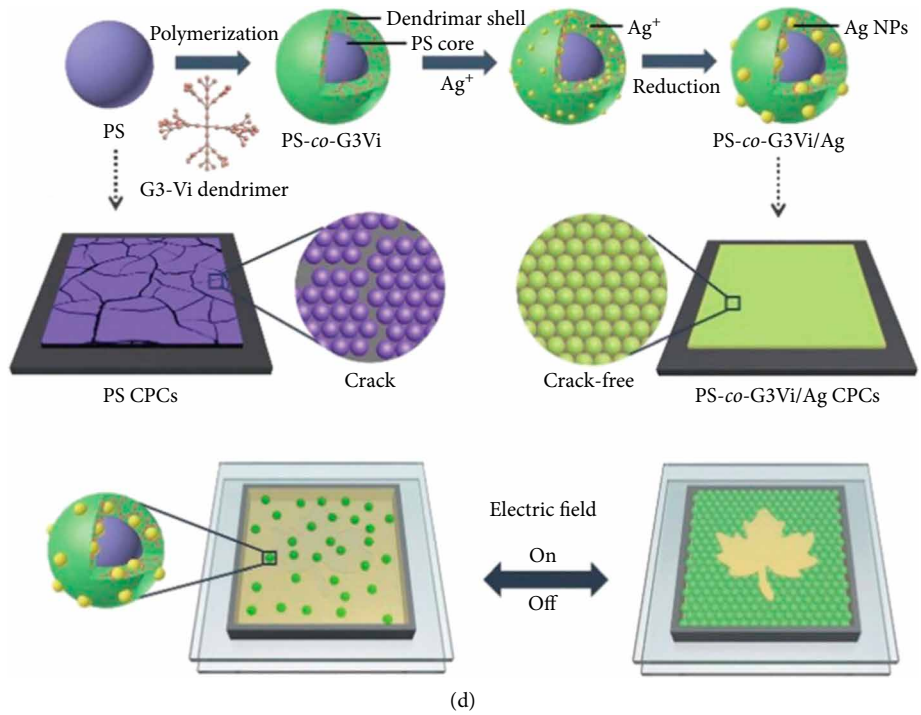

Figure 6: (a) Fabrication of a field-responsive PDMS composite embedded with droplets of EG solution of Fe_3O_4@SiO_2 colloids and patterned letters on a flexible PDMS film magnetically induced colour change. Adapted from [167]. (b) Photographs of slides with printed-graphics designed on a computer and latent graphics on P-papers revealed by a magnetic field. Adapted from [169]. (c) Schematic representation of the triphase microfluidic device, the balance of the three interfacial tensions, and the formation of Janus and core –shell CPC supraballs, and their applications as switches and displays. Adapted from [175]. (d) PS-co-G3Vi/Ag microspheres fabricated crack-free CPC and switch of photonic display devices under an electronic field. Adapted from [176].

diameters/shell thicknesses (see Figure 6(a)). The letters with small roughness at the edges could be seen clearly with striking blue letters on green background when a magnetic field was applied. Similarly, they also studied superparamagnetic Fe_3O_4 colloidal nanocrystal clusters (CNCs), ethanol and the photocurable resin as a three-phase material system [168]. Hu et al. [169] dispersed the carbon-coated superparamagnetic particles in a solution of ethylene glycol and polydimethylsiloxane precursors, and polymerized them to obtain photonic crystal paper. After polymerization, the ethylene glycol solution enveloped the magnetic particles to form a droplet in the PDMS matrix. In order to achieve the printing of the invisible pattern, they partially polymerized the photonic crystal paper under a photomask to form an invisible pattern. In the initial state, the background and the pattern were both brown (see Figure 6(b)). When a magnetic field was added, the unpolymerized pattern produced a colloidal crystal assembly under a magnetic field, and showed a structural colour. Under the same magnetic field, magnetic particles with three different diameters exhibited different structural colours after assembly. They also synthesised monodisperse carbon-capped superparamagnetic colloidal nanoparticles [170], anti-counterfeiting labels were prepared by background (filled with EG/PDMS precursor containing carbon black) and plastic templates (filled with the glycol solution containing carbon-capped SCNps). The carbon-capped SCNps in the glycol droplets could exhibit colours by a vertical magnetic field. Continually, this photonic anti-counterfeiting watermark technique provide double security information to identify the authenticity of banknotes [171]. Wang et al. [172] manipulated responsive free-writing based on magnetic response, and chalcogenides were designed by Cd^{2+} loaded polystyrene (PS), N-isopropylacrylamide (NIPAm) and Fe_3O_4 nanoparticles. The construction technology of Janus suprabeads (JSs) was achieved by synthesis of monodisperse functionalized PS-PMMA microspheres, CdS QD-loaded fluorescent microspheres. The suprabeads was structured by microfluidic device filled with discontinuous phases (QDs-loaded CPC latexes) and continuous phases (methylsilicone oil). Images of "JANUS" were prepared for responsive display. The display colour was reversible by temperature response and magnetic response, and chalcogenide could pattern images with both the electronic confinement and photon confinement response. Xuan and Ge [173] accomplished a novel photonic printing process by repeating the magnetic alignment, orientational tuning, and lithographical photopolymerization. To print labels composed of multiple orientations, the patterns printed by multiple photonic orientations (magnetic inks were first placed above a cubic magnet with a field angle of 90°, and the logo was patterned with UV polymerization under a photomask. Backgrounds were printed onto a cylindrical magnet with changeable colour as controlling the angle of incident light from angle 1–4°. This printing technique was also capable of fabricating colourful or invisible binary codes and recognized with transmission

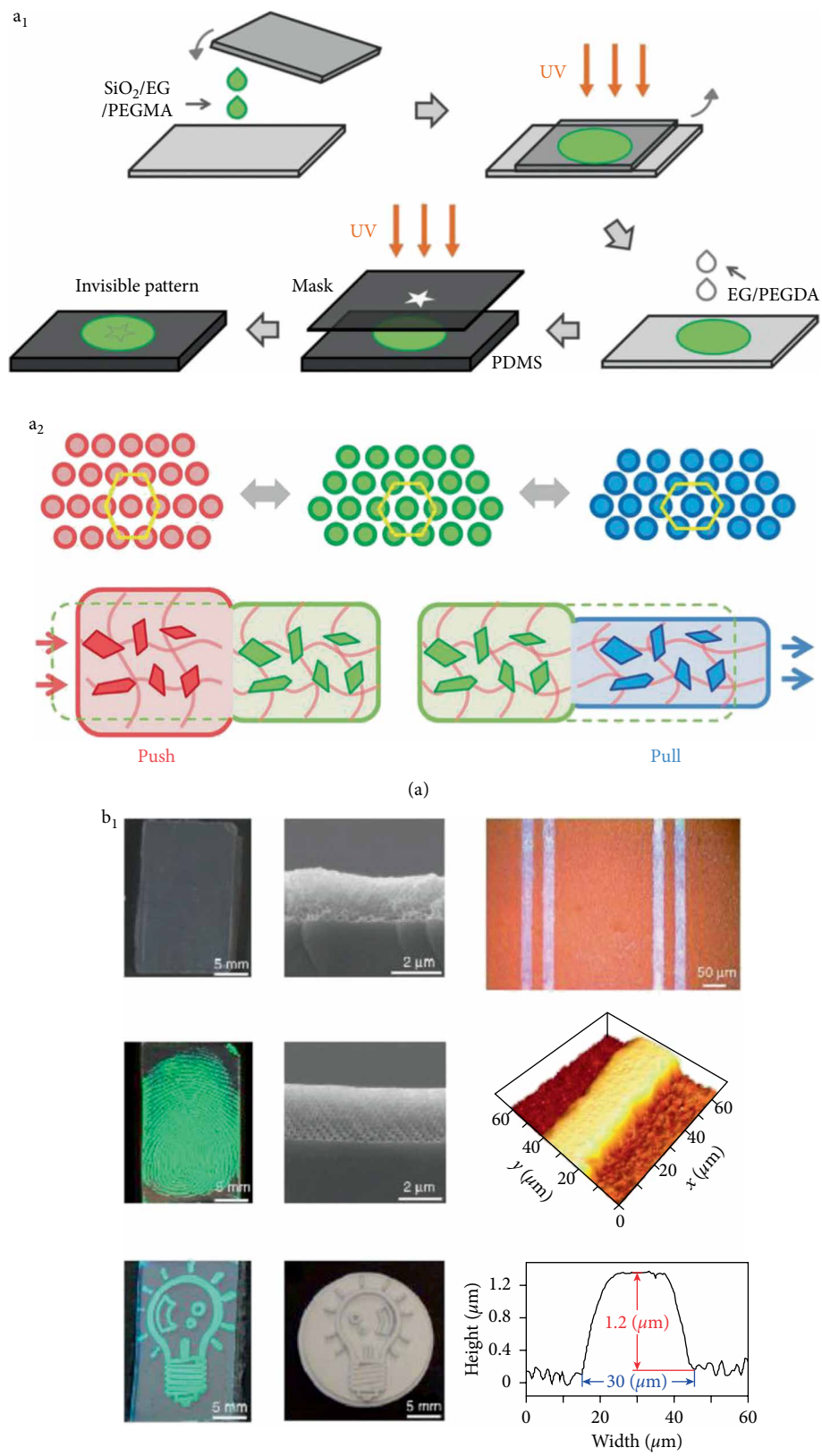

Figure 7: Continued.

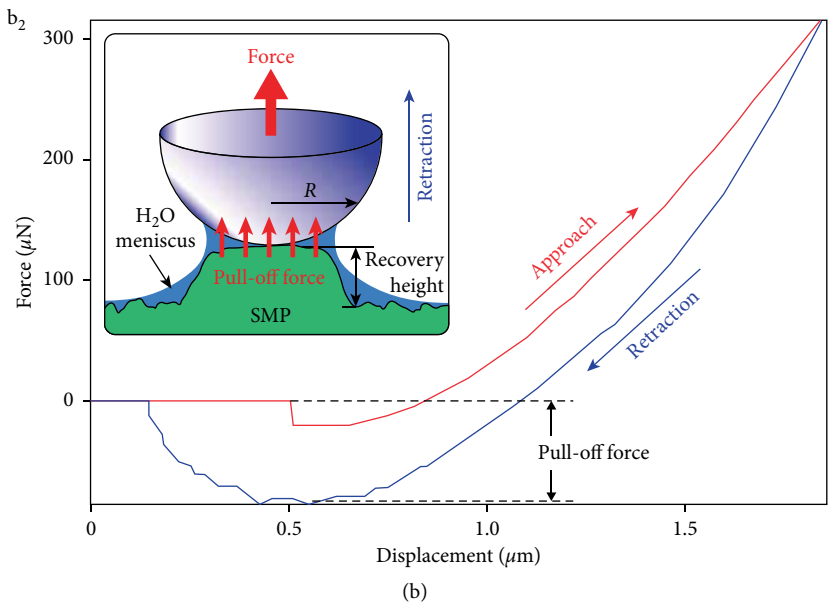

FIGURE 7: (a_1) Printing process of invisible photonic patterns shown by deformation, adapted from [177] and (a_2) its mechanism. Adapted from [178]. (b_1) Arbitrary photonic crystal patterns printed on the new SMP membranes and (b_2) macropore recovery induced by pull-off forces. Adapted from [183].

signals. Zhao et al. [174] constructed Janus particles with controllable and predictable shape by microfluidic directed self-assembly method. Subsequently, Liu et al. tried approaches to assemble two kinds of colloidal photonic crystals into different hemispheres of a single Janus supraball (PS/SiO_2 and PS/Fe_3O_4 CPC JSs and PS@SiO_2 core–shell CPC supraballs) (see Figure 6(c)) [175]. Supraballs were prepared in a triphase microfluidic device that was made up of a polydimethylsiloxane capillary and a pair of paralleled inner needles (one was injected with mono-dispersed PS colloidal microspheres and the other injected with photopolymerizable monomer along with monodispersed SiO_2 microspheres), and uniform biphasic droplets were formed by the outer PDMS capillary broking the inner solutions at the tip of the pair of needles. Patterns of PS/Fe_3O_4 JSs (J-1 and J-2) were fabricated using the magnetic field that could easily switch and rotate as well as exhibit different dual optical properties. Chen et al. [176] prepared large-area crack-free multifunctional photonic crystal film by grafting PS with carbosilane-thioether generation 3 vinyl-terminated (G3-Vi) dendrimers (see Figure 6(d)). Later-generation carbosilane-thioether of PS-co-G3Vi microspheres could enable the ingress of Ag ions into the interiors, and form Ag nanoparticles to improve the interaction among the microspheres, the crack-free CPC films technology was used to pattern photonic display devices as a switch with good stability and reproducibility under an electronic field.

3.5. Stress Responsiveness. The photonic crystal combines some elastomer materials to change the interface distances of the microspheres in the colloidal layer by stretching or compressing. Some scholars have reported that the movement of polymer molecular chains can be controlled by force to realize the change of photonic crystal anti-protein structure cycle from disordered to ordered.

Ye et al. [177] prepared photonic crystal by fixing metastable SiO_2 colloidal crystalline array in the matrix of EG and poly (ethylene glycol) methacrylate (PEGMA) through photo-polymerization (see Figure 7(a_1)). Patterns were achieved by soaking the film with poly(ethylene glycol) diacrylate by a mask, and they were hard to be distinguished in relaxed condition as the unshielded region caused slight change, it could be instant by non-uniform deformation caused by the different elasticity between the cross-linked and uncrosslinked sections. Simultaneously, this strategy was extended to pattern on PDMS rubbers with deformation (see Figure 7(a_2)) [178]. Sun et al. [179] prepared mechanochromic photonic-crystal fibers by electrophoretically depositing polymer microspheres. Firstly, elastic fiber was prepared by curing the PDMS precursor in a mold, then the arrays were wrapped onto the PDMS through a rotation translation strategy fibers with a high conductivity. Afterwards the PS microspheres were deposited onto the elastic fiber by a fast electrophoretic deposition process. Several colourful patterns that were fade-resistant, durable, sensitive and responsive to mechanical strain were prepared with different elastic photonic-crystal fibers. The patterns exhibited brilliant colour changes and maintained very high sensitivity, reversibility, and stability for thousands of cycles of stretching in the vertical, horizontal and bilateral direction. Schäfer et al. [180] reported a preparation of adjustable thermoresponsive spherical core–shell architectures with poly (diethylene glycol methylether methacrylate-co-ethyl acrylate) (PDEGMEMA-co-PEA) shells and hard polystyrene cores. This polymer opal films behaved as photonic rubbers that could be tuned by stretching with quick recover. At first, there was little variation of the reflection spectra between irradiated and non-irradiated regions, while under the same stress, the irradiated and non-irradiated regions produced different strains so that strong contrast

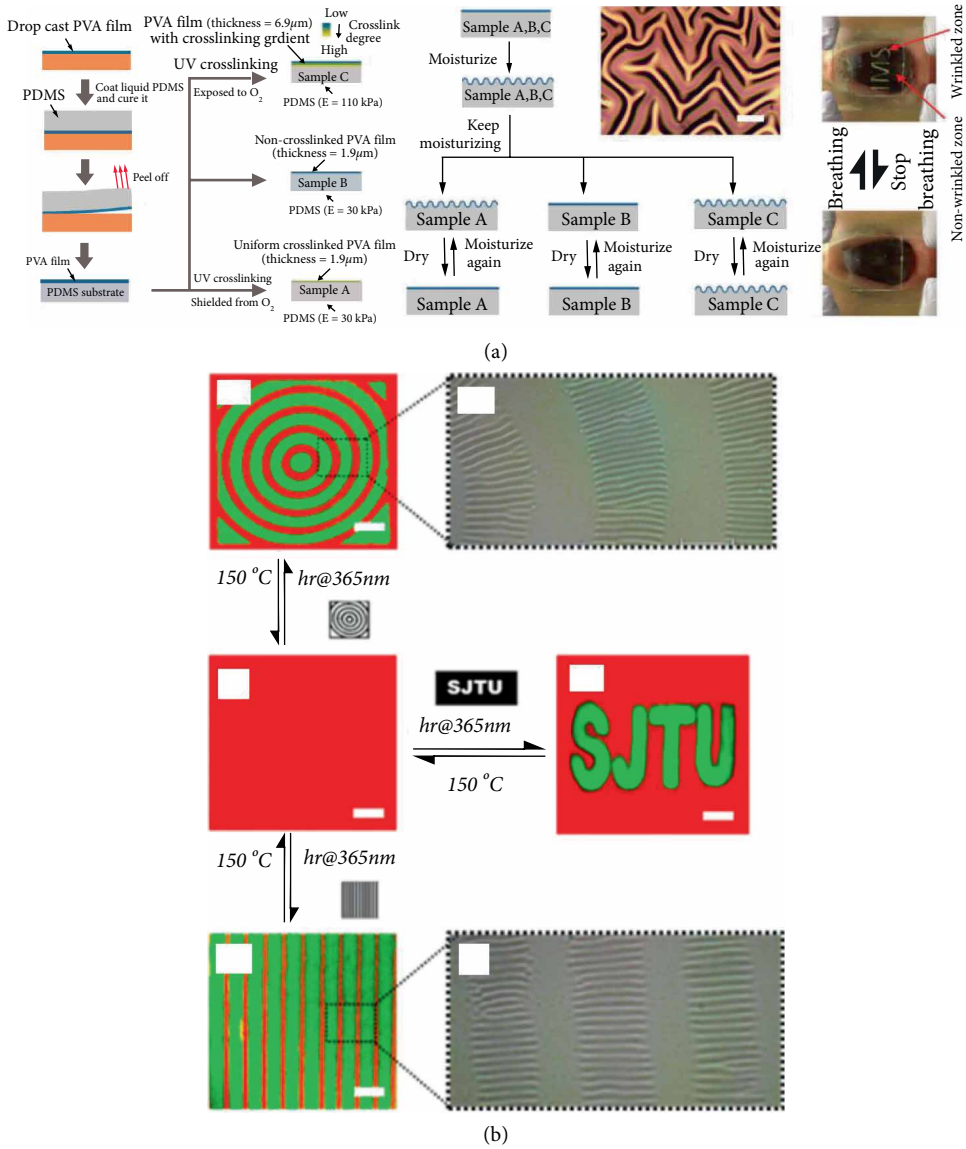

Figure 8: Continued.

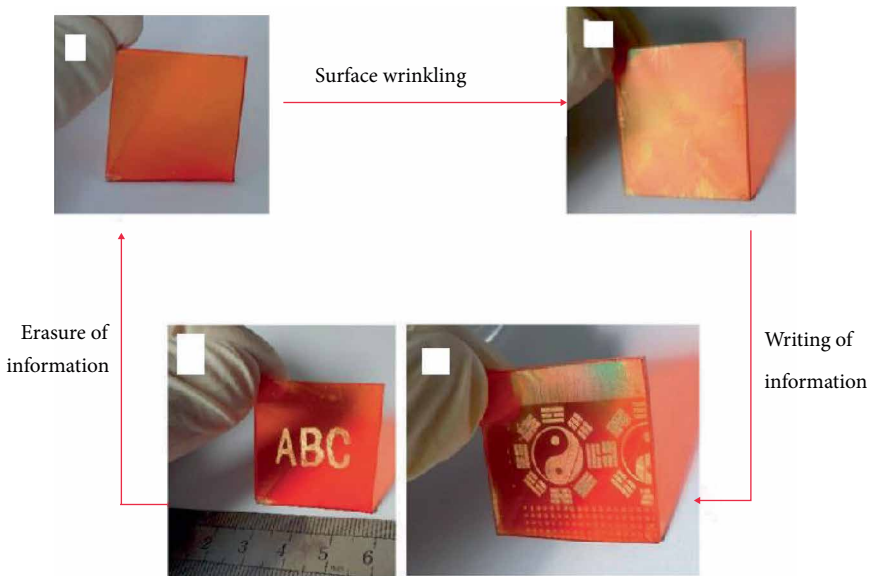

(c)

Figure 8: (a) Preparation approaches for the three moisture-responsive wrinkling devices with different responsive dynamics, and the hidden pattern "IMS" could be reversibly revealed by breathing toward the anti-counterfeit tab. Adapted from [184]. (b) Reversible dual-pattern with fluorescence and hierarchical wrinkles obtained through photomasks. Adapted from [187]. (c) Application of the optically erasable wrinkling system for the repetitive optical writing/erasure of information by multiple cycles of stimulus-induced wrinkling, selective exposure, and blanket exposure. Adapted from [185].

produced clear images [181]. Fang et al. [182, 183] reported shape memory polymers (SMPs) with instantaneous shape recovery triggered by a contact pressure. This process was controlled by unusual "cold" programming that the polymers deformed to a temporary shape at or below room temperature. Macroporous SMPs membranes were prepared by templates of silica microspheres and copolymers of ethoxylated (20) trimethylolpropane triacrylate (ETPTA, $T_g \approx 40°C$) and polyethylene glycol (600) diacrylate (PEGDA, $T_g \approx 42°C$). The membranes exhibited colours in water and became translucent with a pale and no ordering of the deformed macropores when dehydrated. When finger, a "light bulb" relief pattern and printed pairs of parallel lines were under a small contact pressure on the collapsed macroporous membranes, several patterns immediately appeared (see Figure 7(b_1)). The raising up of the smoother line patterns were tested by Atomic Force Microscope (AFM) image, and the corresponding depth profile. The paper elucidated this unusual shape-recovery mechanism due to an apparent adhesive pull-off force of the attractive Van Der Waals interactions and the capillary force of layer between the indenter tip and the SMP membrane (see Figure 7(b_2)).(a)(c)

4. Surface Wrinkles Technology in Patterns Construction and Anti-Counterfeiting Application

Micropatterns by molecular self-assembly and interface self-organization technology can be prepared in a large area, but the local surface is prone to defects, so it is still in the laboratory development stage. The interface self-organizing technology utilizes the inherent Van Der Waals force, polarity, steric hindrance and electrostatic force of the polymer film to produce yield deformation to relax the internal instability of the system to form micropatterns. The main response methods are heat, force and electromagnetic field, humidity, phase separation, osmotic pressure, capillary force and polymerization shrinkage stress, etc. Micropatterns can be obtained by controlling the induced surface instability factors. Material surface wrinkle technology of patterning micro-nano structure is a more conventional method. Polydimethylsiloxane elastomer is usually used as base material, also other hard film and soft substrate can achieve wrinkles by adjusting modulus of elasticity, coefficients of thermal expansion, and swelling abilities of the solvents. Typically, the shape memory material is one of the main ways of wrinkle formation by controlling the melting temperature of the crystalline phase adjusted within a certain temperature range.

Zeng et al. [184] proposed a series of moisture-sensitive film-substrate bilayer devices that consisted of hydrophilic polyvinyl alcohol film onto hydrophobic PDMS. Three states (repeated reversible folds, disposable folds and permanent fold) were controlled by the thickness of the PVA film, PVA crosslinking degree/gradient, PDMS modulus, and PVA-PDMS interface (see Figure 8(a)). Letters "IMS" were patterned sustained for 30 s as moisture penetration to polymeric network and reduction modulus with a degree of hydrolysis of 88% PVA. These unique responsive dynamics also could motivate the invention of anti-counterfeit tabs, encryption devices, water indicators, light diffusors, and anti-glare films. Zong et al. [185] reported a simple method to dynamically tune and/or erase wrinkling patterns by photoisomerization on an azo-containing poly (disperse orange 3) (PDO3) film

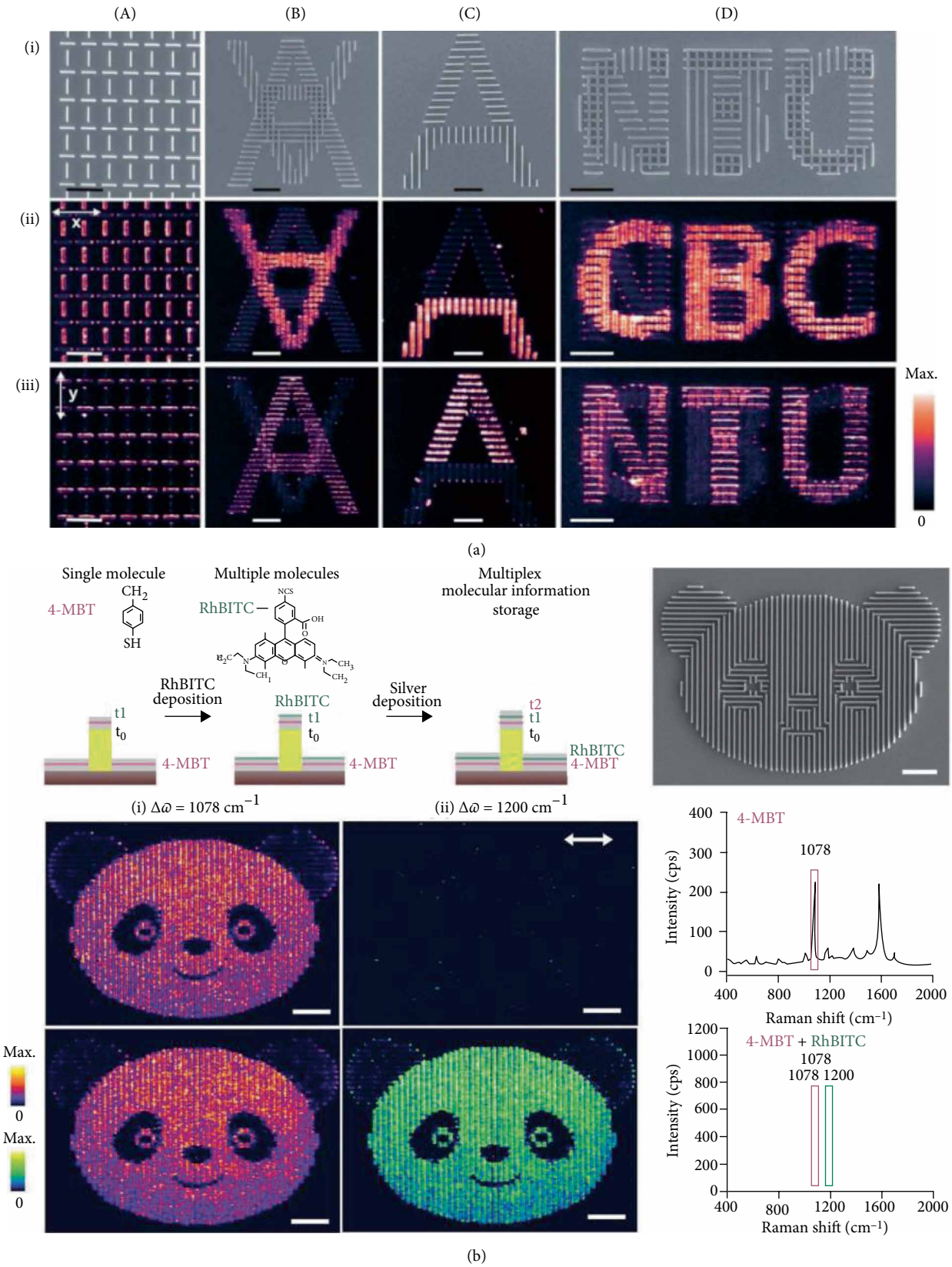

Figure 9: Continued.

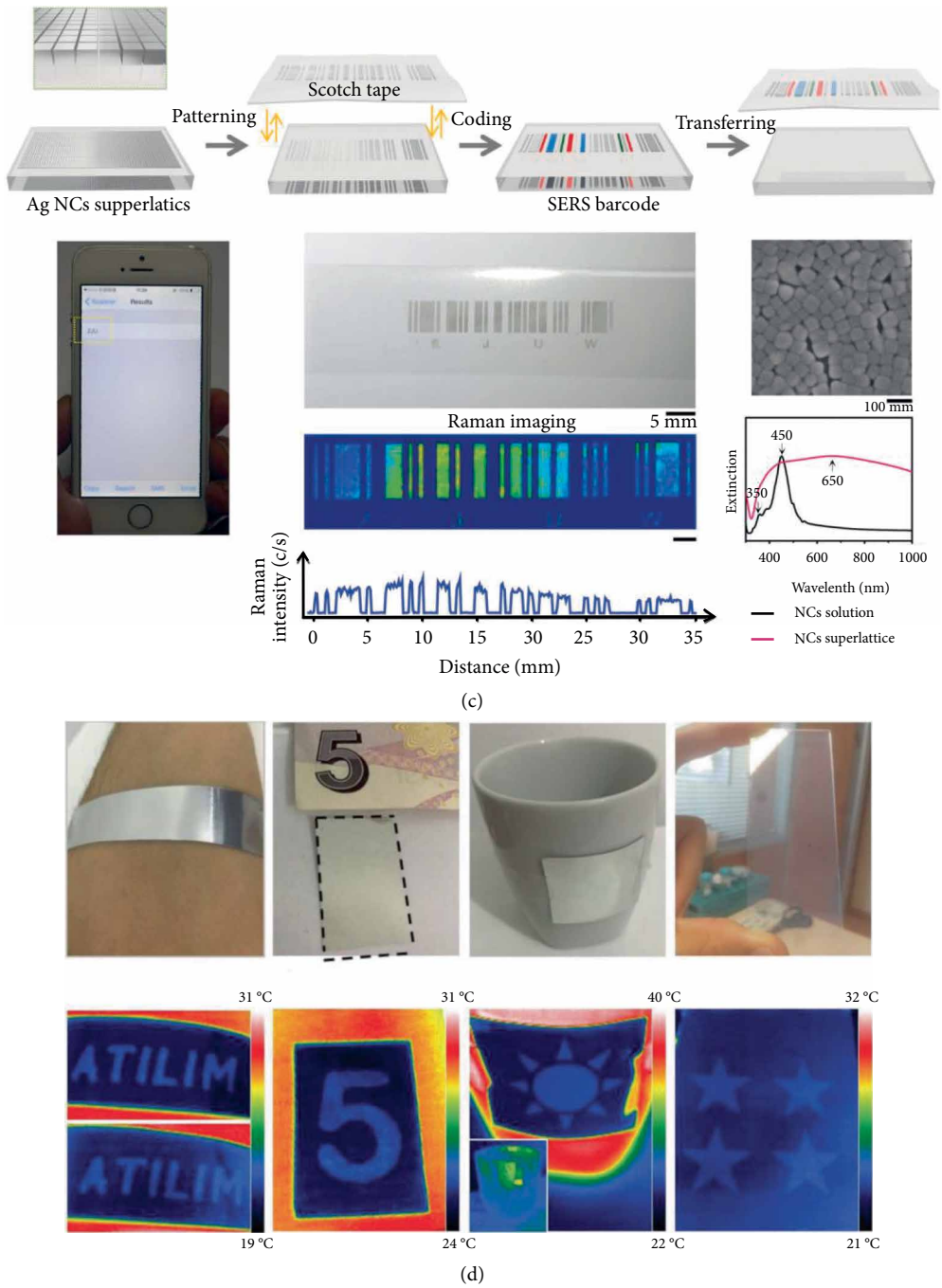

Figure 9: (a) (i) SEM images, (ii and iii) x- and y-polarized 2D SERS imaging of different molecularly encrypted nanostructures formed by horizontal and vertical Ag nanowires. Adapted from [191] and (b) homogeneous plasmonic anti-counterfeiting security labels. Adapted from [192]. (c) Schematic illustration and optical image of the fabrication of the SERS barcode and its application. Adapted from [194]. (d) Photograph and thermal image of alternative mirror layers. Adapted from [198].

bonded to PDMS substrate. Reversible photoisomerization of the azobenzene moieties led to the release of the internal stress upon light irradiation (see Figure 8(c)). Patterns were obtained highly ordered by selective exposure. The unexposed part had a lower transmittance and stronger scattering, and it could be erased by blanket exposure. The writing/erasure velocity was determined by the light power density and the film thickness. Li et al. [186] fabricated near-infrared light-responsive dynamic wrinkles by bilayer systems (carbon nanotube and PDMS elastomer) and top stiff layers (functional polymers). The elastic CNT-PDMS substrate could be obtained with the reversible wrinkle patterns due to the high photon-to-thermal energy conversion efficiency and absorption by NIR irradiation. Switchable optical transparency in the wrinkled and wrinkle-free states were controlled by on/off cyclic NIR irradiation of 20 s and 30 s respectively. A positive letter "S" was

obtained selectively by 365 nm UV light, then converted to a fully wrinkled surface. After that, a negative letter "T" was selectively erased by 254 nm UV light. Interestingly the information could temporarily be erased and swiftly restored to the original state. Xie et al. [187] demonstrated an approach to fabricate patterns by fluorescence and wrinkled topography controlling simultaneously by light. The bilayer system contained a top layer (anthracene (AN) and naphthalene diimide (NDI) moieties containing a copolymer, PAN-NDI-BA and a substrate of PDMS. Upon irradiation by 365 nm UV light, photodimerization leads to a cross-linked top layer with a higher modulus and a red to blue-green fluorescence change. A reversible dynamic dual-pattern with wrinkled topography and fluorescence was generated reversibly upon exposure to 254 nm UV light or 150°C (see Figure 8(b)). By masks of "stripe", "annulus", and "SJTU", positive images with a green fluorescence patterned and erased followed by 365 nm UV light for 15 ,min and a thermal treatment at 70°C in red fluorescence background respectively.

5. Plasmonic Micro–Nano Technology in Pattern Construction and Anti-Counterfeiting Application

Many studies proved that the coherent oscillation of conduction electrons in plasmonic nanostructures with incident light could enhance the electromagnetic field strength on their surfaces and increases scattering [188–190]. Surface-enhanced Raman scattering (SERS) is a detection method to incorporate into security labels as its signal was strongly dependent on the incident field polarization and wavelength of plasmonic nanostructures. Some researchers used surface plasmon resonance to study the structural colour to form a clear and identifiable pattern identification for hiding or reading encrypted information at higher anti-counterfeiting level.

Cui et al. [191] prepared a proof-of-concept novel plasmonic SERS security label with Ag nanowire structures. They designed full encrypted molecular images that was authenticated by polarized SERS imaging in both x- and y-polarizations. The vertical and horizontal nanowires exhibited strong SERS intensity correspondingly in an alternating fashion under the x-polarization and y-polarization respectively (see Figure 9(a)). Similarly, the upright "A" and the inverted "A" written by horizontal and vertical nanowires respectively could be clearly read-out or invisibly controlled, also an alphabet "A" fabricated using 50% horizontal nanowires and 50% vertical nanowires could hide visible molecular information of only half of the "A" under x- or y-polarization. Based on the above mentioned design, the alphabetical "CBC" and "NTU" could be clearly distinguished by x- and y-polarizations, respectively. Subsequently, their teams developed a multiplex plasmonic anti-counterfeiting platform with superior nanometer scale spectral and spatial resolution to increase the complexity of these plasmonic security labels. Sandwich nanowire structures functionalized with 4-methylbenzenethiol (4-MBT) and rhodamine B isothiocyanate (RhBITC) could generate unique security features when individual vibrational modes were selected. For a single sandwich structure with only 4-MBT, the SERS image of a panda was shown visibly with vibrational modes at 1078 cm^{-1} while invisibly at 1200 cm^{-1}. For a sandwich structure with 4-MBT and RhBITC, the image of a panda could be shown with vibrational modes at 1078 cm^{-1} and 1200 cm^{-1} respectively (see Figure 9(b)) [192]. After that, their team studied the spatially selective encapsulation of dye molecules with Ag nanopillar array to fabricated molecular information which was revealed using fluorescence, SERS, and their signal intensities. They fabricated a "yin-yang" pattern with rhodamine 6G (R6G) and eosin Y and dimethyl sulfoxide (EY) encapsulated nanopillars. Bright-field microscopic nanopillars and fluorescence images of patterns with the R6G half and EY half were shown, the image could not fully reveal the "yin-yang" due to the higher fluorescence quantum yield of R6G. However, the SERS image of left- and right-half of "yin-yang" were selectively exhibited. The technology of multiple-layer platform with enhanced information security made anti-counterfeiting more practical in the near future [193]. Li et al. [194] fabricated flexible patterned plasmonic metafilms by bottom-up self-assembly of PS and top-down laser engraving of PS beads with a Langmuir-Blodgett technique. The patterned PS beads loosely bounded to the glass/silica surface could be completely transferred to the tape, then silver was deposited onto the tape to a get flexible plasmonic meta-structures, then a multidimensional SERS barcode was fabricated (see Figure 9(c)). Firstly, the NCs super-lattice sheet was fabricated on glass, then it was patterned into a barcode by an adhesive stencil tape to remove the excessive sheet on the substrate and leave the remaining pattern barcodes. The obtained barcode with an encoding text of Zhejiang University was readable by a photo. Ag NCs were mostly assembled in face-to-face orientations with a strong LSPR due to the dipole-dipole coupling between the neighboring NCs. The patterns shown in the Raman maps perfectly matched the optical image of the NCs barcode. Huge coding capacity could be achieved by adjusting barcodes and choices of Raman dyes. The simple, low-cost, and efficient approach to fabricate a flexible plasmonic material displayed tunable plasmonic properties and excellent flexibility for anti-counterfeiting applications [195]. Kang et al. [196] fabricated multiwavelength thermoplasmonic images by inkjet printing nanoparticle inks of gold nanorod (GNR) and gold nanosphere (GNS), the thermoplasmonic metal nanoparticles could generate localized heat to enhanced light absorption at a particular wavelength by localized surface plasmons, so patterns that are difficult to distinguish with the naked eye could be visible by thermal imaging infrared cameras. This method could operate instantaneously and for an unlimited period of time, also it was fully reversible. Park et al. [197] prepared a secure label with a combination of two codes which was composed of AgNPs formed on the adhesive scotch tape and the UCNCs on the Ag film, respectively, and then the decryption code with MUM structure was assembled by overlapping the tape and the Ag on the mask aligner. The code of "KIST" could not be visually or microscopically identified, however, it could be seen with green luminescence by irradiation of NIR light. Bakan et al. [198] constructed invisible patterns by ultrathin dielectrics which was transparent in the visible and exhibited strong infrared absorption in the spectral range of thermal cameras (see Figure 9(d)). To expand the

possibilities of applications, they used bendable substrates of Al foils from rigid Si wafers. Al foils laminated with polyethylene film and paper were studied in the maximum SiO_2 thickness that was imperceptible to the naked eye. Alternative mirror layers showed not only a security feature but also angle-independent absorbance/emissivity of the surfaces. Conductive oxides fluorine doped tin oxide (FTO) coated glasses were used as another alternative layer, however, the contrast between the SiO_2 patterns and the background was weaker due to the ultrathin SiO_2 ($\approx$5 nm) and greater absorbance/emissivity of FTO, it could only be observed at higher temperatures.

6. Summary and Outlook

In this review, we have considered various published literature on fabrication of micro-nano structures for patterns including styles, materials, method. For better understanding the difference of fabrication methods of micro-nano structures, Table 1 summarized inkjet printing, angle-independent photonic crystal, self-assembled photonic crystals by magnetic field force, gravity, electric field, inverse opal photonic crystal, electron beam etching, ion beam etching, laser holographic lithography, imprinting technology and surface wrinkle technology. In addition, we have reviewed studies aimed at photonic papers with micro-nano structure patterns of photonic crystal by inkjet printing technology, ink responsiveness, photomask technology, electromagnetic responsiveness, stress responsiveness and a summary of figures have been adapted from published literature, which can be manipulated by common solvents, salts or reactive monomers, electric and magnetic field and stress. Finally, we have briefly introduced the surface wrinkle anti-counterfeiting technology and the plasmonic micro-nano anti-counterfeiting technology. These methods have simple steps and can be prepared in a large area, but are still in the laboratory development stage. We put forward some suggestions. Future research may pattern based on the design of micro-nano structure and optical properties, explore the intrinsic connection and law between optical micro-patterns and colours, and adjust the interface strain state of polymer surface topography or apply stress to achieve nano-scale manipulation of light. In particular, micro-nano structure, surface chemistry, interfacial adhesion, and hydrophobicity may be used as optical switches to study patterning and intelligent anti-counterfeiting.

Conflicts of Interest

The authors declare that they have no conflicts of interest.

Acknowledgments

The authors gratefully acknowledge financial support from GDAS' Project of Science and Technology Development (2019GDASYL-0103041, 2018GDASCX-0105).

References

[1] S. S. Sunku, G. X. Ni, B. Y. Jiang et al., "Photonic crystals for nano-light in moiré graphene superlattices," *Science*, vol. 362, no. 6149, pp. 1153–1156, 2018.

[2] D. Y. Kim, S. Choi, H. Cho, and J. Y. Sun, "Synesthetic devices: electroactive soft photonic devices for the synesthetic perception of color and sound," *Advanced Materials*, vol. 31, no. 2, p. 1804080, 2019.

[3] J. Zhou, P. Han, M. Liu et al., "Self-healable organogel nanocomposite with angle-independent structural colors," *Angewandte Chemie International Edition*, vol. 56, no. 35, pp. 10462–10466, 2017.

[4] Y. Zhu, P. Wang, S. Xiao et al., "Manipulating three-dimensional bending to extraordinarily stiffen two-dimensional membranes by interference colors," *Nanoscale*, vol. 10, no. 46, pp. 21782–21789, 2018.

[5] D. Beaton, "Gems & gemology challenge winners," *Gems & Gemology*, vol. 52, p. 217, 2016.

[6] G. H. Lee, T. M. Choi, B. Kim, S. H. Han, J. M. Lee, and S. H. Kim, "Chameleon-inspired mechanochromic photonic films composed of nonclose-packed colloidal arrays," *ACS Nano*, vol. 11, no. 11, pp. 11350–11357, 2017.

[7] Y. Li, Z. Lu, H. Yin, X. Yu, X. Liu, and J. Zi, "Structural origin of the brown color of barbules in male peacock tail feathers," *Physical Review E Statistical, Nonlinear, and Soft Matter Physics*, vol. 72, no. 1, p. 010902, 2005.

[8] J. Matějková-Plšková, D. Jančik, and M. Mašláň, "Photonic crystal structure of wing scales in *Sasakia charonda* butterflies," *Materials Transactions*, vol. 51, no. 2, pp. 202–208, 2010.

[9] M. Vatankhah-Varnosfaderani, A. N. Keith, Y. Cong et al., "Chameleon-like elastomers with molecularly encoded strain-adaptive stiffening and coloration," *Science*, vol. 359, no. 6383, pp. 1509–1513, 2018.

[10] F. Marlow, P. Muldarisnur, R. Sharifi, and C. Brinkmann, "Opals: status and prospects," *Mendive, Angewandte Chemie International Edition*, vol. 48, pp. 6212–6233, 2009.

[11] J. Zi, X. Yu, Y. Li et al., "Coloration strategies in peacock feathers," *Proceedings of the National Academy of Sciences*, vol. 100, no. 22, pp. 12576–12578, 2003.

[12] M. R. Snow, A. Pring, P. Self, D. Losic, and J. Shapter, "The origin of the color of pearls in iridescence from nano-composite structures of the nacre," *American Mineralogist*, vol. 89, no. 10, pp. 1353–1358, 2004.

[13] F. Liu, B. Q. Dong, X. H. Liu, Y. M. Zheng, and J. Zi, "Structural color change in longhorn beetles Tmesisternus isabellae," *Optics Express*, vol. 17, no. 18, pp. 16183–16191, 2009.

[14] A. R. Parker, "515 million years of structural colour," *Journal of Optics A: Pure and Applied Optics*, vol. 2, no. 6, pp. R15–R28, 2000.

[15] P. Vukusic and J. R. Sambles, "Photonic structures in biology," *Nature*, vol. 424, no. 6950, pp. 852–855, 2003.

[16] Z. Gao, D. Gao, C. Huang, H. Zhang, J. Guo, and J. Wei, "Dual-responsive SPMA-modified polymer photonic crystals and their dynamic display patterns," *Macromolecular Rapid Communications*, vol. 39, no. 20, p. 1800134, 2018.

[17] R. Hirayama, T. Suzuki, T. Shimobaba et al., "Inkjet printing-based volumetric display projecting multiple full-colour 2D patterns," *Scientific Reports*, vol. 7, no. 1, Article ID 46511, 2017.

[18] G. Liu, L. Zhou, G. Zhang et al., "Fabrication of patterned photonic crystals with brilliant structural colors on fabric substrates using ink-jet printing technology," *Materials & Design*, vol. 114, pp. 10–17, 2017.

[19] L. Sun, M. Yang, J. Huang, D. Yu, W. Hong, and X. Chen, "Freestanding graphitic carbon nitride photonic crystals for enhanced photocatalysis," *Advanced Functional Materials*, vol. 26, no. 27, pp. 4943–4950, 2016.

[20] W. Lin, W. Hong, L. Sun, D. Yu, D. Yu, and X. Chen, "Bioinspired mesoporous chiral nematic graphitic carbon nitride photocatalysts modulated by polarized light," *Chemsuschem*, vol. 11, no. 1, pp. 114–119, 2018.

[21] P. Li, J. Li, Z. Zhao et al., "A general electrode design strategy for flexible fiber micro-pseudocapacitors combining ultrahigh energy and power delivery," *Advanced Science*, vol. 4, no. 8, p. 170003, 2017.

[22] A. Sandhyarani, M. K. Kokila, G. P. Darshan et al., "Versatile core–shell SiO_2 @$SrTiO_3$: Eu 3+, Li+ nanopowders as fluorescent label for the visualization of latent fingerprints and anti-counterfeiting applications," *Chemical Engineering Journal*, vol. 327, pp. 1135–1150, 2017.

[23] J. Chen, L. Xu, X. Lin et al., "Self-healing responsive chiral photonic films for sensing and encoding," *Journal of Materials Chemistry C*, vol. 6, no. 29, pp. 7767–7775, 2018.

[24] J. H. Lee, B. Fan, T. D. Samdin et al., "Phage-based structural color sensors and their pattern recognition sensing system," *ACS Nano*, vol. 11, no. 4, pp. 3632–3641, 2017.

[25] W. Hong, X. Hu, B. Zhao, F. Zhang, and D. Zhang, "Tunable photonic polyelectrolyte colorimetric sensing for anions, cations and zwitterions," *Advanced Materials*, vol. 22, no. 44, pp. 5043–5047, 2010.

[26] W. Hong, W. Li, X. Hu, B. Zhao, F. Zhang, and D. Zhang, "Highly sensitive colorimetric sensing for heavy metal ions by strong polyelectrolyte photonic hydrogels," *Journal of Materials Chemistry*, vol. 21, no. 43, pp. 17193–17201, 2011.

[27] W. Hong, Y. Chen, X. Feng et al., "Full-color CO_2 gas sensing by an inverse opal photonic hydrogel," *Chemical Communications*, vol. 49, no. 74, pp. 8229–8231, 2013.

[28] X.-Y. Han, Z.-L. Wu, S.-C. Yang et al., "Recent progress of imprinted polymer photonic waveguide devices and applications," *Polymers*, vol. 10, no. 6, p. 603, 2018.

[29] R. Arppe and T. J. Sørensen, "Physical unclonable functions generated through chemical methods for anti-counterfeiting," *Nature Reviews Chemistry*, vol. 1, no. 4, p. 0031, 2017.

[30] M. K. Khan, A. Bsoul, K. Walus, W. Y. Hamad, and M. J. MacLachlan, "Photonic patterns printed in chiral nematic mesoporous resins," *Angewandte Chemie International Edition England*, vol. 54, no. 14, pp. 4304–4308, 2015.

[31] R. Lee, in *Optical Security and Counterfeit Deterrence Techniques*, R. L. VanRenesse, Ed., pp. 350–368, vol. 5310, SPIE Digital Library, 2004.

[32] J. Liu, M. Li, Y. Yang et al., "Metal conductive surface patterning on photoactive polyimide," *Advanced Functional Materials*, vol. 27, no. 33, p. 1701674, 2017.

[33] T. Ding, L. Luo, H. Wang et al., "Micropatterning and defect engineering of colloidal photonic crystals via laser direct writing," *Journal of Materials Chemistry C*, vol. 21, p. 11330, 2011.

[34] C. Liu, H. Ding, Z. Wu et al., "Tunable structural color surfaces with visually self-reporting wettability," *Advanced Functional Materials*, vol. 26, no. 43, pp. 7937–7942, 2016.

[35] U. Y. Lau, S. S. Saxer, J. Lee, E. Bat, and H. D. Maynard, "Direct write protein patterns for multiplexed cytokine detection from live cells using electron beam lithography," *ACS Nano*, vol. 10, no. 1, pp. 723–729, 2015.

[36] W. Hong, H. Li, X. Hu, B. Zhao, F. Zhang, and D. Zhang, "Independent multifunctional detection by wettability controlled inverse opal hydrogels," *Chemical Communications*, vol. 48, no. 38, pp. 4609–4611, 2012.

[37] H. Jeong, R. Salas-Montiel, G. Lerondel, and M. S. Jeong, "Indium gallium nitride-based ultraviolet, blue, and green light-emitting diodes functionalized with shallow periodic hole patterns," *Scientific Reports*, vol. 7, no. 1, p. 45726, 2017.

[38] W. Hong, Y. Zhang, L. Gan, X. Chen, and M. Zhang, "Control of plasmonic fluorescence enhancement on self-assembled 2-D colloidal crystals," *Journal of Materials Chemistry C*, vol. 3, no. 24, pp. 6185–6191, 2015.

[39] G. Chen, D. Wang, W. Hong, L. Sun, Y. Zhu, and X. Chen, "Fluorescence enhancement on large area self-assembled plasmonic-3D photonic crystals," *Small*, vol. 13, no. 9, p. 1602612, 2017.

[40] M. Parchine, J. McGrath, M. Bardosova, and M. E. Pemble, "Large area 2D and 3D colloidal photonic crystals fabricated by a roll-to-roll langmuir–blodgett method," *Langmuir*, vol. 32, no. 23, pp. 5862–5869, 2016.

[41] B. Chang, C. Zhou, A. T. Tarekegne et al., "Large area three-dimensional photonic crystal membranes: single-run fabrication and applications with embedded planar defects," *Advanced Optical Materials*, vol. 7, no. 2, p. 1801176, 2019.

[42] M. Liu, W. Xu, J. Bai et al., "Investigation of the size effect for photonic crystals," *Nanotechnology*, vol. 27, no. 40, p. 405703, 2016.

[43] S.-H. Kim, S.-J. Jeon, G.-R. Yi, C.-J. Heo, J. H. Choi, and S.-M. Yang, "Optofluidic assembly of colloidal photonic crystals with controlled sizes, shapes, and structures," *Advanced Materials*, vol. 20, no. 9, pp. 1649–1655, 2008.

[44] H. Y. Ryu, J. K. Hwang, and Y. H. Lee, "Effect of size nonuniformities on the band gap of two-dimensional photonic crystals," *Physical Review B*, vol. 59, no. 8, pp. 5463–5469, 1999.

[45] G. Scalari, J. Faist, L. A. Dunbar, and R. Houdré, "Design and fabrication technology for high performance electrical pumped terahertz photonic crystal band edge lasers with complete photonic band gap," *Journal of Applied Physics*, vol. 108, no. 9, p. 093104, 2010.

[46] Z. Li, Y. Xin, W. Wu, B. Fu, and Z. Zhang, "Phosphorus cation doping: a new strategy for boosting photoelectrochemical performance on TiO_2 nanotube photonic crystals," *ACS Applied Materials & Interfaces*, vol. 8, pp. 30972–30979, 2016.

[47] D. Li, D. Zhou, W. Xu et al., "Plasmonic photonic crystals induced two-order fluorescence enhancement of blue perovskite nanocrystals and its application for high-performance flexible ultraviolet photodetectors," *Advanced Functional Materials*, vol. 28, no. 41, p. 1804429, 2018.

[48] K. W. Kimble, J. P. Walker, D. N. Finegold, and S. A. Asher, "Progress toward the development of a point-of-care photonic crystal ammonia sensor," *Analytical and Bioanalytical Chemistry*, vol. 385, no. 4, pp. 678–685, 2006.

[49] J. S. King, D. P. Gaillot, E. Graugnard, and C. J. Summers, "Conformally back-filled, non-close-packed inverse-opal photonic crystals," *Advanced Materials*, vol. 18, no. 8, pp. 1063–1067, 2006.

[50] R. A. Lee, "Micro-technology for anti-counterfeiting," *Microelectronic Engineering*, vol. 53, pp. 513–516, 2000.

[51] S. Shikha, T. Salafi, J. Cheng, and Y. Zhang, "Versatile design and synthesis of nano-barcodes," *Chemical Society Reviews*, vol. 46, no. 22, pp. 7054–7093, 2017.

[52] A. F. Smith and S. E. Skrabalak, "Metal nanomaterials for optical anti-counterfeit labels," *Journal of Materials Chemistry C*, vol. 5, pp. 3207–3215, 2017.

[53] R. Hirayama, T. Suzuki, T. Shimobaba et al., "Inkjet printing-based volumetric display projecting multiple full-colour 2D patterns," *Scientific Reports*, vol. 7, p. 46511, 2017.

[54] B. Ye, F. Rong, H. Gu et al., "Bioinspired angle-independent photonic crystal colorimetric sensing," *Chemical Communications*, vol. 49, no. 46, pp. 5331–5333, 2013.

[55] I. L. Lyubchanskii, N. N. Dadoenkova, M. I. Lyubchanskii, E. A. Shapovalov, and T. H. Rasing, "Magnetic photonic crystals," *Journal of Physics D: Applied Physics*, vol. 36, no. 18, pp. R277–R287, 2003.

[56] L. Sun, M. Yang, J. Huang, D. Yu, W. Hong, and X. Chen, "Freestanding graphitic carbon nitride photonic crystals for enhanced photocatalysis," *Advanced Functional Materials*, vol. 26, pp. 4943–4950, 2016.

[57] A. Yethiraj, J. H. J. Thijssen, A. Wouterse, and A. van Blaaderen, "Large-area electric-field-induced colloidal single crystals for photonic applications," *Advanced Materials*, vol. 16, no. 7, pp. 596–600, 2004.

[58] C. I. Aguirre, E. Reguera, and A. Stein, "Tunable colors in opals and inverse opal photonic crystals," *Advanced Functional Materials*, vol. 20, no. 16, pp. 2565–2578, 2010.

[59] W. Hong, H. Li, X. Hu et al., "Wettability gradient colorimetric sensing by amphiphilic molecular response," *Chemical Communications*, vol. 49, no. 7, pp. 728–730, 2013.

[60] J. Kim, D. C. Joy, and S. Y. Lee, "Controlling resist thickness and etch depth for fabrication of 3D structures in electron-beam grayscale lithography," *Microelectronic Engineering*, vol. 84, no. 12, pp. 2859–2864, 2007.

[61] D. W. Reagor and V. Y. Butko, "Highly conductive nanolayers on strontium titanate produced by preferential ion-beam etching," *Nature Materials*, vol. 4, no. 8, pp. 593–596, 2005.

[62] L. L. Yuan and P. R. Herman, "Laser scanning holographic lithography for flexible 3D fabrication of multi-scale integrated nano-structures and optical biosensors," *Scientific Reports*, vol. 6, no. 1, p. 22294, 2016.

[63] C.-C. Yu and H.-L. Chen, "Nanoimprint technology for patterning functional materials and its applications," *Microelectronic Engineering*, vol. 132, pp. 98–119, 2015.

[64] Y. Mei, S. Kiravittaya, S. Harazim, and O. G. Schmidt, "Principles and applications of micro and nanoscale wrinkles," *Materials Science and Engineering: R: Reports*, vol. 70, no. 3–6, pp. 209–224, 2010.

[65] Z. Zhu, J. Zhang, C.-F. Wang, and S. Chen, "Construction of hydrogen-bond-assisted crack-free photonic crystal films and their performance on fluorescence enhancement effect," *Macromolecular Materials and Engineering*, vol. 302, p. 1700013, 2017.

[66] C. Osuji, C. Y. Chao, I. Bita, C. K. Ober, and E. L. Thomas, "Temperature-dependent photonic bandgap in a self-assembled hydrogen-bonded liquid-crystalline diblock copolymer," *Advanced Functional Materials*, vol. 12, no. 112, pp. 753–758, 2002.

[67] J. D. Chinn, W. Phillips, I. Adesida, and E. D. Wolf, "Ion beam etching of silicon, refractory metals, and refractory metal silicides using a chemistry assisted technique," *Journal of The Electrochemical Society*, vol. 131, no. 2, pp. 375–380, 1984.

[68] A. P. Schenning and E. W. Meijer, "Supramolecular electronics; nanowires from self-assembled π-conjugated systems," *Chemical Communications*, vol. 26, pp. 3245–3258, 2005.

[69] P. Datskos, G. Polizos, M. Bhandari, D. A. Cullen, and J. Sharma, "Colloidosome like structures: self-assembly of silica microrods," *RSC Advances*, vol. 6, pp. 26734–26737, 2016.

[70] S. Stepanow, M. Lingenfelder, A. Dmitriev et al., "Steering molecular organization and host–guest interactions using two-dimensional nanoporous coordination systems," *Nature Materials*, vol. 3, no. 4, pp. 229–233, 2004.

[71] X. Huang, Z. Yang, L. Sun et al., "Synthesis and characterization of potassium bismuth titanate inverse opal photonic crystals by sol–gel technique," *Materials Chemistry and Physics*, vol. 114, no. 1, pp. 23–25, 2009.

[72] J. W. Galusha, C.-K. Tsung, G. D. Stucky, and M. H. Bartl, "Optimizing sol–gel infiltration and processing methods for the fabrication of high-quality planar titania inverse opals," *Chemistry of Materials*, vol. 20, no. 15, pp. 4925–4930, 2008.

[73] W. Li, F. Wang, S. Feng et al., "Sol–gel design strategy for ultradispersed TiO_2 Nanoparticles on graphene for high-performance lithium ion batteries," *Journal of the American Chemical Society*, vol. 135, no. 49, pp. 18300–18303, 2013.

[74] A. Blanco, E. Chomski, S. Grabtchak et al., "Large-scale synthesis of a silicon photonic crystal with a complete three-dimensional bandgap near 1.5 micrometres," *Nature*, vol. 405, no. 6785, pp. 437–440, 2000.

[75] J. S. King, E. Graugnard, and C. J. Summers, "TiO_2 inverse opals fabricated using low-temperature atomic layer deposition," *Advanced Materials*, vol. 17, no. 8, pp. 1010–1013, 2005.

[76] J. S. King, E. Graugnard, and C. J. Summers, "Photoluminescence modification by high-order photonic bandsin TiO_2/ZnS:Mn multilayer inverse opals," *Applied Physics Letters*, vol. 88, no. 8, p. 081109, 2006.

[77] H. Yan, Y. Z. Yang, B. Fu et al., "Cathodic electrodeposition of ordered porous titania films by polystyrene colloidal crystal templating," *Chemistry Letters*, vol. 35, no. 8, pp. 864–865, 2006.

[78] Y. Xu, X. Zhu, Y. Dan et al., "Electrodeposition of three-dimensional titania photonic crystals from holographically patterned microporous polymer templates," *Chemistry of Materials*, vol. 20, no. 5, pp. 1816–1823, 2008.

[79] P. Yao, G. J. Schneider, D. W. Prather, E. D. Wetzel, and D. J. O'Brien, "Fabrication of three-dimensional photonic crystals with multilayer photolithography," *Optics Express*, vol. 13, no. 7, pp. 2370–2376, 2005.

[80] M. Yemini, B. Hadad, Y. Liebes, A. Goldner, and N. Ashkenasy, "The controlled fabrication of nanopores by focused electron-beam-induced etching," *Nanotechnology*, vol. 20, no. 24, p. 245302, 2009.

[81] S. Chattopadhyay and P. W. Bohn, "Direct-write patterning of microstructured porous silicon arrays by focused-ion-beam Pt deposition and metal-assisted electroless etching," *Journal of Applied Physics*, vol. 96, pp. 6888–6894, 2004.

[82] M. Campbell, D. N. Sharp, M. T. Harrison, R. G. Denning, and A. J. Turberfield, "Fabrication of photonic crystals for the visible spectrum by holographic lithography," *Nature*, vol. 404, no. 6773, pp. 53–56, 2000.

[83] X. Wang, J. F. Xu, H. M. Su et al., "Three-dimensional photonic crystals fabricated by visible light holographic lithography," *Applied Physics Letters*, vol. 82, no. 14, pp. 2212–2214, 2003.

[84] X. Hu, H. Wang, C. Zhai, H. Ge, and Y. Cui, "Fabrication of metallic patterns on highly curved substrates via nanoimprint lithography in association with an etch-in process," *Journal of Materials Chemistry C*, vol. 4, no. 47, pp. 11104–11109, 2016.

[85] X. Cheng and L. Jay Guo, "A combined-nanoimprint-and-photolithography patterning technique," *Microelectronic Engineering*, vol. 71, no. 3-4, pp. 277–282, 2004.

[86] Y. Chen, Z. Wang, M. M. Kulkarni et al., "Hierarchically patterned elastomeric and thermoplastic polymer films through nanoimprinting and ultraviolet light exposure," *ACS Omega*, vol. 3, no. 11, pp. 15426–15434, 2018.

[87] Y. Chen, Z. Wang, M. M. Kulkarni et al., "Hierarchically patterned elastomeric and thermoplastic polymer films through nanoimprinting and ultraviolet light exposure," *ACS Omega*, vol. 3, no. 11, pp. 15426–15434, 2018.

[88] P. Müller-Buschbaum, E. Bauer, O. Wunnicke, and M. Stamm, "The control of thin film morphology by the interplay of dewetting, phase separation and microphase separation," *Journal of Physics: Condensed Matter*, vol. 17, no. 9, pp. S363–S386, 2005.

[89] A. M. Higgins and R. A. L. Jones, "Anisotropic spinodal dewetting as a route to self-assembly of patterned surfaces," *Nature*, vol. 404, no. 6777, pp. 476–478, 2000.

[90] L. F. Pease and W. B. Russel, "Charge driven, electrohydrodynamic patterning of thin films," *The Journal of Chemical Physics*, vol. 125, no. 18, p. 184716, 2006.

[91] N. Wu, L. F. Pease, and W. B. Russel, "Toward large-scale alignment of electrohydrodynamic patterning of thin polymer films," *Advanced Functional Materials*, vol. 16, no. 15, pp. 1992–1999, 2006.

[92] G. Nisato, B. D. Ermi, J. F. Douglas, and A. Karim, "Excitation of surface deformation modes of a phase-separating polymer blend on a patterned substrate," *Macromolecules*, vol. 32, no. 7, pp. 2356–2364, 1999.

[93] E. Schaffer, S. Harkema, M. Roerdink, R. Blossey, and U. Steiner, "Morphological Instability of a confined polymer film in a thermal gradient," *Advanced Materials*, vol. 15, pp. 514–517, 2003.

[94] H. Katsuragi, "Diffusion-induced spontaneous pattern formation on gelation surfaces," *Europhysics Letters (EPL)*, vol. 73, no. 5, pp. 793–799, 2006.

[95] P. Kim, Y. Hu, J. Alvarenga, M. Kolle, Z. Suo, and J. Aizenberg, "Rational design of mechano-responsive optical materials by fine tuning the evolution of strain-dependent wrinkling patterns," *Advanced Optical Materials*, vol. 1, no. 5, pp. 381–388, 2013.

[96] T. Ohzono and M. Shimomura, "Ordering of microwrinkle patterns by compressive strain," *Physical Review B*, vol. 69, no. 13, p. 132202, 2004.

[97] S. Zeng, D. Zhang, W. Huang et al., "Bio-inspired sensitive and reversible mechanochromisms via strain-dependent cracks and folds," *Nature Communications*, vol. 7, no. 1, p. 11802, 2016.

[98] M. Guvendiren, S. Yang, and J. A. Burdick, "Swelling-induced surface patterns in hydrogels with gradient crosslinking density," *Advanced Functional Materials*, vol. 19, no. 19, pp. 3038–3045, 2009.

[99] M. Guvendiren, J. A. Burdick, and S. Yang, "Kinetic study of swelling-induced surface pattern formation and ordering in hydrogel films with depth-wise crosslinking gradien," *Soft Matter*, vol. 6, no. 9, pp. 2044–2049, 2010.

[100] M. K. Kang and R. Huang, "Swell-induced surface instability of confined hydrogel layers on substrates," *Journal of the Mechanics and Physics of Solids*, vol. 58, no. 10, pp. 1582–1598, 2010.

[101] M. K. Kang and R. Huang, "Swelling-induced instability of substrate-attached hydrogel lines," *International Journal of Applied Mechanics*, vol. 3, no. 2, pp. 219–233, 2011.

[102] J. Wu, L. Liu, B. Jiang et al., "A coating of silane modified silica nanoparticles on {PET} substrate film for inkjet printing," *Applied Surface Science*, vol. 258, pp. 5131–5134, 2012.

[103] K. N. Al-Milaji, R. R. Secondo, T. N. Ng, N. Kinsey, and H. Zhao, "Interfacial self-assembly of colloidal nanoparticles in dual-droplet inkjet printing," *Advanced Materials Interfaces*, vol. 5, no. 10, p. 1701561, 2018.

[104] Y. S. Yang, D.-H. Youn, S. H. Kim et al., "Preparation and characteristics of {PMMA} microlens array for a {BLU} application by an inkjet printing method," *Molecular Crystals and Liquid Crystals*, vol. 520, no. 1, pp. 515–520, 2010.

[105] P. Wilson, C. Lekakou, and J. F. Watts, "A comparative assessment of surface microstructure and electrical conductivity dependence on co-solvent addition in spin coated and inkjet printed poly(3,4-ethylenedioxythiophene):polystyr ene sulphonate ({PEDOT}:{PSS})," *Organic Electronics*, vol. 13, no. 3, pp. 409–418, 2012.

[106] P. Wilson, C. Lekakou, and J. F. Watts, "In-plane conduction characterisation and charge transport model of {DMSO} co-doped, inkjet printed poly(3,4-ethylenedioxythiophene): polystyrene sulfonate ({PEDOT}:{PSS})," *Organic Electronics*, vol. 14, no. 12, pp. 3277–3285, 2013.

[107] T.-T.-N. Nguyen, C.-Y. Chan, and J.-L. He, "One-step inkjet printing of tungsten oxide-poly(3,4-ethylenedioxythiophene):polystyrene sulphonate hybrid film and its applications in electrochromic devices," *Thin Solid Films*, vol. 603, pp. 276–282, 2016.

[108] P. Wilson, C. Lei, C. Lekakou, and J. F. Watts, "Transverse charge transport in inkjet printed poly(3,4-ethylenedioxythiophene) polystyrene sulfonate ({PEDOT}:{PSS})," *Organic Electronics.*, vol. 15, no. 9, pp. 2043–2051, 2014.

[109] R. Xing, S. Wang, B. Zhang et al., "Inkjet printed polystyrene sulfuric acid-doped poly(3,4-ethylenedioxythiophene) (PEDOT) uniform thickness films in confined grooves through decreasing the surface tension of PEDOT inks," *RSC Advances*, vol. 7, no. 13, pp. 7725–7733, 2017.

[110] C. Lee, B. J. Kang, and J. H. Oh, "High-resolution conductive patterns fabricated by inkjet printing and spin coating on wettability-controlled surfaces," *Thin Solid Films*, vol. 616, pp. 238–246, 2016.

[111] P. Q. Nguyen, L. P. Yeo, B. K. Lok, and Y. C. Lam, "Patterned surface with controllable wettability for inkjet printing of flexible printed electronics," *ACS Applied Materials Interfaces*, vol. 6, no. 6, pp. 4011–4016, 2014.

[112] S. H. Lee, K. Y. Shin, J. Y. Hwang, K. T. Kang, and H. S. Kang, "Silver inkjet printing with control of surface energy and substrate temperature," *Journal of Micromechanics and Microengineering*, vol. 18, no. 7, p. 075014, 2008.

[113] S. Biswas, S. Gawande, V. Bromberg, and Y. Sun, "Effects of particle size and substrate surface properties on deposition dynamics of inkjet-printed colloidal drops for printable

photovoltaics fabrication," *Journal of Solar Energy Engineering*, vol. 132, no. 2, p. 021010, 2010.

[114] I. M. T. Moutinho, P. J. T. Ferreira, and M. L. Figueiredo, "Impact of surface sizing on inkjet printing quality," *Industrial Engineering Chemistry Research*, vol. 46, no. 19, pp. 6183–6188, 2007.

[115] S. Yoshioka and Y. Takeoka, "Production of colourful pigments consisting of amorphous arrays of silica particles," *Chemphyschem*, vol. 15, no. 11, pp. 2209–2215, 2014.

[116] Y. Xue, F. Wang, Y. Qin, B. Lu, L. Wang, and J. Zhu, "Angle-independent structurally colored PS@TiO_2 film with excellent underwater superoleophobicity in harsh environments," *Langmuir*, vol. 35, no. 21, pp. 6956–6961, 2019.

[117] X. Su, H. Xia, S. Zhang, B. Tang, and S. Wu, "Vivid structural colors with low angle dependence from long-range ordered photonic crystal films," *Nanoscale*, vol. 9, no. 9, pp. 3002–3009, 2017.

[118] G. Peng, Z. Zhu, Y. Tian et al., "Dendrimer-induced colloids towards robust fluorescent photonic crystal films and high performance WLEDs," *Journal of Materials Chemistry C*, vol. 6, no. 30, pp. 8187–8193, 2018.

[119] C. Zhang, B.-H. Wu, Y. Du, M.-Q. Ma, and Z.-K. Xu, "Mussel-inspired polydopamine coatings for large-scale and angle-independent structural colors," *Journal of Materials Chemistry C*, vol. 5, no. 16, pp. 3898–3902, 2017.

[120] J. D. Forster, H. Noh, S. F. Liew et al., "Biomimetic isotropic nanostructures for structural coloration," *Advanced Materials*, vol. 22, no. 26-27, pp. 2939–2944, 2010.

[121] A. Kahlouche, A. Hocini, and D. Khedrouche, "Band-gap properties of 2D photonic crystal made by silica matrix doped with magnetic nanoparticles," *Journal of Computational Electronics*, vol. 13, no. 2, pp. 490–495, 2014.

[122] B. Gates and Y. N. Xia, "Photonic crystals that can be addressed with an external magnetic field," *Advanced Materials*, vol. 13, no. 21, pp. 1605–1608, 2001.

[123] H. Wang, Y. B. Sun, Q. W. Chen, Y. F. Yu, and K. Cheng, "Synthesis of carbon-encapsulated superparamagnetic colloidal nanoparticles with magnetic-responsive photonic crystal property," *Dalton Transactions*, vol. 39, no. 40, pp. 9565–9569, 2010.

[124] H. Ma, M. Zhu, W. Luo et al., "Free-standing, flexible thermochromic films based on one-dimensional magnetic photonic crystals," *Journal of Materials Chemistry C*, vol. 3, no. 12, pp. 2848–2855, 2015.

[125] A. You, Y. Cao, and G. Cao, "Facile fabrication of a magnetically assembled colloidal photonic crystal film via radical polymerization," *RSC Advances*, vol. 5, no. 114, pp. 93945–93950, 2015.

[126] T.-S. Deng, J.-Y. Zhang, K.-T. Zhu, Q.-F. Zhang, and J.-L. Wu, "Highly monodisperse vinyl functionalized silica spheres and their self-assembled three-dimensional colloidal photonic crystals," *Colloid. Surfaces A*, vol. 356, no. 1–3, pp. 104–111, 2010.

[127] S.-L. Kuai, X.-F. Hu, A. Haché, and V.-V. Truong, "High-quality colloidal photonic crystals obtained by optimizing growth parameters in a vertical deposition technique," *Journal of Crystal Growth*, vol. 267, no. 1-2, pp. 317–324, 2004.

[128] A. Yethiraj, J. H. J. Thijssen, A. Wouterse, and A. van Blaaderen, "Large-area electric-field-induced colloidal single crystals for photonic applications," *Advanced Materials*, vol. 16, no. 7, pp. 596–600, 2004.

[129] K. Chen, Q. Fu, S. Ye, and J. Ge, "Invisible photonic prints shown by deformation," *Advanced Functional Materials*, vol. 27, no. 41, Article ID 1702825, pp. 6430–6438, 2017.

[130] G. I. N. Waterhouse and M. R. Waterland, "Opal and inverse opal photonic crystals: fabrication and characterization," *Polyhedron*, vol. 26, no. 2, pp. 356–368, 2007.

[131] R. C. Schroden, M. Al-Daous, C. F. Blanford, and A. Stein, "Optical properties of inverse opal photonic crystals," *Chemistry of Materials*, vol. 14, no. 8, pp. 3305–3315, 2002.

[132] M. A. Bruk, E. N. Zhikharev, D. R. Streltsov, V. A. Kalnov, and A. V. Spirin, "The new dry method of mask (relief) formation by direct electron-beam etching of resist," *Microelectronic Engineering*, vol. 112, pp. 1–4, 2013.

[133] T. Yoshikawa, "Smooth etching of various III/V and II/VI semiconductors by Cl_2 reactive ion beam etching," *Journal of Vacuum Science & Technology B: Microelectronics and Nanometer Structures*, vol. 14, no. 3, p. 1764, 1996.

[134] T. Ohzono and M. Shimomura, "Ordering of microwrinkle patterns by compressive strain," *Physical Review B*, vol. 69, no. 13, p. 132202, 2004.

[135] J. Y. Chung, T. Q. Chastek, M. J. Fasolka, H. W. Ro, and C. M. Stafford, "Quantifying residual stress in nanoscale thin polymer films via surface wrinkling," *ACS Nano*, vol. 3, no. 4, pp. 844–852, 2009.

[136] T. Xie, X. Xiao, J. Li, and R. Wang, "Encoding localized strain history through wrinkle based structural colors," *Advanced Materials*, vol. 22, no. 39, pp. 4390–4394, 2010.

[137] P. Yang, R. M. Baker, J. H. Henderson, and P. T. Mather, "In vitro wrinkle formation via shape memory dynamically aligns adherent cells," *Soft Matter*, vol. 9, no. 18, p. 4705, 2013.

[138] Z. Chen, Y. Young Kim, and S. Krishnaswamy, "Anisotropic wrinkle formation on shape memory polymer substrates," *Journal of Applied Physics*, vol. 112, no. 12, p. 124319, 2012.

[139] C. M. Gabardo, J. Yang, N. J. Smith, R. C. Adams-McGavin, and L. Soleymani, "Programmable wrinkling of self-assembled nanoparticle films on shape memory polymers," *ACS Nano*, vol. 10, no. 9, pp. 8829–8836, 2016.

[140] C. M. Gabardo, R. C. Adams-McGavin, B. C. Fung, E. J. Mahoney, Q. Fang, and L. Soleymani, "Rapid prototyping of all-solution-processed multi-lengthscale electrodes using polymer-induced thin film wrinkling," *Scientific Reports*, vol. 7, no. 1, p. 42543, 2017.

[141] B. Kolaric, H. Vandeparre, S. Desprez, R. A. L. Vallee, and P. Damman, "In situ tuning the optical properties of a cavity by wrinkling," *Applied Physics Letters*, vol. 96, no. 4, p. 043119, 2010.

[142] S. H. Chae, W. J. Yu, J. J. Bae et al., "Transferred wrinkled Al2O3 for highly stretchable and transparent graphene–carbon nanotube transistors," *Nature Materials*, vol. 12, no. 5, pp. 403–409, 2013.

[143] J. Rodriguez-Hernandez, "Toward "smart" nano-objects by self-assembly of block copolymers in solution," *Progress in Polymer Science*, vol. 42, pp. 1–41, 2015.

[144] H. Y. Ko, J. Park, H. Shin, and J. Moon, "Rapid self-assembly of monodisperse colloidal spheres in an ink-jet printed droplet," *Chemistry of Materials*, vol. 16, no. 22, pp. 4212–4215, 2004.

[145] J. Park, J. Moon, H. Shin, D. Wang, and M. Park, "Direct-write fabrication of colloidal photonic crystal microarrays by ink-jet printing," *Journal of Colloid and Interface Science*, vol. 298, no. 2, pp. 713–719, 2006.

[146] H. Nam, K. Song, D. Ha, and T. Kim, "Inkjet printing based mono-layered photonic crystal patterning for anti-counterfeiting structural colors," *Scientific Reports*, vol. 6, no. 1, p. 30885, 2016.

[147] C. Monteux and F. Lequeux, "Packing and sorting colloids at the contact line of a drying drop," *Langmuir*, vol. 27, no. 6, pp. 2917–2922, 2011.

[148] V. L. Morales, J. Y. Parlange, M. Wu et al., "Surfactant-mediated control of colloid pattern assembly and attachment strength in evaporating droplets," *Langmuir*, vol. 29, no. 6, pp. 1831–1840, 2013.

[149] T. A. H. Nguyen, M. A. Hampton, and A. V. Nguyen, "Evaporation of nanoparticle droplets on smooth hydrophobic surfaces: the inner coffee ring deposits," *The Journal of Physical Chemistry C*, vol. 117, no. 9, pp. 4707–4716, 2013.

[150] L. Cui, Y. Li, J. Wang et al., "Fabrication of large-area patterned photonic crystals by ink-jet printing," *Journal of Materials Chemistry*, vol. 19, pp. 5499–5502, 2009.

[151] X. Yang, V. H. Chhasatia, J. Shah, and Y. Sun, "Coalescence, evaporation and particle deposition of consecutively printed colloidal drops," *Soft Matter*, vol. 8, no. 35, p. 9205, 2012.

[152] A. B. Pawar, M. Caggioni, R. Ergun, R. W. Hartel, and P. T. Spicer, "Arrested coalescence in Pickering emulsions," *Soft Matter*, vol. 7, no. 17, p. 7710, 2011.

[153] D. Soltman and V. Subramanian, "Inkjet-printed line morphologies and temperature control of the coffee ring effect," *Langmuir*, vol. 24, pp. 2224–2231, 2008.

[154] P. Kang, S. O. Ogunbo, and D. Erickson, "High resolution reversible color images on photonic crystal substrates," *Langmuir*, vol. 27, pp. 9676–9680, 2011.

[155] L. Wang, J. Wang, Y. Huang et al., "New tetraphenylethene-based efficient blue luminophors: aggregation induced emission and partially controllable emitting color," *Journal of Materials Chemistry*, vol. 22, no. 6, p. 21405, 2012.

[156] L. Bai, Z. Xie, W. Wang et al., "Bio-inspired vapor-responsive colloidal photonic crystal patterns by inkjet printing," *ACS nano*, vol. 8, pp. 11094–11100, 2014.

[157] S. Wu, B. Liu, X. Su, and S. Zhang, "Structural color patterns on paper fabricated by inkjet printer and their application in anticounterfeiting," *The Journal of Physical Chemistry Letters*, vol. 8, no. 13, pp. 2835–2841, 2017.

[158] H. Fudouzi and Y. N. Xia, "Colloidal crystals with tunable colors and their use as photonic papers," *Langmuir*, vol. 19, no. 23, pp. 9653–9660, 2003.

[159] J. Liu, G. Li, Z. Wu, Q. An, and Y. Qiu, "A poly(4-vinylpyridine)-based inverse opal," *Chemphyschem*, vol. 8, no. 9, pp. 1298–1302, 2007.

[160] J. Ge, J. Goebl, L. He, Z. Lu, and Y. Yin, "Rewritable photonic paper with hygroscopic salt solution as ink," *Advanced Materials*, vol. 21, no. 42, pp. 4259–4264, 2009.

[161] H. Gu, Y. Zhao, Y. Cheng et al., "Tailoring colloidal photonic crystals with wide viewing angles," *Small*, vol. 9, pp. 2266–2271, 2013.

[162] X. Du, T. Li, L. Li, Z. Zhang, and T. Wu, "Water as a colorful ink: transparent, rewritable photonic coatings based on colloidal crystals embedded in chitosan hydrogel," *Journal of Materials Chemistry C*, vol. 3, no. 15, pp. 3542–3546, 2015.

[163] J. Chen, P. Liu, X. Du, and Z. Xie, "Clickable colloidal photonic crystals for structural color pattern," *Langmuir*, vol. 34, no. 44, pp. 13219–13224, 2018.

[164] Z. Wang, J. Zhang, J. Xie et al., "Patterning organic/inorganic hybrid bragg stacks by integrating one-dimensional photonic crystals and macrocavities through photolithography: toward tunable colorful patterns as highly selective sensors," *ACS Applied Materials & Interfaces*, vol. 4, no. 3, pp. 1397–1403, 2012.

[165] H. S. Lee, T. S. Shim, H. Hwang, S.-M. Yang, and S.-H. Kim, "Colloidal photonic crystals toward structural color palettes for security materials," *Chemistry of Materials*, vol. 25, no. 13, pp. 2684–2690, 2013.

[166] J. Zhang, Y. Tian, W.-Q. Ji, Z. Zhu, C.-F. Wang, and S. Chen, "Ultrasensitive responsive photonic crystal films derived from the assembly between similarly charged colloids and substrates towards trace electrolyte sensing," *Journal of Materials Chemistry C*, vol. 4, no. 28, pp. 6750–6755, 2016.

[167] J. Ge and Y. Yin, "Magnetically tunable colloidal photonic structures in alkanol solutions," *Advanced Materials*, vol. 20, no. 18, pp. 3485–3491, 2008.

[168] H. Kim, J. Ge, J. Kim et al., "Structural colour printing using a magnetically tunable and lithographically fixable photonic crystal," *Nature Photonics*, vol. 3, no. 9, pp. 534–540, 2009.

[169] H. Hu, J. Tang, H. Zhong, Z. Xi, C. Chen, and Q. Chen, "Invisible photonic printing: computer designing graphics, UV printing and shown by a magnetic field," *Scientific Reports*, vol. 3, no. 1, p. 1484, 2013.

[170] H. Hu, Q.-W. Chen, J. Tang, X.-Y. Hu, and X.-H. Zhou, "Photonic anti-counterfeiting using structural colors derived from magnetic-responsive photonic crystals with double photonic bandgap heterostructures," *Journal of Materials Chemistry*, vol. 22, no. 22, pp. 11048–11053, 2012.

[171] H. Hu, H. Zhong, C. Chen, and Q. Chen, "Magnetically responsive photonic watermarks on banknotes," *Journal of Materials Chemistry C*, vol. 2, p. 3695, 2014.

[172] H. Wang, S. Yang, S. N. Yin, L. Chen, and S. Chen, "Janus suprabead displays derived from the modified photonic crystals toward temperature magnetism and optics multiple responses," *ACS Applied Materials & Interfaces*, vol. 7, no. 16, pp. 8827–8833, 2015.

[173] R. Xuan and J. Ge, "Photonic printing through the orientational tuning of photonic structures and its application to anticounterfeiting labels," *Langmuir*, vol. 27, no. 9, pp. 5694–5699, 2011.

[174] Y. Zhao, H. Gu, Z. Xie, H. C. Shum, B. Wang, and Z. Gu, "Bioinspired multifunctional janus particles for droplet manipulation," *Journal of the American Chemical Society*, vol. 135, no. 1, pp. 54–57, 2013.

[175] S.-S. Liu, C.-F. Wang, X.-Q. Wang et al., "Tunable Janus colloidal photonic crystal supraballs with dual photonic band gaps," *Journal of Materials Chemistry C*, vol. 2, pp. 9431–9438, 2014.

[176] M. Chen, Y. Tian, J. Zhang et al., "Fabrication of crack-free photonic crystal films via coordination of microsphere terminated dendrimers and their performance in invisible patterned photonic displays," *Journal of Materials Chemistry C*, vol. 4, no. 37, pp. 8765–8771, 2016.

[177] S. Ye, Q. Fu, and J. Ge, "Invisible photonic prints shown by deformation," *Advanced Functional Materials*, vol. 24, no. 41, pp. 6430–6438, 2014.

[178] D. Yang, S. Ye, and J. Ge, "From metastable colloidal crystalline arrays to fast responsive mechanochromic photonic gels: an organic gel for deformation-based display panels," *Advanced Functional Materials*, vol. 24, no. 21, pp. 3197–3205, 2014.

[179] X. Sun, J. Zhang, X. Lu, X. Fang, and H Peng, "Mechanochromic photonic-crystal fibers based on continuous sheets of aligned

carbon nanotubes," *Angewandte Chemie International Edition England*, vol. 54, no. 12, pp. 3630–3634, 2015.

[180] C. G. Schafer, C. Lederle, K. Zentel, B. Stuhn, and M. Gallei, "Utilizing stretch-tunable thermochromic elastomeric opal films as novel reversible switchable photonic materials," *Macromolecular Rapid Communications*, vol. 35, pp. 1852–1860, 2014.

[181] T. Ding, G. Cao, C. G. Schafer et al., "Revealing invisible photonic inscriptions: images from strain," *ACS Applied Materials & Interfaces*, vol. 7, no. 24, pp. 13497–13502, 2015.

[182] Y. Fang, Y. Ni, S. Y. Leo et al., "Direct writing of three-dimensional macroporous photonic crystals on pressure-responsive shape memory polymers," *ACS Applied Materials & Interfaces*, vol. 7, no. 42, pp. 23650–23659, 2015.

[183] Y. Fang, Y. Ni, S. Y. Leo, C. Taylor, V. Basile, and P. Jiang, "Reconfigurable photonic crystals enabled by pressure-responsive shape-memory polymers," *Nature Communications*, vol. 6, no. 1, p. 7416, 2015.

[184] S. Zeng, R. Li, S. G. Freire et al., "Wrinkling devices: moisture-responsive wrinkling surfaces with tunable dynamics," *Advanced Materials*, vol. 29, no. 24, p. 1700828, 2017.

[185] C. Zong, Y. Zhao, H. Ji et al., "Tuning and erasing surface wrinkles by reversible visible-light-induced photoisomerization," *Angewandte Chemie International Edition England*, vol. 55, no. 12, pp. 3931–3935, 2016.

[186] F. Li, H. Hou, J. Yin, and X. Jiang, "Near-infrared light–responsive dynamic wrinkle patterns," *Science Advances*, vol. 4, no. 4, p. 5762, 2018.

[187] M. X. Xie, F. G. Xu, L. Z. Zhang, J. Yin, and X. S. Jianet, "Reversible surface dual-pattern with simultaneously dynamic wrinkled topography and fluorescence," *ACS Macro Letters*, vol. 7, no. 5, pp. 540–545, 2018.

[188] Y. N. Xia and N. J. Halas, "Shape-controlled synthesis of metal nanocrystals," *MRS Bulletin*, vol. 30, no. 4, pp. 338–344, 2005.

[189] J. A. Fan, C. Wu, K. Bao et al., "Self-assembled plasmonic nanoparticle clusters," *Science*, vol. 328, no. 5982, pp. 1135–1138, 2010.

[190] M. Hu, J. Chen, Z. Y. Li et al., "Gold nanostructures: engineering their plasmonic properties for biomedical applications," *Chemical Society Reviews*, vol. 35, no. 8, pp. 1084–1094, 2006.

[191] Y. Cui, R. S. Hegde, I. Y. Phang, H. K. Lee, and X. Y. Ling, "Encoding molecular information in plasmonic nanostructures for anti-counterfeiting applications," *Nanoscale*, vol. 6, no. 1, pp. 282–288, 2014.

[192] Y. Cui, I. Y. Phang, Y. H. Lee, M. R. Lee, Q. Zhang, and X. Y. Ling, "Multiplex plasmonic anti-counterfeiting security labels based on surface-enhanced Raman scattering," *Chemical Communications*, vol. 51, no. 25, pp. 5363–5366, 2015.

[193] Y. Liu, Y. H. Lee, Q. Zhang, Y. Cui, and X. Y. Ling, "Plasmonic nanopillar arrays encoded with multiplex molecular information for anti-counterfeiting application," *Journal of Materials Chemistry C*, vol. 4, no. 19, pp. 4312–4319, 2016.

[194] D. Li, L. Tang, J. Wang, X. Liu, and Y. Ying, "Multidimensional SERS barcodes on flexible patterned plasmonic metafilm for anticounterfeiting applications," *Advanced Optical Materials*, vol. 4, pp. 1475–1480, 2016.

[195] X. Liu, J. Wang, L. Tang, L. Xie, and Y. Ying, "Flexible plasmonic metasurfaces with user-designed patterns for molecular sensing and cryptography," *Advanced Functional Materials*, vol. 26, no. 30, pp. 5515–5523, 2016.

[196] H. Kang, J. W. Lee, and Y. Nam, "Inkjet-printed multiwavelength thermoplasmonic images for anticounterfeiting applications," *ACS Applied Materials & Interfaces*, vol. 10, no. 7, pp. 6764–6771, 2018.

[197] K. Park, M. Park, H. S. Jang et al., "Highly secure plasmonic encryption keys combined with upconversion luminescence nanocrystals," *Advanced Functional Materials*, vol. 28, no. 21, p. 1800369, 2018.

[198] G. Bakan, S. Ayas, M. Serhatlioglu, C. Elbuken, and A. Dana, "Invisible thin-film patterns with strong infrared emission as an optical security feature," *Advanced Optical Materials*, vol. 6, no. 21, p. 1800615, 2018.

Hindawi
Advances in Polymer Technology
Volume 2019, Article ID 4273253, 25 pages
https://doi.org/10.1155/2019/4273253

Review Article

Nanoreinforcements of Two-Dimensional Nanomaterials for Flame Retardant Polymeric Composites: An Overview

Shaolin Lu, Wei Hong, and Xudong Chen

Key Laboratory for Polymeric Composite and Functional Materials of Ministry of Education, School of Chemistry, Sun Yat-sen University, Guangzhou 510275, China

Correspondence should be addressed to Wei Hong; hongwei9@mail.sysu.edu.cn

Received 19 June 2019; Revised 13 August 2019; Accepted 17 August 2019; Published 4 December 2019

Academic Editor: Gyorgy Szekely

Polymer materials are ubiquitous in daily life. While polymers are often convenient and helpful, their properties often obscure the fire hazards they may pose. Therefore, it is of great significance in terms of safety to study the flame retardant properties of polymers while still maintaining their optimal performance. Current literature shows that although traditional flame retardants can satisfy the requirements of polymer flame retardancy, due to increases in product requirements in industry, including requirements for durability, mechanical properties, and environmental friendliness, it is imperative to develop a new generation of flame retardants. In recent years, the preparation of modified two-dimensional nanomaterials as flame retardants has attracted wide attention in the field. Due to their unique layered structures, two-dimensional nanomaterials can generally improve the mechanical properties of polymers via uniform dispersion, and they can form effective physical barriers in a matrix to improve the thermal stability of polymers. For polymer applications in specialized fields, different two-dimensional nanomaterials have potential conductivity, high thermal conductivity, catalytic activity, and antiultraviolet abilities, which can meet the flame retardant requirements of polymers and allow their use in specific applications. In this review, the current research status of two-dimensional nanomaterials as flame retardants is discussed, as well as a mechanism of how they can be applied for reducing the flammability of polymers.

1. Introduction

Polymer materials, due to the continuous development of science and technology, have been widely used in all aspects of humankind's basic life necessities [1]. Due to the environmental adaptability of polymer materials, they have been widely used in construction, transportation, agriculture, electronics and electrical systems, textile, and other major economic areas. However, most of polymer materials are highly flammable, with fast combustion propagation rates and are not easily extinguished. A large portion of annual fires worldwide are related to polymer materials. According to statistics, 237,000 fires were reported in China in 2018, resulting in 1407 deaths, 798 injuries, and direct property losses amounting to 3.675 billion RMB [2]. Therefore, it is critical to research and develop effective flame retardants so as to reduce the risks of accidental fires, costly damage to buildings materials, and to widespread health and safety [3].

Polymer flame retardants are mainly divided into halogen and halogen-free categories. However, halogen flame retardants have limited use because they release toxic gases and corrosive smoke during combustion. Therefore, halogen-free compounds are currently being considered as promising flame retardants, based on their more environmentally friendly properties [4]. Numerous efforts have been made to find suitable halogen-free flame retardants polymers. Traditional inorganic flame retardants, including aluminium hydroxide [5, 6] and ammonium polyphosphate [7, 8], are usually added to polymers in large quantities, which can often lead to a decline in the processability and mechanical properties of these doped materials. Organic phosphorus flame retardants [9, 10] have high flame retardant efficiency, but most of these are liquids with poor heat resistance. In recent years, in addition to graphene, two-dimensional nanomaterials, such as hexagonal boron nitride (h-BN) [11–16], molybdenum disulfide (MoS_2) [17–20] and black phosphorus [21] (Figure 1), have also been developed, which has greatly expanded the properties and applications of two-dimensional materials in this realm. Notably, two-dimensional materials and their derivatives have been extensively studied as photocatalysts

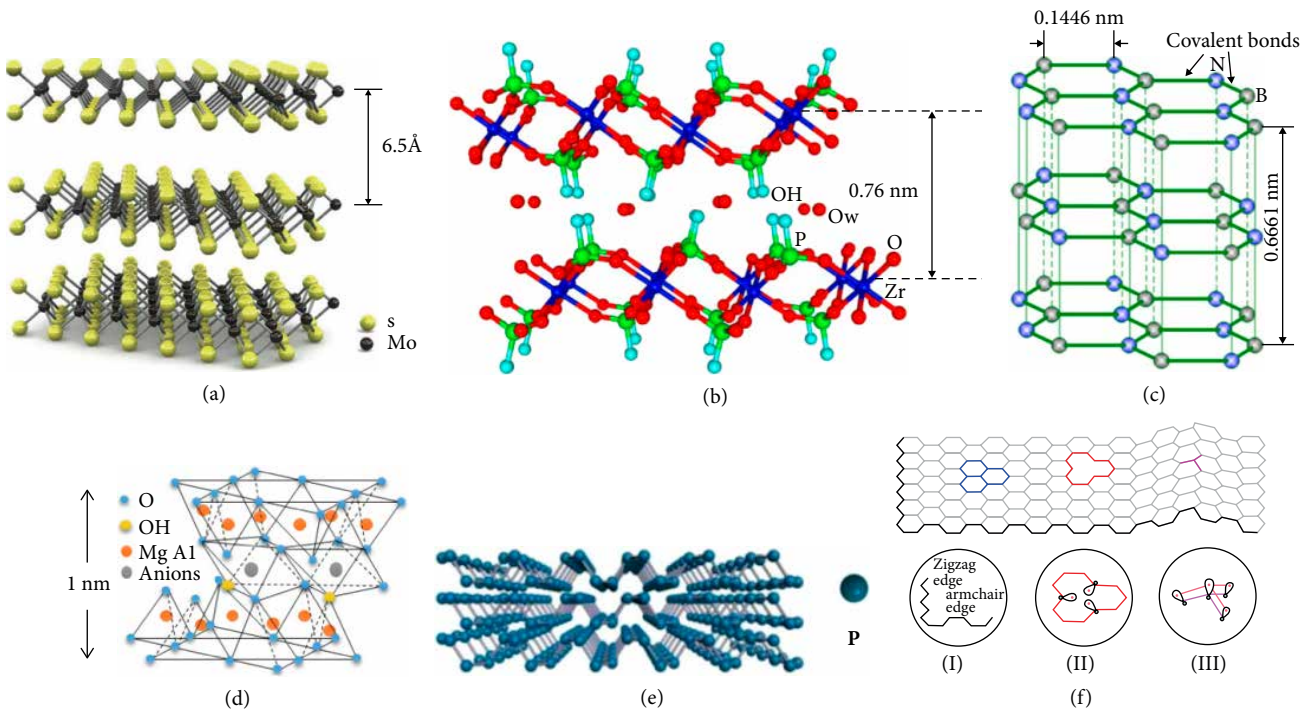

Figure 1: Structure of some two-dimensional nanomaterials. (a) Molybdenum disulfide [52]. (b) α-zirconium phosphate [53]. (c) Hexagonal boron nitride [54]. (d) Layered double hydroxide [55]. (e) Black phosphorus [56]. (f) Graphene with (I) Zigzag and armchair edges, (II) Monovacancy, (III) Local structure of a curved graphene sheet [57].

[22, 23], sensors [24], drug delivery vehicles [25], transistors [26], lithium ion batteries [27], water treatment agents [28], ion exchange [29], fuel cells [30], nanofiltration membranes [31], conductive inks [32], quantum dots [33], adsorbents [34] and supercapacitors [35]. Moreover, two-dimensional nanomaterials/polymer composites have also been investigated. Lin et al. [36] realized the intercalation of polythiophene into MoS_2 could be achieved by means of in situ polymerization of intercalated monomers. This method has contributed to enhancing the conductivity of composites at ambient temperature. Wang et al. [37] prepared a high-performance thermal interface material based on exfoliated boron nitride nanosheets (BNNSs) and polystyrene (PS) microspheres. Yan et al. [38] reported that g-C_3N_4-poly(3-hexylthiophene) polymer composites achieve enhanced hydrogen production using water as a substrate under visible light. Particularly, two-dimensional nanomaterials have attracted extensive attention in the field of flame retardant and smoke suppression due to their unique structure and properties [39].

Compared with zero-dimensional nanomaterials and one-dimensional nanomaterials, two-dimensional nanomaterials have emerged as a superior flame retardant option due to their layered structures, which have high thermal stability and can form a physical barrier in a polymer matrix [17, 40]. Additionally, homogeneous dispersion of a small amount of two-dimensional nanomaterials in polymers can effectively improve the mechanical properties of polymers [41, 42]. A well-dispersed layered structure in a polymer can not only greatly improve the thermal stability of a polymer [43, 44] but it can also further enhance the action of char residual in the inhibition of heat and mass transfer [39, 45]. It is believed that the biggest obstacle to the application of two-dimensional nanomaterials as flame retardant additives is the high cost and the low yield of the peeled sheet structures [46]. Recently, as the number of publications related to these emerging two-dimensional nanomaterials has increased dramatically, a large number of studies on the large-scale production of two-dimensional nanosheets have paved the way for flame-retardant applications [47, 48]. Yao et al. [49] reported a facile and scalable method for the preparation of monolayer and few-layer of BN, MoS_2, and graphene using a combination of low-energy ball milling and sonication. These prepared 2D nanosheets could be well dispersed in high concentrations of aqueous solutions as 1.2 mg/ml (for BN), 0.8 mg/ml (for Mos_2) and 0.9 mg/ml (for graphene). These advantages make it possible to apply high performance 2D nanomaterials/polymers at low cost with great potential, which is beneficial to the application of such new 2D nanomaterials in the flame retardant field. If suitable two-dimensional nanomaterials are selected for the application of specific polymers and the functionally controllable two-dimensional nano flame retardants associated are prepared via a simple and versatile method, the multi-functional application challenges of polymers can be overcome. It is well known that nano-fillers can easily achieve good flame retardant effects (below 6 wt%) at low load, meaning that they have potential industrial prospects [50, 51].

Recent progress and future development trends in flame-retardant materials using two-dimensional materials were summarized above. This also highlighted the effects of two-dimensional nanomaterials and the unique flame retardant mechanisms of sulfur, phosphorus, nitrogen, silicon, layered double hydroxide, and carbon skeleton.

2. The Flame-Retardant Mechanism of Two-Dimensional Nanomaterials

The combustion of polymer materials involves the evolution of combustible volatiles through decomposition in an oxygen-rich atmosphere. No matter which flame retardant is used, its flame-retardant mechanism is through one of the following two processes (or occasionally a combination of the two): (i) condensed phase or (ii) gas phase [58]. Figure 2 shows three possible processes of flame retardant mechanisms.

2.1. Condensed-Phase Mechanism

2.1.1. Physical Barrier. Two-dimensional nano-layered flame retardants can function as an effective insulating barrier, to inhibit mass loss during the thermal degradation process.

Shi et al. [61] reported a ternary PS/g-C_3N_4/aMWCNT assembled system using LBL technology, which led to the improved thermal stability of the PS matrix, including $T_{-10\%}$, $T_{-\max,}$ and char residue increased by 11°C, 20.0°C and 6.5%, respectively. The generation of total gaseous products was also distinctly inhibited by the ternary assembled systems. Moreover, the ternary assembled systems showed outstanding improvements in flame retardancy; i.e., HRR and THR decreased by around 45% and 47%, respectively. These enhancements were attributed to the LBL assembly strategy being conducive to building extremely tight barriers.

Hu et al. [62] synthesized a functionalized graphene oxide (FGO) that was grafted by hyper-branching as a flame retardant to reduce the combustion and toxicity of PS. The addition of 0.1% FGO significantly increased the $T_{-5\%}$ of PS-FGO0.1 nanocomposites compared to that of pure PS. This effect was attributed to the combined effect of the physical barrier and the capture of oxygen molecules and free radicals by FGO layers under atmospheric air. This enhanced barrier effect was also demonstrated by a suppressed mass loss rate, implying the retardation of mass transfer from nanocomposites to the flame zone.

2.1.2. Formation of a Continuous Char Layer. During the combustion process, a compact and stable char layer is formed on the surface of a polymer, which acts as a thermal insulating barrier to heat and separates oxygen from burning materials, thus preventing mass and heat transfer, reducing the heat release rate and total amount of flammable volatile gases after the char layer is established.

Xie et al. [63] synthesized a ZrP-decorated macromolecular charring agent (ZrP-d-MCA), which was then introduced into polypropylene. A mechanistic study showed that ZrP-d-MCA/APP effectively involved PP incorporation into the charring reaction, forming a compact and firm intumescent char layer with outstanding barrier properties. ZrP first catalyzed the carbonization of MCA on its surface, forming closed micro-nano char-cages, which then trapped the degradation products of PP and further catalyzed them into a thermostable graphitized char.

Feng et al. [64] proposed a ternary thermal interface material based on epoxy resin (EP), silver nanowires (AgNWs), and a small amount of flame-retardant functionalized graphene (GP-DOPO). Char analysis confirmed that the char's yield and quality (integrality and compact degree) were increased dramatically by incorporating GP-DOPO into EP/AgNWs, due to the strong catalytic charring effect. The increased organic chars not only protected the AgNWs from melting and wicking action but also connected the AgNWs network to form a protective char layer with a compact and robust structure, which acted as a barrier to prevent the transfer of heat, oxygen, and flammable volatile products between the inside and outside of the polymer melt, thus improving the flame retardancy of the EP/AgNWs/GP-DOPO composite.

2.2. Gas-Phase Mechanism

2.2.1. Dilution of Oxygen by Inert Gases. The gas dilution flame retardant mechanism is typified by a large amount of nonflammable gases being produced during the decomposition process of a flame retardant at high temperatures, and these nonflammable gases can prevent the combustion of a polymer by diluting the oxygen concentration.

Wang et al. [65] reported Cardanol-BS modified layered double hydroxide (M-LDH) being synthesized by a coprecipitation method, and its subsequent incorporation into EP at different loadings. The degradation gaseous products could be mainly divided into two categories: one was inflammable gases, such as water vapor and CO_2, and the other was flammable gases, such as carbonyl, aromatic compounds, and esters. The maximum absorbance intensity of inflammable volatiles for EP/LDH-6% and EP/m-LDH-6% composites was much higher than that for pure EP, which effectively diluted the concentration of flammable volatiles.

Xu et al. [66] reported a hybrid RGO-LDH/Mo system through RGO-LDH modified by heptaheptamolybdate ($Mo_7O_{24}{}^{6-}$) via ion exchange method, and introduced it into polyurethane elastomer (PUE). Compared with pristine PUE, the pHRR of PUE1 was decreased by 36.4% because the LDH layer and carbon residue inhibited the volatilization of combustible gases produced during polymer decomposition, isolated oxygen, and reduced the thermal radiation of materials. At the same time, due to the generated water vapor, the temperature was lowered and the combustion process of the composites was delayed, so the heat was absorbed in the endothermic decomposition process of LDH.

2.2.2. Gas Phase Free Radical Inhibition. Flame retardants can also capture and annihilate active free radicals, thus preventing and inhibiting free radical chain reactions, reducing the flame burning rate and extinguishing a flame.

Yang et al. [67] used organophilic α-zirconium phosphate (α-ZRP, OZRP) as a synergistic agent with aluminium hydroxide (ATH), and introduced it into low-density polyethylene and ethylene-vinyl acetate (LDPE/EVA) blends. As LDPE/EVA/(ATH, OZrP) hybrids burned, ATH first decomposed rapidly with the release of hydration water. This endothermic decomposition lowers the temperature of the reaction, and the released water vapor dilutes flammable volatile gasses. Second, a small amount of phosphorus monoxide (PO•) produced by the combustion of OZrP can quench active radicals produced by the burning of the gas phase, while the exfoliated OZrP layers can efficiently promote the formation of compact

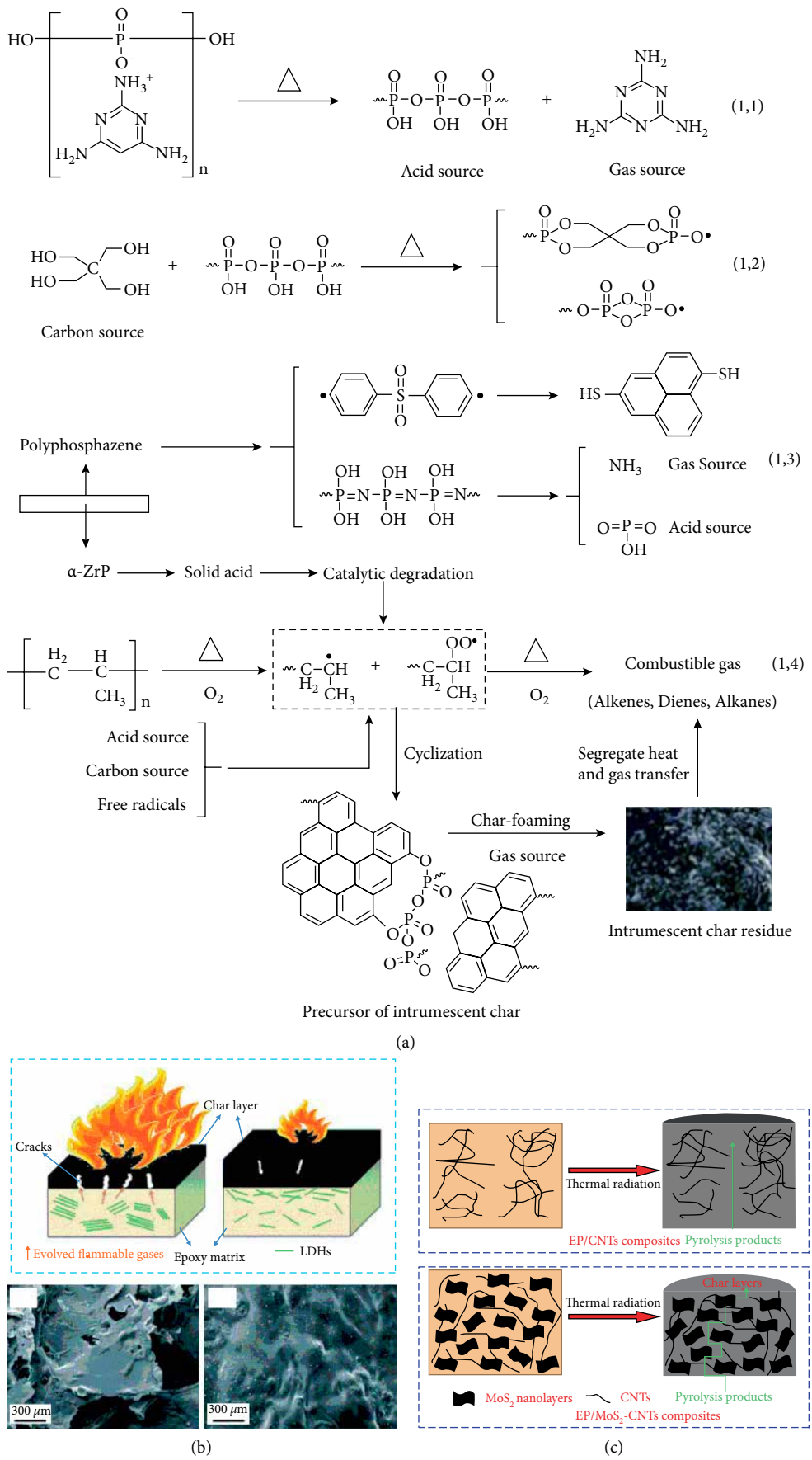

Figure 2: Flame retardant mechanisms of partial two-dimensional materials. (a) The free radicals of PP chain scission are inhibited, and then a coherent, thermally stable, and tough swollen char is formed under the catalysis of solid acid sites on the surface of a-zrp core [59]. (b) LDHs catalyze the formation of a thick char layer on the surface of EP [60]. (c) A MoS_2-CNT hybrid acts as a physical barrier in an EP [19].

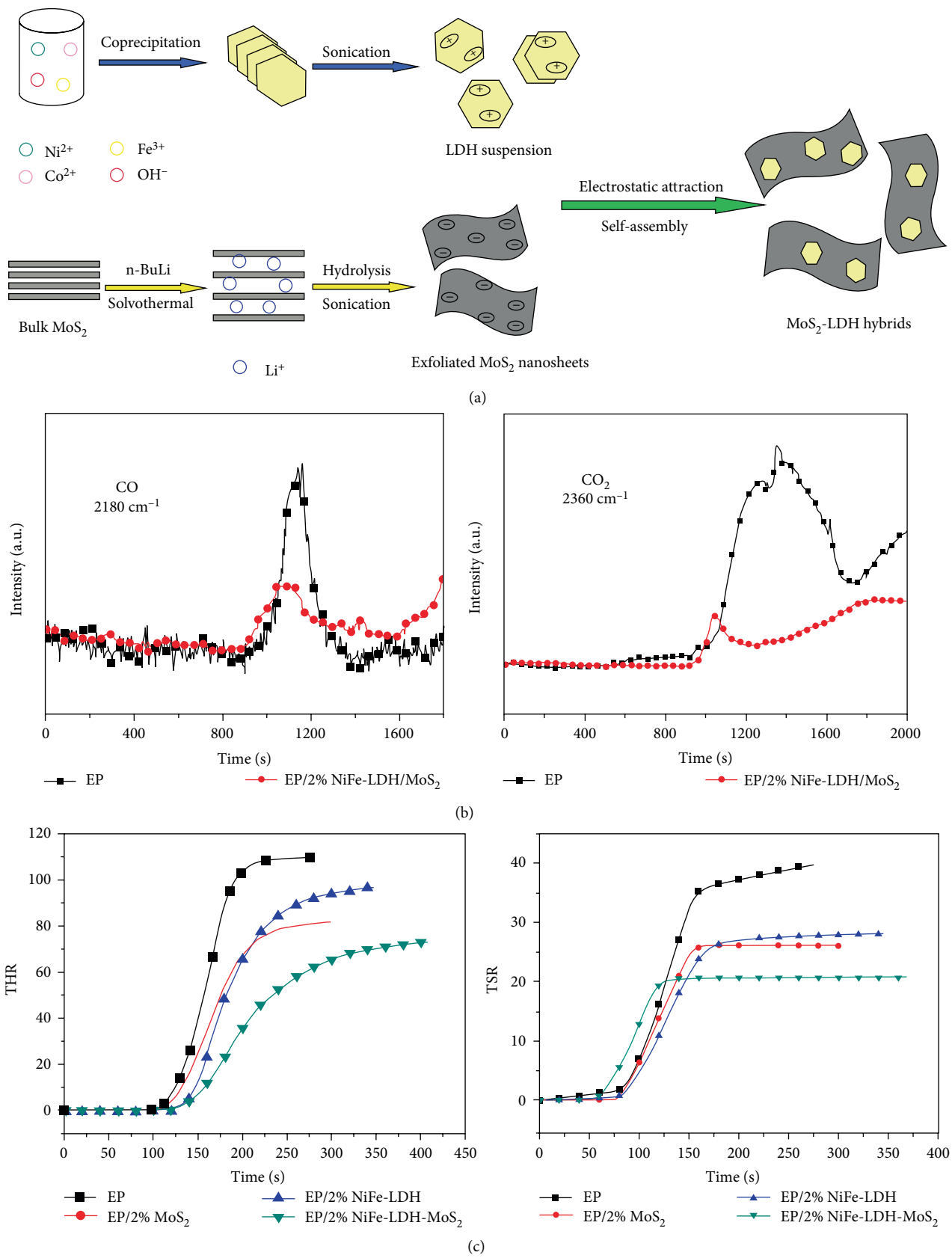

FIGURE 3: (a) Illustration of the preparation of MoS_2-LDH nanohybrids via a self-assembly method. (b) Intensity of characteristic peaks for pyrolysis products of EP and EP/2% NiFe-LDH-MoS_2 composites. (c) The TSP and THR of EP and EP composites. Adapted from [39].

charred layers in the condensed phase and hinder the diffusion of oxygen and flammable volatile products.

Ren et al. [68] prepared black phosphorene/graphene (BP/G) composites by high-pressure nano-homogenizer machine (HNHM) and distributed them uniformly in WPU. The addition of graphene could reduce pHRR by 21.2%, and the addition of BP/G could reduce pHRR by 48.18% when compared with the pristine WPU. This was because the special layered structure of graphene and BP had barrier effects during degradation process, which could prevent materials from oxygen and heat transfer. In addition, BP could form PO• free radicals, diffuse in surrounding gases, and react with H• or OH• free radicals produced by polymer under combustion, hence reducing the flame.

3. Research Progress on Polymer/Two-Dimensional Nanomaterial Flame Retardant Composites

3.1. Sulfur-Containing Compounds. Various 2D nanosheets, such as molybdenum disulfide (MoS_2) and tungsten disulfide (WS_2), have attracted tremendous attention due to the unusual properties associated with their ultrathin nanosheet structures. MoS_2 is composed of three stacked atomic layers (S-Mo-S) held together by van der Waals forces [17]. Mechanically exfoliated atomically thin sheets of WS_2 have been shown to exhibit high in-plane carrier mobility and electrostatic modulation of conductance similar to MoS_2 [69]. These have been extensively studied in the field of polymer flame retardation because of their outstanding mechanical properties, which can be attributed to their small size, typically in the range of 40–180 nm, and their chemical inertness [70].

On the one hand, MoS_2 has been used for enhancing the thermal, flame-retardant, and mechanical properties of polymer composites [18–20, 71–83] due to its small size and high thermal stability. For instance, cellulose nanofibers (CNFs) were nano-wrapped with ultrathin 1T phase MoS_2 nanosheets via chemical crosslinking to produce an aerogel. Thermal and combustion characterization revealed highly desirable properties (thermal conductivity $k = 28.09\,\mathrm{mW\,m^{-1}\,K^{-1}}$, insulation R value = 5.2, limit oxygen index (LOI) = 34.7%, total heat release = $0.4\,\mathrm{MJ\,m^{-2}}$). Considering the inherently low density of this material, there was significant opportunity for its use in a number of insulating applications [72]. Wang et al. reported the synthesis of MoS_2 nanosheets via a "thiol-ene" click reaction between defect-rich MoS_2 nanosheets with sulfydryl groups and ene-terminated hyperbranched polyphosphate acrylate (HPA), and characterized these nanosheets by FTIR and XPS to confirm their covalent functionalization through C–S bonds. The combustion behavior of unsaturated polyester resin (UPR) composites was also investigated, demonstrating an obvious reduction of 43.2% and 39.6% in Peak Heat Release Rate (pHRR) and Total Heat Release (THR), respectively [74]. To solve the problem of homogeneous dispersion of MoS_2 nanosheets in a polymer matrix and exact interface control, hierarchical polystyrene@MoS_2 core-shell structures were constructed by combining latex technology and self-assembly of oppositely charged MoS_2 nanosheets onto the surface of PS spheres. This method proved to be an efficient and facile approach to fabricate polymer/MoS_2 nanocomposites with good dispersion and improved properties [75].

On the other hand, MoS_2 and its derivatives have been used for smoke suppression of various polymers, including polystyrene [17, 84], polyvinyl alcohol [85], epoxy [86–89], polyurethane [90], and polyamide 6 [91]. For example, Zhou et al. [86] reported LDH/MoS_2 hybrids were facilely prepared by self-assembly of exfoliated MoS_2 nanosheets and LDH via electrostatic forces. This approach endowed excellent fire resistance to an epoxy matrix, which was reflected by the significantly reduced peak heat release rate, total heat release, and total smoke production (Figure 3). Qiu et al. [88] showed that polyphosphazene nanoparticles (PPN) functionalized with MoS_2 nanosheets have been successfully fabricated, followed by high temperature polymerization. The incorporation of P and N atoms efficiently reduced the stacking of MoS_2 nanolayers and formed a large number of active sites. It was also demonstrated that the introduction of MoS_2@PPN nanohybrids significantly improved the flame retardancy of EP. Feng et al. [91] used supramolecular self-assembly to prepare sandwich-like melamine cyanurate/MoS_2 sheets as hybrid flame retardants for PA6. The introduction of MoS_2 sheets functioned not only as a template to induce the formation of two-dimensional melamine cyanurate capping layers, but also as a synergist to generate integrated flame-retarding effects in the hybrid sheets, in addition to a high-performance smoke suppressor to reduce the fire hazards of PA6 materials.

WS_2 is one of the most commonly used compounds in semiconductor TMS's. In recent years, materials such as WS_2 have attracted increased attention in the field of nanocomposite fillers, due to their high thermal and mechanical properties [69, 92]. Díez-Pascual et al. prepared an inorganic fullerene-like tungsten disulfide (IF-WS_2) lubricant, and then used this to manufacture PPS/IF-WS_2/CF laminates via melt-blending and hot-press processing. These multiscale laminates exhibited higher ignition points and notably reduced pHRR compared to PPS/CF alone. The coexistence of micro- and nano-scale fillers resulted in synergistic effects that enhanced the stiffness, strength, thermal conductivity, and flame retardancy of the matrix [70]. Wenelska et al. reported WS_2 functionalized with metal oxides (iron oxide and nickel oxide) as a filler for PEs. This showed that composites can provide a certain physical barrier and inhibit the diffusion of heat and gaseous products during combustion [69].

3.2. Phosphorus-Containing Compounds. Phosphorus-containing compounds, including α-zirconium phosphate (α-ZrP), black phosphorus (BP), and vanadium dehydrated phosphate ($VOPO_4$), may replace halogenated variants that are still widely used in flame retardants. Phosphorous flame retardants can play a role in both the gas phase and condensed phase extinguishing mechanisms during a fire [3]. In the following, different P-containing flame retardants are explored in detail.

3.2.1. α-Zirconium Phosphate. α-ZrP is a type of solid acid, which represents a wide range of chemical substances that are able to accept electrons and create coordinate bonds. The

dehydrogenation of a polymer occurs and these unsaturated sites then lead to crosslinking and ultimately graphitization. Therefore, solid acid-type α-ZrP can play an effective role as a crosslinking catalyst through the catalysis of carbonization of the polymer itself during thermal decomposition [93]. However, two main subjects have to be addressed before their further applications as flame retardants: the inherent agglomeration of nano-sized α-ZrP and their incompatibility with polymers [59, 63, 67, 93–114].

Planar-like α-ZrP particles have been modified with a kind of cyclophosphazene derivative (named HAC) by a three-step hybridization method [113]. The combination of (intumescent flame retardant) IFR and HAC can significantly improve the yield and graphitization of these residues, make them more stable, compact, and continuous, and allowing the inhibition of the thermo-oxygen contact of the underlying poly (vinyl alcohol) (PVA). In addition, the mechanical properties of such composites could be enhanced and toughened by specific HAC content.

Xie et al. [63] reported a macromolecular charring agent (MCA) decorated with zirconium phosphate nanosheets. This was then combined with ammonium polyphosphate (APP) to reduce the flammability of polypropylene. The limiting oxygen index (LOI) of PP/ZrP-d-MCA/APP reached 32.5% and a UL-94-V0 rating when the content of ZrP-d-MCA and APP was 5%wt and 15%wt, respectively. The flame-retardant mechanism of ZrP-d-MCA/APP was further studied. It was shown that a ZrP nanosheet could effectively catalyze the carbonization reaction of MCA to form a closed micro-nano carbon cage during the combustion process.

Fu et al. [114] reported the synthesis of a hybrid cardanol-derived zirconium phosphate (CZrP) from the renewable resource cardanol. Their results showed that the enlarged interlayer spacing of CZrP facilitated the homogeneous dispersion of the nano-additive in an epoxy resin. The suppressed fire hazards of EP were attributed to the physical barrier effect induced by the 2D-CZrP. In addition, the tensile strength and the elongation at break were enhanced simultaneously due to the reinforcing effect of the inorganic platelet and the plasticizing effect of the long alkyl chains in this unique hybrid.

3.2.2. Black Phosphorus and Dehydrated Vanadyl Phosphate. Mono or multi-layer BP is a two-dimensional nanomaterial with distinct physical/chemical properties due to dimensionality effects [21, 68]. BP can catalyze the formation of char and capture free radicals, and its unique layered structure can also serve as a physical barrier for insulation from heat and oxygen during the combustion process [115]. For example, Qiu et al. [115] reported a stable cross-linked polyphosphazene-functionalized BP (BP-PZN) synthesized in the presence of air. The BP-PZN was developed with abundant -NH_2 groups via a one-pot polycondensation of 4,4′-diaminodiphenyl ether and hexachlorocyclotriphosphazene on the surface of BP nanosheets. Results demonstrated that the introduction of 2 wt% BP-PZN distinctly improved the flame-retardant properties of EP. For instance, there was a 59.4% decrease in pHRR and a 63.6% reduction in THR. The diffusion of pyrolysis products from an EP during combustion was obviously suppressed after incorporating BP-PZN nanosheets. Digital photos, SEM, and Raman spectra of char residue from such an EP are shown in Figure 4.

$VOPO_4$ is a new two-dimensional graphene material with a typical layered structure where $VOPO_4$ has been formed by connecting VO_6 octahedra with vertex-sharing with phosphate PO_4 tetrahedra. An ultrathin $VOPO_4$ nanosheet is expected to improve the thermal stability, flame retardancy, and mechanical properties of a polymer. In addition, $VOPO_4$ nanosheets can also catalyze the dehydrogenation of a polymer and promote the carbonization of a polymer [116]. For example, a $VOPO_4$ ultrathin nanosheet was synthesized by a simple refluxing method and then modified with typical organic surfactants (VOP) [117]. Afterwards, this nanosheet was incorporated into PS for reducing fire hazards. With a loading of 1 wt% of modified VOP, $T_{5\%}$, $T_{10\%}$, $T_{50\%}$, and T_{max} values increased 15, 22, 29, and 33°C, respectively. Furthermore, the presence of VOP nano-sheet reduced the decomposition rate of PS and increased the char residue.

3.3. Nitrogen-Containing Compounds. As a structural analogue of graphene, monolayer 2D hexagonal boron nitride (h-BN), with the alternate use of boron and nitrogen atoms instead of carbon atoms in the 2D conjugate layers, has attracted increased attention due to its high-temperature stability, excellent thermal conductivity, superior chemical inertness, and low friction coefficients [16, 118]. Considering the ionic properties of the B–N bond in the boron nitride layer, which is different from the covalent C–C bond of graphene, boron nitride nanosheets have outstanding resistance to oxidation (the degradation temperature in air is 840°C) and corrosion [119]. Most notably, boron nitride with a 2D morphology and high thermal resistance can be used as an effective nano flame retardant to improve the thermal stability, thermal conductivity, and flame retardancy of a polymer.

It is believed that H–BN can be used as a rigid barrier for the transfer of decomposed fragments due to its highly thermal stability via its layered structure, thus improving the fire safety of polymers [11–16, 42, 51, 118–133]. Zhang et al. [16] reported a multifunctional CPBN that was successfully prepared via the wrapping of a phytic acid doped polypyrrole shell, followed by the adsorption of copper ions. The significant suppression of CO and HCN release could be observed from a TG-IR test. Tensile tests showed that the addition of CPBN was beneficial to the mechanical properties of TPU.

Additionally, super paramagnetic zinc ferrite (ZF) has been used to modify the surface of boron nitride nanosheets (BNN) via a typical solvothermal method [133]. The prepared ZF-BNNS nanofiller was then loaded in an EP and placed in a weak magnetic field (0.05 T) to achieve an orderly orientation of the EP matrix. Results showed that this weak magnetic field could adjust the orderly arrangement of ZF-BNNS nanofillers in an EP matrix, and well-ordered ZF-BNNS nanofillers were superior to randomly distributed ZF-BNNS nano-fillers in enhancing EP fire resistance.

With the rapid development of electronic devices, there is an increasing demand for high heat-dissipation polymers [13, 118, 126, 129]. We found that a high thermal conductivity (TC) is also an important factor for the high flame retardancy

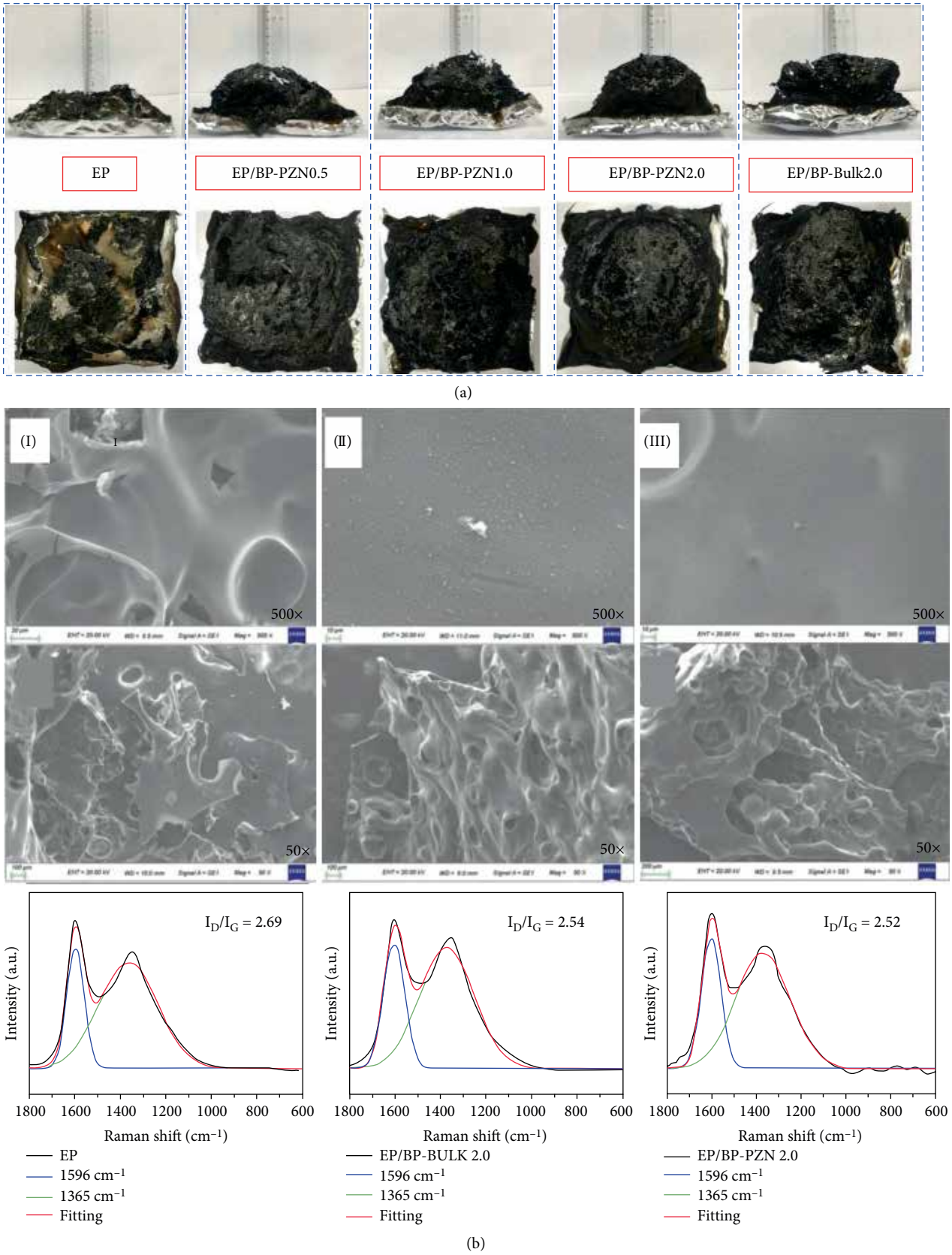

Figure 4: (a) Micrographs of external residues from a top and side view for EP and its nanocomposites. (b) SEM images and Raman spectra of external and interior char residues for (I) EP, (II) EP/BP-Bulk2.0, and (III) EP/BP-PZN2.0 nanocomposites. Adapted from [115].

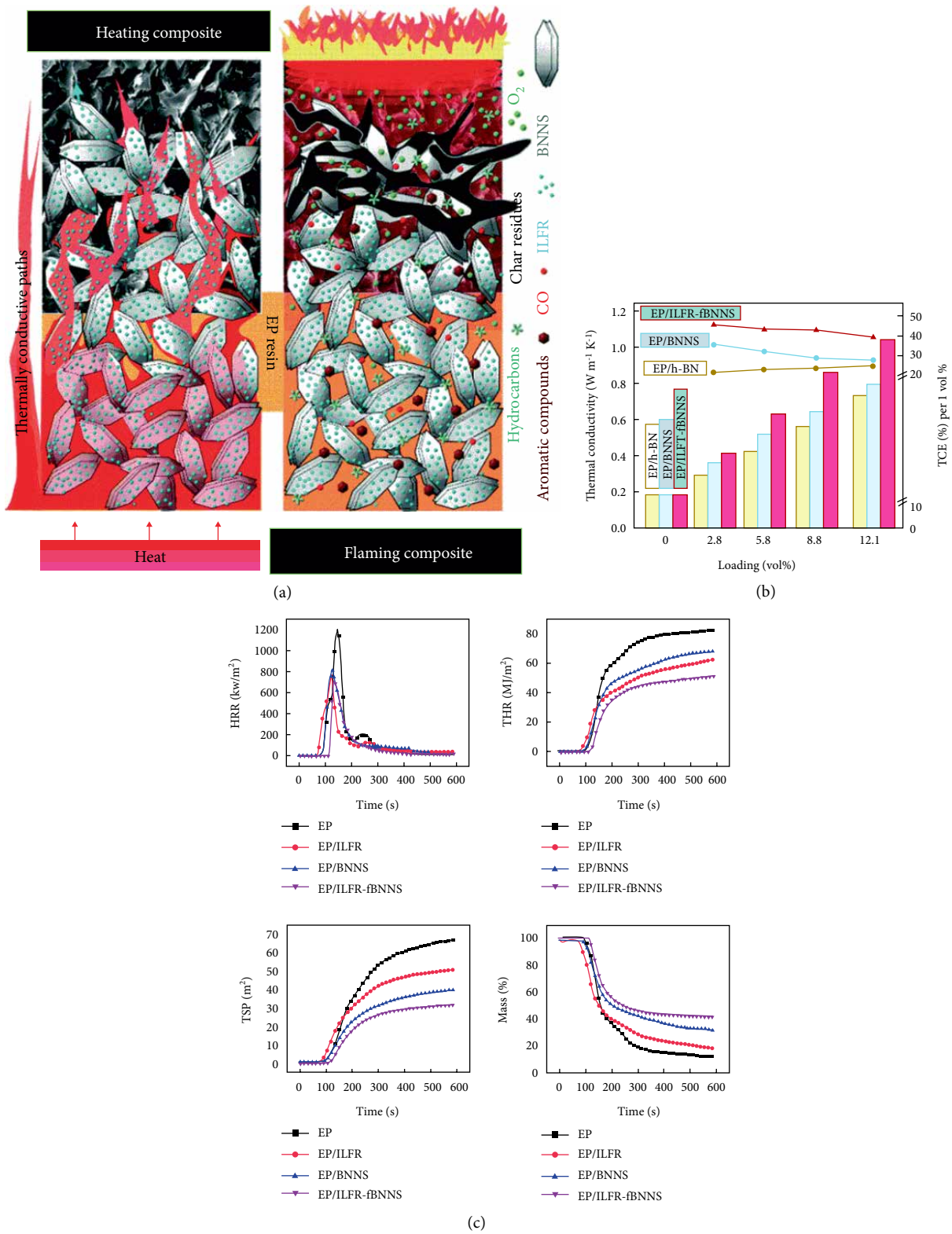

Figure 5: (a) Schematic illustration of thermal conduction and flame retardation mechanisms of EP/ILFR-fBNNS nanocomposites. (b) Thermal conductivity of EP/h-BN, EP/BNNS, and EP/ILFR-fBNNS composites. (c) The HRR, THR, TSP, and mass loss versus time curves of neat EP, EP/ILFR, EP/BNNS 12.1% vol and EP/ILFR-fBNNS 12.1% vol samples obtained from cone calorimeter tests. Adapted from [118].

of boron nitride nanosheets. Non covalent ionic liquid flame retardant-functionalized boron nitride nanosheets (ILFR-fBNNSs) were used as a multifunctional nano-additive for fabricating EP-based nanocomposites with both superior TC and flame retardancy [118]. These ILFR-fBNNS trigger resin crosslinking at a given temperature, while conferring

Table 1: Formulations and flammability test results of TPU composites [45].

Sample	TPU [g]	APP [g]	CS [g]	ACS [g]	OMMT [g]	LOI [%]	UL-94 rating
TPU	100	0	0	0	0	20.8 ± 0.3	None
TPU/APP/CS	90	5	5	0	0	26.6 ± 0.2	None
TPU/APP/ACS	90	5	0	5	0	28.6 ± 0.1	V-2
TPU/APP/ACS/ OMMT	90	4.5	0	4.5	1	29.0 ± 0.1	V-0

Table 2: Burning parameters of two-dimensional nanomaterials/polymer composites.

Polymer matrix	Recipes	pHRR	THR	TSR	Year and reference
EP	2 wt% MoS_2 @PPN	−30.7%	−23.6%	−43.0%	2018 [88]
PE	2 wt% WS_2/Ni_2O_3	−34.9%	−17.0%	/	2018 [69]
EP	6 wt% MCPA-ZrP	−42.2%	−21.4%	/	2018 [114]
EP	2 wt% BP-PZN	−59.4%	−63.6%	−32.0%	2019 [115]
PS	3 wt% C-VOP	−48.3%	−43.6%	/	2017 [117]
EP	3 wt% ZF-BNNS	−48.5%	/	−6.5%	2019 [133]
PP	4 wt% Co-OMt/19 wt%IFR	−63.8%	−17.6%	/	2017 [143]
EP	7 wt% fCD-DBS-Ph-LDH	−72.3%	/	−63.7%	2016 [180]
EP	2 wt% RGO-LDH/$CuMoO_4$	−47.6%	−28.5%	−38.0%	2018 [191]
PS	4 wt% g-C_3N_4/DAHPi	−42.8%	−20.8%	/	2017 [233]
EP	2 wt% ZIF-67/RGO-B	−65.1%	−41.4%	−37.6%	2019 [223]
EP	2 wt% MoS_2-CNTs	−26.4%	−31.3%	/	2015 [19]

improvements in the dispersion and interfacial adhesion, thereby forming a thermally conductive network with reduced interfacial phonon scattering and a high-efficiency nano-barrier network acting synergistically with ILFR-induced char residues during thermal degradation. Figure 5 shows the relationship between thermal conductivity and flame retardancy.

Liu et al. [13] demonstrated the use of exfoliated h-BN nanosheets as a high-performance, binder-free fire-resistant coating for wood. The surface of a wood substrate remained intact after exposure to fire. The anisotropic thermal conductivity and low thermal diffusivity and effusivity of h-BN make it an excellent wood protection coating.

3.4. Silicon-Containing Compounds. Among nanofillers, layered silicates are the most widely used for preparing polymer nanocomposites because they are readily available and well characterized. Montmorillonite (MMT) is a crystalline 2 : 1 layered clay mineral where a central alumina octahedral sheet is sandwiched between two silica tetrahedral sheets, and it has been shown to be safe in animals or humans [134, 135].

There are various methods that have been used to realize flame-retardant polymer/montmorillonite nanocomposites, including intercalation, synergy, organic modification, hybridization, layer-by-layer assembly, and self-assembly [134–152]. Inspired by nacre, Xie et al. [151] developed a super-efficient fire-safe nanocoating based on carboxymethyl chitosan and modified MMT via one-step self-assembly. The nanocoating possessed a well-arranged nacre-like hierarchical microstructure, exhibiting high transparency and specific nacre-like iridescence. Most importantly, the peak heat release rate, total heat release, peak smoke production rate, and total smoke production of polyurethane foam were decreased by 84.1%, 89.4%, 84.4%, and 95.2%, respectively. A polyimide (PI) composite aerogel was also prepared by freeze-drying with graphene and MMT as additives [141]. Through the strong interaction between the two components, GO/MMT complexes could be synergistically dispersed in water and have good dispersion in a PI matrix, thus endowing the composite aerogel with enhanced mechanical, thermal, and flame-retardant properties. In order to improve the flame retardant performance of IFR/PP composites, OMMT intercalation cobalt compounds (Co-OMt) have been prepared and modified using acidified chitosan to further expand the interlayer spacing of MMT [143]. CO-OMT/IFR/PP nanocomposites have been prepared by a melt blending method. With addition of 4% mass Co-OMt, 4% mass Co-OMt/IFR/PP nanocomposites have surpassed a UL-94 V-0 rating, with an LOI value as high as 32.1%.

The use of MMT as a synergic additive to flame retardants for designing polymers with better flame-retardant properties has already been extensively studied [45, 153–166]. The effect of APP/zinc borate (ZB) for making highly efficient flame retardants and ceramics of ethylene-vinyl acetate/mica powder/organic modified montmorillonite (EVA/MP/OMMT) composites has been shown [166]. In a fire test, the EVA/MP/OMMT/APP/ZB system displayed obvious flame-retardant features, showing a much lower THR and TSR than pure EVA. Zhang et al., [45] reported a flame retardant (ACS) prepared by crosslinking chitosan with bis-(4-formylphenyl)-phenyl-phosphonate. Flame-retardant TPU composites were then prepared by melt blending of ACS, APP, and OMMT. For TPU

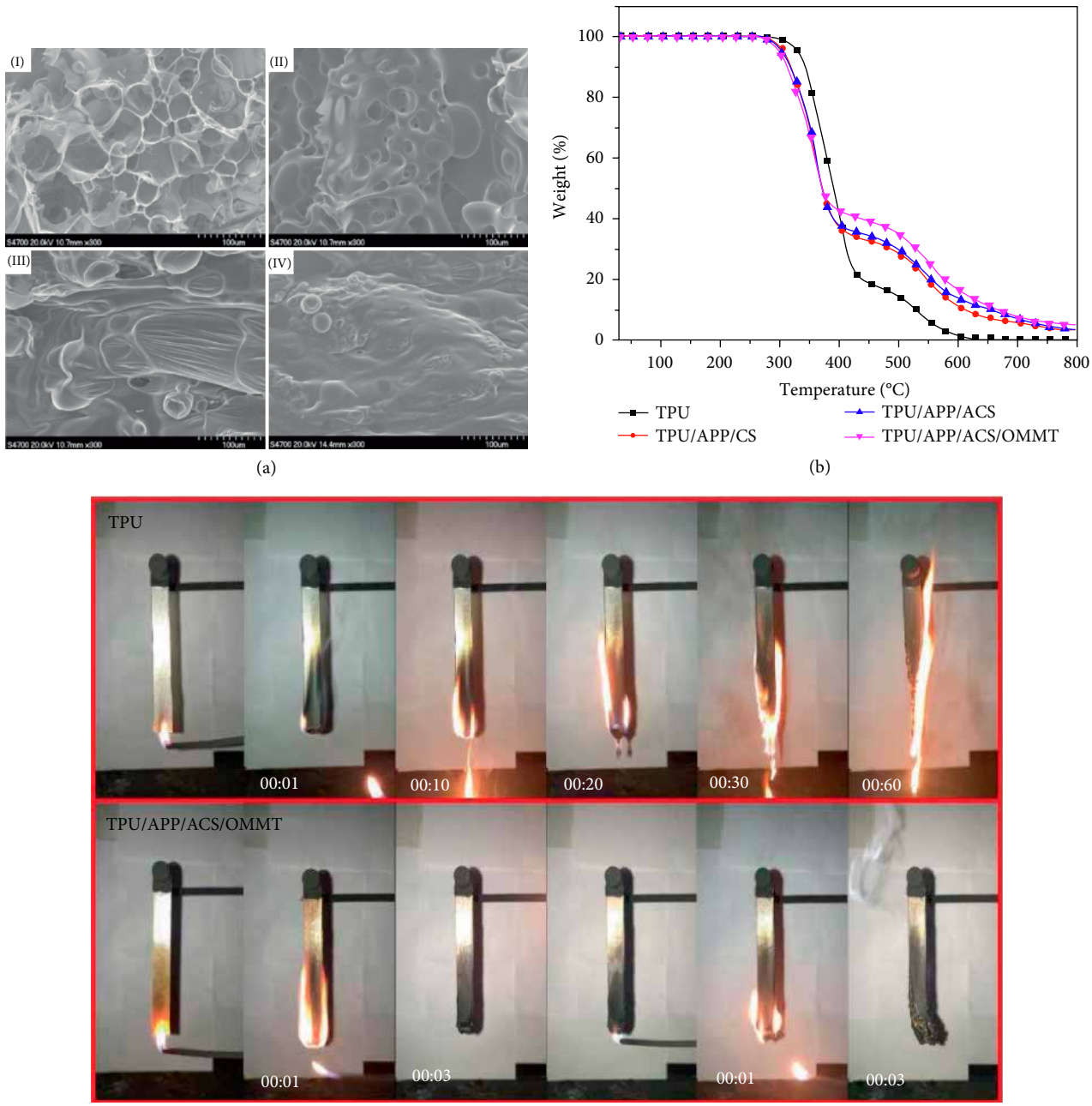

Figure 6: (a) SEM images of the surfaces residues of (I) neat TPU, (II) TPU/APP/CS, (III) TPU/APP/ACS, and (IV) TPU/APP/ACS/OMMT. (b) TGA curves of TPU composites in air. (c) Screenshots from UL-94 test videos of TPU and TPU/APP/ACS/OMMT samples. Adapted from [45].

samples containing 10% flame retardant, the LOI increased from 20.8 to 29.0, the UL-94 rating increased from no to V-0, and the pHRR decreased from 1090 to 284 kW/m^2, respectively. The test results for added OMMT and non-added samples are shown in Figure 6 and Table 1.

3.5. Layered Double Hydroxides. Layered double hydroxides (LDH) are a kind of synthetic anionic clay with host and guest nano-layered materials, which contain positively charged metal hydroxide nanosheets, intercalated anions, and water molecules [167]. LDHs can be represented by the chemical formula $[M_{1-x}{}^{2+}\ M_x{}^{3+}(OH)_2]^{x+}\cdot[A_{x/n}{}^{n-}\cdot yH_2O]^{x-}$, where M^{2+}, M^{3+}, and A^{n-} represent divalent metal cations, trivalent metal cations, and an inorganic or organic anion with negative charge n, respectively [168]. When used as flame retardant for polymer materials, it has been shown that the flame-retardant mechanism of LDHs are via the "barrier effect" of nano-layers, inert gas dilution of oxygen and the formation of ceramic-like materials [169].

LDHs can be directly used as flame retardant additives because of their unique chemical properties and layered structures [170–177]. For example, flexible polyurethane foam with

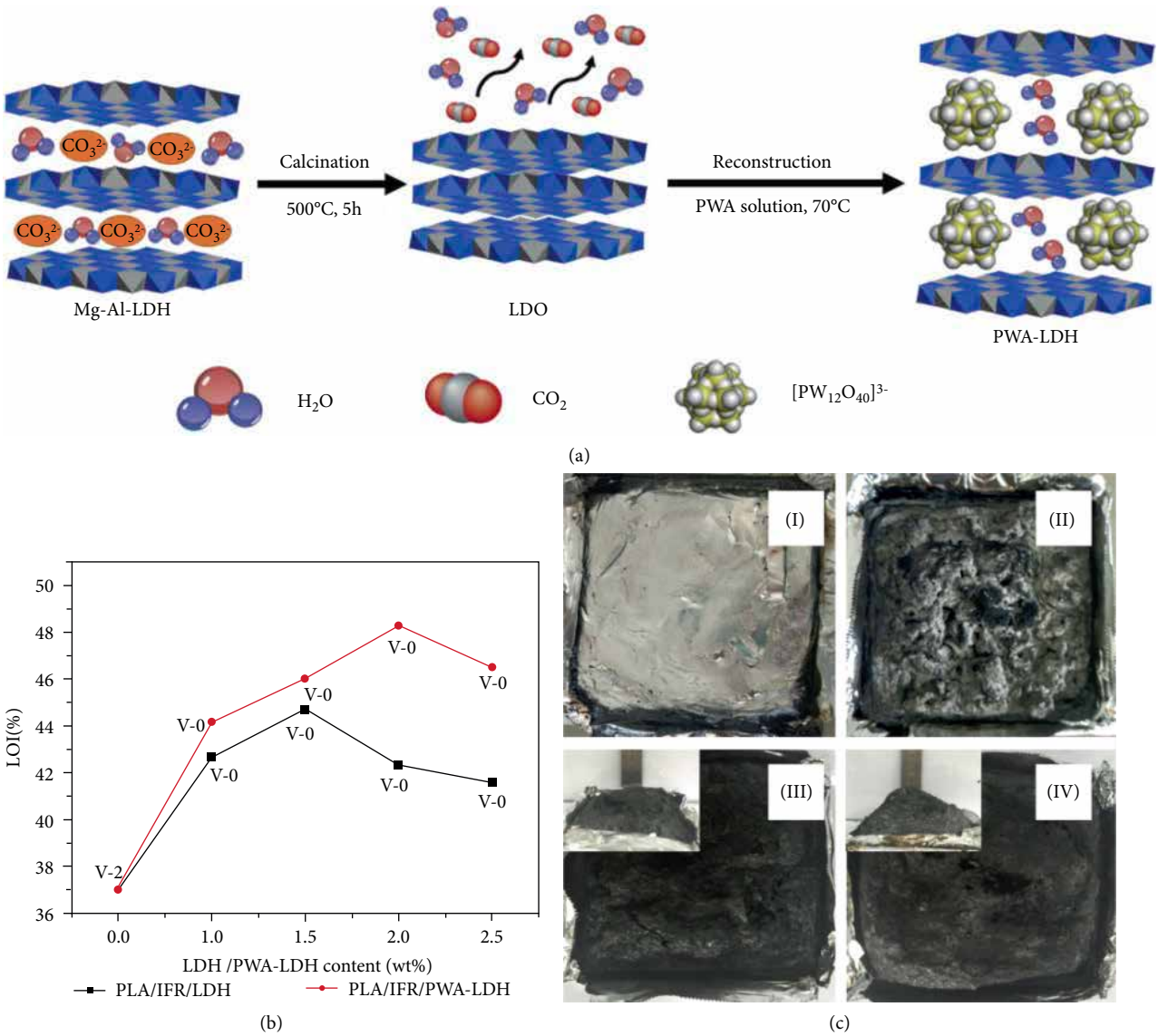

Figure 7: (a) The preparation process of PWA-LDH. (b) The LOI and UL-94 results of PLA composites. (c) Digital photos of (I) PLA, (II) PLA/IFR, (III) PLA/IFR/2.0LDH, and (IV) PLA/IFR/2.0PWA-LDH samples after cone calorimeter tests. Adapted from [167].

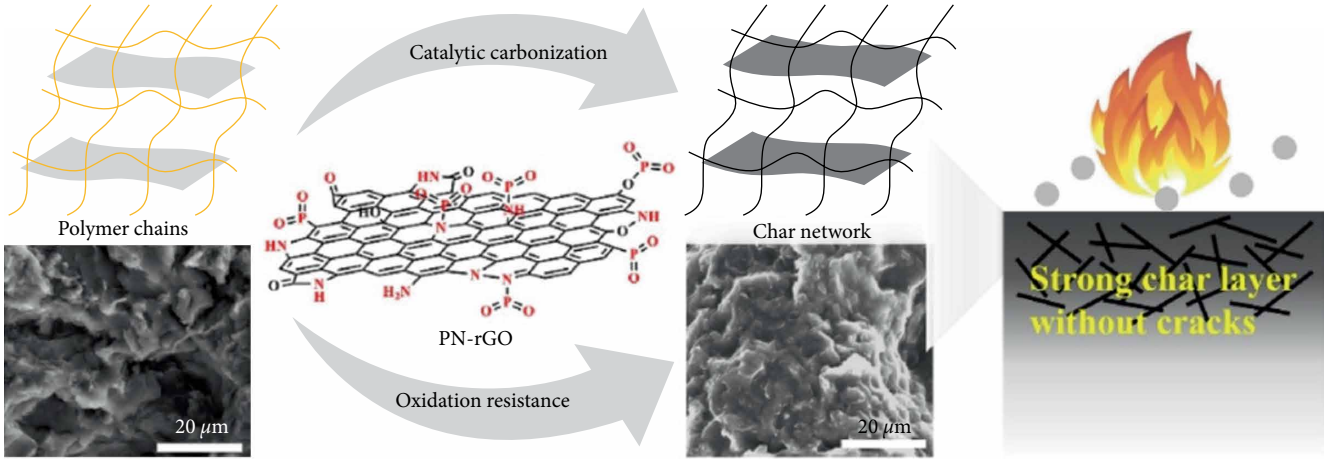

Figure 8: Schematic illustration of PN-rGO improving oxidation resistance of the char layer and catalytic carbonization capacity for EP chains. Adapted from [214].

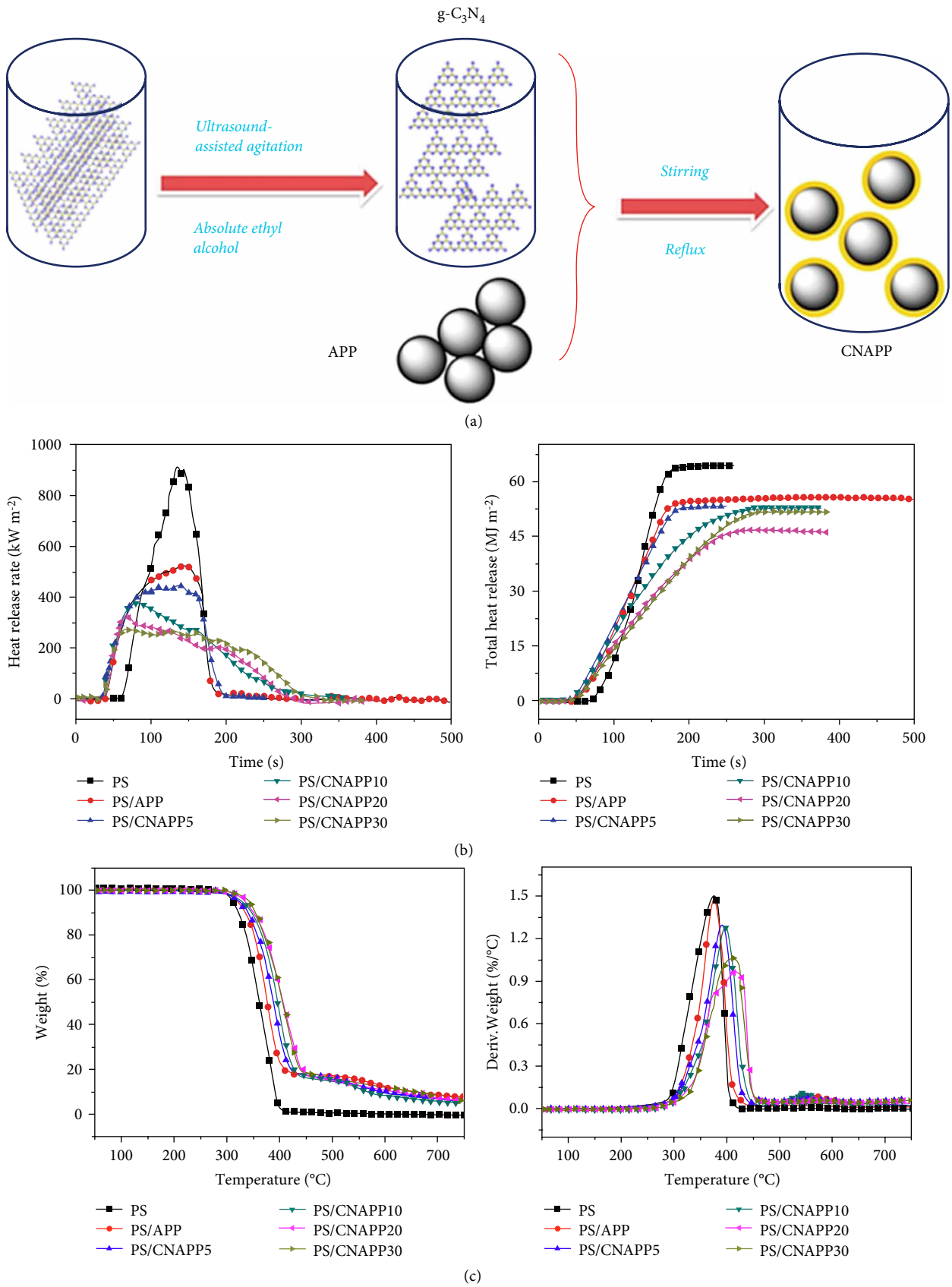

Figure 9: (a) The preparation process of CNAPP. (b) The HRR and THR curves of PS and its composites. (c) TG and DTG curves of PS and its composites. Adapted from [232].

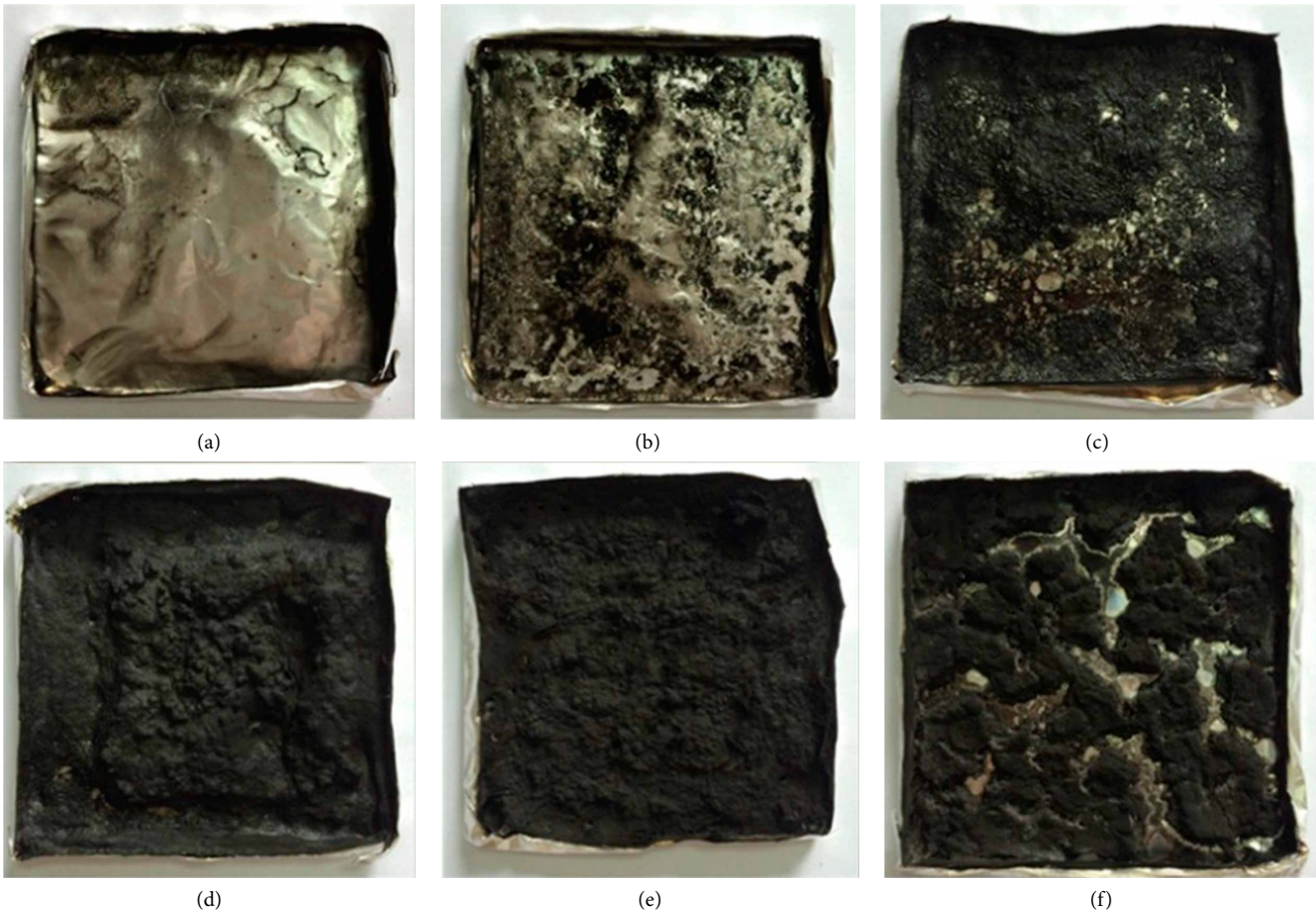

Figure 10: Digital photos of char residues of (a) PS, (b) PS/APP, (c) PS/CNAPP5, (d) PS/CNAPP10, (e) PS/CNAPP20, and (f) PS/CNAPP30 after the cone calorimetry measurement. Adapted from [232].

a density of $40 \pm 2\,\mathrm{kg\,m^{-3}}$ was prepared by combining LDH and kraft lignin (a byproduct of the pulp and paper industry) with phosphorous polyol (E560) [175]. The effects of fillers on the mechanical properties and combustion properties of fibers were then studied. The presence of such low amounts of lignin by itself did not increase the flame retardancy of FPF, but the addition of E560 increased the charring efficiency, while the addition of LDH contributed to reinforcing the char layer, yielding a more cohesive protective layer that decreased the pHRR to 47% as compared with an unfilled foam 0E. Wang et al. [176] investigated the synergistic effects of trace amounts of chloride on char formation and flame retardancy of linear low density polyethylene (LLDPE) filled with NiAl-LDHs. Their results showed that the char yield of 20% LDH/LLDPE (20 wt% NiAl-LDH) increased from 10.4% to 49.6% with the addition of 0.5 wt% NH_4Cl.

Moreover, the modification of LDHs via the intercalation of some flame-retardant molecules has been shown to be very effective in improving their compatibility with polymer matrices and flame retardants[44, 60, 65, 66, 167, 168, 178–185]. Zhang et al., prepared MgAl-LDH intercalated with phosphotungstic acid (PWA-LDH) by a reconstruction method and melted it with IFR and poly (lactic acid) (PLA) to prepare a flame-retardant biodegradable resin. Their studies showed that the maximum LOI value of composite materials containing 18.0 wt% IFR and 2.0 wt% PWA-LDH was 48.3%, passed the UL-94 V-0 rating, and the pHRR of pure PLA was significantly reduced from 306.3 kw/m^2 to 40.1 kw/m^2 [167]. As shown in Figure 7, the introduction of LDH into PLA/IFR composites significantly improved the flame retardancy of the condensed phase. By designing composite multi-modifiers with varied functions, multifunctional intercalation of LDHs has been developed, including functionalized hydroxypropyl-sulfobutyl-beta-cyclodextrin (sCD), phytic acid (Ph), sodium dodecylbenzenesulfonate (SDBS), and chalcone, and these functions have been transferred to epoxy materials using nanocarriers [180]. Studies have shown that at only 7 wt% fCD-DBS-Ph-LDH, the resultant EP nanocomposites passed the UL-94 V-0 rating. Compared with a pure epoxy resin, the pHRR (−72%) in a cone calorimeter test decreased significantly.

Lastly, the modification of LDHs via the covering surfaces with hydrophobic flame-retardant molecules is also generally believed to be very effective in improving their compatibility with other polymer matrices for flame retardation [40, 44, 66, 179, 186–194]. DBS intercalated LDH (LDH-DBS) nanosheets have been surface-assembled by an ultrafine $Ni(OH)_2$ nanocatalyst via circular coordination-induced growth, with the aim of imbuing EP with high-efficient fire retardant properties [193]. An LDH-DBS@$Ni(OH)_2$ material was designed to

exploit a spatial-dependent catalytic strategy to improve the interfacial structure between LDH nanosheets and an EP matrix during dynamic charring. The results showed that 3 wt% LDH-DBS@Ni$(OH)_2$ led to an EP matrix with a UL-94 V-0 rating. Xu et al. [191] synthesized a hybrid compound containing MgAl-LDH loaded graphene (RGO-LDH) by a co-precipitation method. An RGO-LDH/$CuMoO_4$ hybrid was then prepared by introducing $CuMoO_4$ onto the surface of RGO-LDH. Their results illustrated that the pHRR and THR of an EP composite with RGO-LDH/$CuMoO_4$ added were decreased significantly. The reason was that the Cu_2O and MoO_3 generated from RGO-LDH/$CuMoO_4$ in the combustion process helped to increase the yield of char residue and the compactness of the char layer.

3.6. Carbon Skeleton. Graphene is one of the most classic flame retardant C-skeleton two-dimensional nanosheets. In recent years, g-C_3N_4 and organic frameworks have also been studied in the field of flame retardant polymers.

3.6.1. Graphene. Graphene is a single-layer carbon plate with high thermal conductivity, excellent mechanical strength, and superior electronic conductivity [195–199]. It has been shown that modified graphene has excellent fire resistance even when exposed to flame [200]. In order to obtain improved flame retardant performance, functionalization of graphene or loading of synergistic flame retardants should effectively improve the flame retardant efficiency of graphene.

Various functional treatments or synergistic addition of flame retardants have been performed on graphene surfaces, including the incorporation of P, N, or Si [201–212]. Hu et al., [62] synthesized a functionalized graphene oxide (FGO) grafted to a hyper-branched flame retardant based on N-aminoethyl piperazine and a phosphonate derivative to reduce the flammability and toxic gas release of polystyrene (PS). The authors attributed the function of this to the homogeneous dispersion of FGO in a PS matrix and enhanced physical barrier effects. Yu et al. [212] successfully prepared functionalized reduced graphene oxide (FRGO) wrapped with P-N flame retardants by a one-pot method, and then covalently incorporated them into EP. The glass transition temperature of FRGO/EP nanocomposites remarkably increased by 29.6°C under 4 wt% loading. The pHRR of EP nanocomposites containing 2 wt% FRGO decreased by 43.0%. Jing et al., [213] reported UL-94 V-0 rating flame retardant PLA composites with a total content of only 3 wt% using bio-based polyphosphonate (BPPT) and polyethyleneimine-modified graphene oxide (M-GO) as flame retardants. Feng et al., [64] used a "branch-like" strategy with a graphene polymer as the backbone and a flame retardant as the branch to functionalize reduced graphene oxide (RGO) to improve the flame retardant grafting rate and compatibility of RGO in a polymer matrix, and then introduced the resulting GP-DOPO into EP/AgNW composites in situ. Phosphorus-nitrogen co-doped rGO (PN-rGO) was also prepared by a scalable hydrothermal and microwave process to improve the flame retardancy of an EP [214]. Figure 8 shows the schematic illustration of the flame retardation mechanism for EP/PN-rGO. Pethsangave et al. [215] reported that functionalized polyaniline (PANI)- and polypyrrole (PPy)-supported graphene nanocomposites were effective flame retardants. These synthesized nanocomposites showed excellent flame-retardant properties when coated on cotton fabric and wood. Li et al. [216] synthesized a hybrid flame retardant (GO-MD-MP) containing methacryloisobutyl polyhedral oligomeric silsesquioxane (POSSMA), reactive glycidyl methacrylate (GMA), bis-9, 10-dihydro-9-oxa-10-phosphaphenanthrene-10-oxide methacrylate (bisDOPOMA) and its derivative functionalized graphene oxide (GO) via a one-step grafting method. Their results showed that the LOI of EP increased to 31.1% after adding 4 wt% GO-MD-MP, and it easily reached a UL-94 V-0 rating.

Graphene incorporated with metal oxides have also been realized for use as flame retardants [217]. CeO_2/RGO [218] hybrids and graphene-zinc stannate (G-ZS) [219] hybrids have been synthesized by hydrothermal methods. They can effectively reduce toxic gases released from the combustion process of polymers. Yuan et al. [220] used an ingenious method to decorate Ni $(OH)_2$ nanosheets onto the surface of GO via the strong affinity of Ni^{2+} with NH_2 groups. Their experiments showed that the addition of functionalized graphene oxide (FGO) reduced the pHRR, THR, and TSP of polypropylene (PP) during combustion. Wang et al. [221] synthesized a series of nitrogenous resorcinol formaldehyde/graphene oxide composite aerogels by using a self-assembly copolymerization strategy. The materials featured with multiple functions, e.g., thermal insulation, ultra light, anti-corrosion, mechanical resilient, high flame-retardant capability.

Graphene has also been incorporated with other inorganic fillers [50, 222–226]. Chen et al. [226] ingeniously prepared a smart fire alarm wallpaper based on ultralong hydroxyapatite nanowires (HNs) and GO thermosensitive sensors. The thermosensitive sensor exhibited a low responsive temperature (126.9°C), fast response (2 s), long working time in flame (at least 5 min), and could be processed into various shapes, dyed with different colors, and printed with the commercial printer. It had broad application prospects in high-security interior decoration of houses. Nanosilica/graphene oxide (m-SGO) hybrids have been prepared by sol-gel and surface treatment processes on a large number of non-flammable silicas on the surface of graphene oxide [41]. These hybrids significantly improved the flame retardancy, mechanical properties, and thermal stability of an EP, endowing the EP resin with high thermal conductivity, low dielectric loss, and high dielectric constants. Zuo et al. [227] prepared polyimide (PI) composite aerogels with enhanced flame retardancy via an eco-friendly freeze-drying method, followed by a thermal imidization process with graphene and MMT as additives. Guo et al. [228] studied the mechanical and flame retardant properties of four composites, EVA with aluminum hydroxide (ATH), EVA with ATH and MoS_2, EVA with ATH and graphene nanoplatelets (GNPs), and EVA with all three components.

3.6.2. g-C_3N_4 and Organic Framework Nanosheets. Analogous to graphene, g-C_3N_4 also has stacked two-dimensional structure [229]. Because of its excellent thermal stability, chemical stability, and catalytic performance [230], it has attracted increased attention in the field of flame retardant and smoke suppression. For example, it

has been used for the improvement of the thermal stability and flame retardancy of polymers. Shi et al. [231] prepared polypropylene-grafted maleic anhydride (PP-g-MA)/g-C_3N_4 nanocomposites via a solvent mixing strategy. Their results showed that the T_{-10} and T_{-50} (temperature at 10% and 50% weight loss, respectively) of the composites increased by 14.6°C and 27.7°C, respectively. Additionally, a flame retardant CNAPP containing g-C_3N_4 wrapped ammonium polyphosphate (APP) was prepared and then incorporated into PS [232]. Experimental results show that the main reason for the improvement in flame retardancy of the resulting composites was that the POC and PCN structures formed after combustion significantly improved the stability of the char layer. When the content of g-C_3N_4 in CNAPP was 20%, the best flame retardant effect was obtained (Figures 9 and 10). g-C_3N_4/organic aluminum diethylhypophosphites (CDAHPI) hybrids have also been synthesized by salification reactions [233]. PS composites were then prepared by a melt blending method. Compared with pure PS, PS/CDAHPI showed additional advantages in terms of inhibiting pyrolysis gas release while reducing HRR and THR of the composite.

Smoke suppression in polymer combustion. The spinel copper cobaltate ($CuCo_2O_4$)/g-C_3N_4 (named C-$CuCo_2O_4$) nanohybrids were synthesized by hydrothermal method, and then incorporate with TPU by a master batch-melt compounding approach [234]. The number of pyrolysis gas products (including combustible volatiles and CO) decreased significantly, while the number of noncombustible gases (CO_2) increased. The g-C_3N_4/organic aluminum hypophosphites hybrid CPDCPAHPI and CBODAHPI [235] were synthesized by esterification and salification reactions, and introduced into PS. The release of flammable aromatic compounds was reduced by introducing these hybrids, which was attributed to the synergy of gas phase action and physical barrier effect in condensed phase. The g-C_3N_4/carbon sphere/Cu (CSACS-C) nanohybrid [236] were prepared by metal ions-induced gel reaction as green template, and the amount of pyrolysis gaseous products; generation and pHRR of TPU/CSACS-C composites were significantly reduced.

Recently, organic frameworks, including covalent organic frameworks and metal organic frameworks, have also begun to be used as flame retardants in polymers [237–239]. Hou et al. [237] synthesized iron-based and cobalt-based metal-organic frameworks (MOFs) by solvothermal method and prepared PS/MOF composites. Compared with pure PS, the pHRR of PS/Fe-MOF and PS/Co-MOF decreased by 14% and 28%, respectively, indicating that MOF has flame retardant effect in polymer. Subsequently, DOPO was used to modify Co-MOF and introduced to PLA to improve the fire safety and mechanical properties of the composites [238]. Mu et al. [239] prepared the original phosphorus-containing flame retardant wrapped covalent organic frameworks (FCOFs) nanosheets and introduced it to EP by in-situ polymerization, which had a positive impact on the flame retardancy, toxic volatiles and the quality of char residue of the composites. Recently, the flame retardant properties of various two-dimensional materials/polymers have been extensively studied. The results are listed in Table 2.

4. Conclusion

Clarifying the special properties of various two-dimensional nanomaterials is pivotal for being able to fully exploit their flame-retardant properties. With increased awareness of the structure and properties of two-dimensional nanomaterials, researchers will be able to realize the potential of two-dimensional nanomaterials for fulfilling required flame-retardant effects under low load conditions. Based on the specific properties of different two-dimensional nanomaterials, they can be reasonably used as additives or reactive components in the design of polymer flame-retardant materials. With additional research, two-dimensional nanomaterials/polymers will be more suitable for specific applications. Although two-dimensional nanomaterials are widely used to prepare fireproofing materials in the laboratory because of their high efficiency and environmental friendliness, many challenges still remain. First is the challenge of the large-scale application of two-dimensional nanomaterials. New two-dimensional nanomaterials, including g-C_3N_4 and black phosphorus, have not been prepared at industrial as of yet. Moreover, the uniform dispersion of many two-dimensional nanomaterials in a polymer matrix depends on their efficient exfoliation and surface modification. The application of hydrophobic technology of two-dimensional nanomaterials in industry is promising. Second is finding suitable flame retardant applications for two-dimensional nanomaterials. In specific applications, polymer materials not only need to meet flame retardant requirements, but also need to face meet requirements for heat dissipation, dielectric properties, etc. In some special cases, appropriate multifunctional nanosheets can be designed to meet specific design challenges according to the molecular components and structure of the two-dimensional nanomaterial. For example, in highly integrated small electronic devices, h-BN nanosheets are a reasonable choice.

The authors are confident that the above-mentioned challenges will be gradually overcome through the continuous development and innovation of two-dimensional nanomaterials due to their intrinsic advantages over other materials. The thorough survey of the current literature presented here offers useful information for realizing the potential of two-dimensional nanomaterials/polymer and should help in guiding the design of novel high-performance flame-retardant composites.

Conflicts of Interest

The authors declare that they have no conflicts of interest.

Acknowledgments

Financial support from the National Key R&D Program of China Grant No. 2016YFB0302303 and the Guangdong YangFan Innovative & Entrepreneurial Research Team Program (Project No. 201633002) is gratefully acknowledged.

References

[1] X. Qiu, Z. Li, X. Li, and Z. Zhang, "Flame retardant coatings prepared using layer by layer assembly: a review," *Chemical Engineering Journal*, vol. 334, pp. 108–122, 2018.

[2] Department of Emergency Management Fire and Rescue Bureau, "Data interpretation of fire and emergency," 2019, http://www.119.gov.cn/xiaofang/hztj/36306.htm.

[3] M. M. Velencoso, A. Battig, J. C. Markwart, B. Schartel, and F. R. Wurm, "Molecular firefighting—how modern phosphorus chemistry can help solve the challenge of flame retardancy," *Angewandte Chemie International Edition*, vol. 57, no. 33, pp. 10450–10467, 2018.

[4] Y. Li, C. Kuan, S. Hsu et al., "Preparation, thermal stability and flame-retardant properties of halogen-free polypropylene composites," *Journal of High Performance Polymers*, vol. 24, pp. 478–487, 2012.

[5] L. Liu, J. L. Liu, X. L. Chen, and C. M. Jiao, "Synergistic effect between hollow glass beads and aluminium hydroxide in flame retardant EVA composites," *Plastics, Rubber and Composites*, vol. 43, pp. 77–81, 2014.

[6] Z. Wang, Y. Liu, and Q. Wang, "Flame retardant polyoxymethylene with aluminium hydroxide/melamine/novolac resin synergistic system," *Polymer Degradation and Stability*, vol. 95, no. 6, pp. 945–954, 2010.

[7] H. Yan, J. Wei, B. Yin, and M. Yang, "Effect of the surface modification of ammonium polyphosphate on the structure and property of melamine–formaldehyde resin microencapsulated ammonium polyphosphate and polypropylene flame retardant composites," *Polymer Bulltin*, vol. 72, no. 11, pp. 2725–2737, 2015.

[8] K. Wu, M. Shen, and Y. Hu, "Synthesis of a novel intumescent flame retardant and its flame retardancy in polypropylene," *Journal of Polymer Research*, vol. 18, no. 3, pp. 425–433, 2011.

[9] S. Chiu, C. Wu, H. Lee, J. Gu, and M. Suen, "Synthesis and characterisation of novel flame retardant polyurethanes containing designed phosphorus units," *Journal of Polymer Research*, vol. 23, no. 10, p. 205, 2016.

[10] U. Braun, A. I. Balabanovich, B. Schartel et al., "Influence of the oxidation state of phosphorus on the decomposition and fire behaviour of flame-retarded epoxy resin composites," *Polymer*, vol. 47, no. 26, pp. 8495–8508, 2006.

[11] C. Kizilkaya, Y. Mülazim, M. Vezir Kahraman, N. Kayaman Apohan, and A. Güngör, "Synthesis and characterization of polyimide/hexagonal boron nitride composite," *Journal of Applied Polymer Science*, vol. 124, no. 1, pp. 706–712, 2012.

[12] A. Yaras, E. Er, H. Çelikkan, A. Disli, and A. Alicilar, "Cellulosic tent fabric coated with boron nitride nanosheets," *Journal of Industrial Textiles*, vol. 45, no. 6, pp. 1689–1700, 2015.

[13] J. Liu, R. G. Kutty, Q. Zheng, V. Eswariah, S. Sreejith, and Z. Liu, "Hexagonal boron nitride nanosheets as high-performance binder-free fire-resistant wood coatings," *Small*, vol. 13, no. 2, Article ID 1602456, 2017.

[14] F. Chu, D. Zhang, Y. Hou et al., "Construction of hierarchical natural fabric surface structure based on two-dimensional boron nitride nanosheets and its application for preparing biobased toughened unsaturated polyester resin composites," *ACS Applied Materials & Interfaces*, vol. 10, no. 46, pp. 40168–40179, 2018.

[15] Y.-R. Zhi, B. Yu, A. C. Y. Yuen et al., "Surface manipulation of thermal-exfoliated hexagonal boron nitride with polyaniline for improving thermal stability and fire safety performance of polymeric materials," *ACS Omega*, vol. 3, lpp. 14942–14952, 2018.

[16] J. Wang, D. Zhang, Y. Zhang et al., "Construction of multifunctional boron nitride nanosheet towards reducing toxic volatiles (CO and HCN) generation and fire hazard of thermoplastic polyurethane," *Journal of Hazardous Materials*, vol. 362, pp. 482–494, 2019.

[17] K. Zhou, S. Jiang, Y. Shi et al., "Multigram-scale fabrication of organic modified MoS_2 nanosheets dispersed in polystyrene with improved thermal stability, fire resistance, and smoke suppression properties," *Royal Society of Chemistry Advances*, vol. 4, no. 76, pp. 40170–40180, 2014.

[18] D. Wang, L. Song, K. Zhou, X. Yu, Y. Hu, and J. Wang, "Anomalous nano-barrier effects of ultrathin molybdenum disulfide nanosheets for improving the flame retardance of polymer nanocomposites," *Journal of Materials Chemistry A*, vol. 3, no. 27, pp. 14307–14317, 2015.

[19] K. Zhou, J. Liu, Y. Shi et al., "MoS_2 nanolayers grown on carbon nanotubes: an advanced reinforcement for epoxy composites," *A. C. S. Applied Materials & Interfaces*, vol. 7, no. 11, pp. 6070–6081, 2015.

[20] K. Zhou, J. Liu, Z. Gui, Y. Hu, and S. Jiang, "The influence of melamine phosphate modified MoS_2 on the thermal and flammability of poly(butylene succinate) composites," *Polymers For Advanced Technologies*, vol. 27, no. 14, pp. 1397–1400, 2016.

[21] X. Ren, Y. Mei, P. Lian et al., "A novel application of phosphorene as a flame retardant," *Polymers-Basel*, vol. 10, no. 3, p. 227, 2018.

[22] W. Zhou, T. Jia, H. Shi, D. Yu, W. Hong, and X. Chen, "Conjugated polymer dots/graphitic carbon nitride nanosheet heterojunctions for metal-free hydrogen evolution photocatalysis," *Journal of Materials Chemistry A*, vol. 7, no. 1, pp. 303–311, 2019.

[23] L. Sun, W. Hong, J. Liu et al., "Cross-linked graphitic carbon nitride with photonic crystal structure for efficient visible-light-driven photocatalysis," *A. C. S. Applied Materials & Interfaces*, vol. 9, no. 51, pp. 44503–44511, 2017.

[24] A. K. Chaudhari, S. S. Nagarkar, B. Joarder, and S. K. Ghosh, "A continuous π-stacked starfish array of two-dimensional luminescent MOF for detection of nitro explosives," *Crystal Growth & Design*, vol. 13, no. 8, pp. 3716–3721, 2013.

[25] Q. Weng, B. Wang, X. Wang et al., "Highly water-soluble, porous, and biocompatible boron nitrides for anticancer drug delivery," *ACS Nano Materials*, vol. 8, no. 6, pp. 6123–6130, 2014.

[26] F. Ahmed, Y. D. Kim, M. S. Choi et al., "High electric field carrier transport and power dissipation in multilayer black phosphorus field effect transistor with dielectric engineering," *Advanced Functional Materials*, vol. 27, no. 4, Article ID 1604025, 2017.

[27] L. Yang, S. Wang, J. Mao et al., "Hierarchical MoS_2/polyaniline nanowires with excellent electrochemical performance for lithium-ion batteries," *Advanced Materials*, vol. 25, no. 8, pp. 1180–1184, 2013.

[28] X. Zeng, D. T. McCarthy, A. Deletic, and X. Zhang, "Silver/reduced graphene oxide hydrogel as novel bactericidal filter for point-of-use water disinfection," *Advanced Functional Materials*, vol. 25, no. 27, pp. 4344–4351, 2015.

[29] L. Cseri, J. Baugh, A. Alabi et al., "Graphene oxide–polybenzimidazolium nanocomposite anion exchange membranes for electrodialysis," *Journal of Materials Chemistry A*, vol. 6, no. 48, pp. 24728–24739, 2018.

[30] K. Bhunia, S. Khilari, D. Pradhan, "Monodispersed PtPdNi trimetallic nanoparticles-integrated reduced graphene oxide

hybrid platform for direct alcohol fuel cell," *A. C. S. Sustain Chemistry & Enginering*, vol. 6, no. 6, pp. 7769–7778, 2018.

[31] F. Fei, L. Cseri, G. Szekely, C. F. Blanford, "Robust covalently cross-linked polybenzimidazole/graphene oxide membranes for high-flux organic solvent nanofiltration," *A. C. S. Applied Materials & Interfaces*, vol. 10, no. 8, pp. 16140–16147, 2018.

[32] K. Pan, Y. Fan, T. Leng et al., "Sustainable production of highly conductive multilayer graphene ink for wireless connectivity and IoT applications," *Nature Communications*, p. 5197, 2018.

[33] R. Wang, G. Xia, W. Zhong et al., "Direct transformation of lignin into fluorescence-switchable graphene quantum dots and their application in ultrasensitive profiling of a physiological oxidant," *Green Chemistry*, vol. 21, no. 12, pp. 3343–3352, 2019.

[34] M. Razali, J. F. Kim, M. Attfield et al., "Sustainable wastewater treatment and recycling in membrane manufacturing," *Green Chemistry*, vol. 17, no. 12, pp. 5196–5205, 2015.

[35] X. Dong, L. Wang, D. Wang, C. Li, and J. Jin, "Layer-by-layer engineered co–al hydroxide nanosheets/graphene multilayer films as flexible electrode for supercapacitor," *Langmuir*, vol. 28, no. 1, pp. 293–298, 2011.

[36] B. Lin, C. Ding, B. Xu, Z. Chen, and Y. Chen, "Preparation and characterization of polythiophene/molybdenum disulfide intercalation material," *Materials Research Bulletin*, vol. 44, no. 4, pp. 719–723, 2009.

[37] X. Wang and P. Wu, "Preparation of highly thermally conductive polymer composite at low filler content via a self-assembly process between polystyrene microspheres and boron nitride nanosheets," *ACS Applied Materials & Interfaces*, vol. 9, no. 23, pp. 19934–19944, 2016.

[38] H. Yan and Y. Huang, "Polymer composites of carbon nitride and poly(3-hexylthiophene) to achieve enhanced hydrogen production from water under visible light," *Chemical Communications*, vol. 47, no. 14, pp. 4168–4170, 2011.

[39] K. Zhou, R. Gao, and X. Qian, "Self-assembly of exfoliated molybdenum disulfide (MoS_2) nanosheets and layered double hydroxide (LDH): towards reducing fire hazards of epoxy," *Journal of Hazardous Materials*, vol. 338, pp. 343–355, 2017.

[40] W. Wang, H. Pan, Y. Shi et al., "Fabrication of LDH nanosheets on β-FeOOH rods and applications for improving the fire safety of epoxy resin," *Composites Part A: Applied Science and Manufacturing*, vol. 80, pp. 259–269, 2016.

[41] R. Wang, D. Zhuo, Z. Weng et al., "A novel nanosilica/graphene oxide hybrid and its flame retarding epoxy resin with simultaneously improved mechanical, thermal conductivity, and dielectric properties," *Journal of Materials Chemistry A*, vol. 3, no. 18, pp. 9826–9836, 2015.

[42] W. Cai, D. Zhang, B. Wang et al., "Scalable one-step synthesis of hydroxylated boron nitride nanosheets for obtaining multifunctional polyvinyl alcohol nanocomposite films: multi-azimuth properties improvement," *Composites Science and Technology*, vol. 168, pp. 74–80, 2018.

[43] Y. Shi, S. Jiang, K. Zhou et al., "Influence of g-C_3N_4 nanosheets on thermal stability and mechanical properties of biopolymer electrolyte nanocomposite films: a novel investigation," *ACS Applied Materials & Interfaces*, vol. 6, no. 1, pp. 429–437, 2013.

[44] P. K. Kaul, A. J. Samson, G. T. Selvan, I. Enoch, and P. M. Selvakumar, "Synergistic effect of LDH in the presence of organophosphate on thermal and flammable properties of an epoxy nanocomposite," *Applied Clay Science*, vol. 135, pp. 234–243, 2017.

[45] S. Zhang, X. Liu, X. Jin, H. Li, J. Sun, and X. Gu, "The novel application of chitosan: effects of cross-linked chitosan on the fire performance of thermoplastic polyurethane," *Carbohydrate Polymers*, vol. 189, pp. 313–321, 2018.

[46] C. Zhi, Y. Bando, C. Tang, H. Kuwahara, and D. Golberg, "Large-scale fabrication of boron nitride nanosheets and their utilization in polymeric composites with improved thermal and mechanical properties," *Advanced Materials*, vol. 21, no. 28, pp. 2889–2893, 2009.

[47] Z. Lin, A. McCreary, N. Briggs et al., "2D materials advances: from large scale synthesis and controlled heterostructures to improved characterization techniques, defects and applications," *2D Materials*, vol. 3, no. 4, Article ID 042001, 2016.

[48] S. I. Kudryashov, L. V. Nguyen, D. A. Kirilenko et al., "Large-scale laser fabrication of antifouling silicon-surface nanosheet arrays via nanoplasmonic ablative self-organization in liquid cs2 tracked by a sulfur dopant," *ACS Applied Nano Materials*, vol. 1, no. 6, pp. 2461–2468, 2018.

[49] Y. Yao, Z. Lin, Z. Li, X. Song, K. Moon, and C. Wong, "Large-scale production of two-dimensional nanosheets," *Journal of Materials Chemistry*, vol. 22, no. 27, pp. 13494–13499 , 2012.

[50] K. Zhou, Z. Gui, and Y. Hu, "The influence of graphene based smoke suppression agents on reduced fire hazards of polystyrene composites," *Composites Part A*, vol. 80, pp. 217–227, 2016.

[51] W. Cai, W. Guo, Y. Pan et al., "Polydopamine-bridged synthesis of ternary h-BN@PDA@SnO_2 as nanoenhancers for flame retardant and smoke suppression of epoxy composites," *Composites Part A*, vol. 111, pp. 94–105, 2018.

[52] B. Radisavljevic, A. Radenovic, J. Brivio, V. Giacometti, and A. Kis, "Single-layer MoS_2 transistors," *Nature Nanotechnology*, vol. 6, pp. 147–150, 2011.

[53] M. Pica, "Zirconium phosphate catalysts in the XXI century: state of the art from 2010 to date," *Catalysts.*, vol. 7, p. 190, 2017.

[54] M. Xu, T. Liang, M. Shi, and H. Chen, "Graphene-like two-dimensional materials," *Chemical Reviews*, vol. 113, no. 5, pp. 3766–3798, 2013.

[55] C. Swearingen, S. Macha, and A. Fitch, "Leashed ferrocenes at clay surfaces: potential applications for environmental catalysis," *Journal of Molecular Catalysts A-Chemistry*, vol. 199, no. 1–2, pp. 149–160, 2003.

[56] S. Qiu, Y. Zhou, X. Zhou et al., "Air-stable polyphosphazene-functionalized few-layer black phosphorene for flame retardancy of epoxy resins," *Small*, vol. 15, Article ID 1805175, 2019.

[57] L. Yan, Y. B. Zheng, F. Zhao et al., "Chemistry and physics of a single atomic layer: strategies and challenges for functionalization of graphene and graphene-based materials," *Chemical Society Reviews*, vol. 41, no. 1, pp. 97–114, 2012.

[58] C. Hobbs, "Recent advances in bio-based flame retardant additives for synthetic polymeric materials," *Polymers-Basel*, vol. 11, no. 2, p. 224, 2019.

[59] L Xu, C. Lei, R. Xu, X. Zhang, and F. Zhang, "Functionalization of α-zirconium phosphate by polyphosphazene and its effect on the flame retardance of an intumescent flame retardant polypropylene system," *RSC Advances*, vol. 6, no. 81, pp. 77545–77552, 2016.

[60] E. N. Kalali, X. Wang, and D. Wang, "Functionalized layered double hydroxide-based epoxy nanocomposites with improved

flame retardancy and mechanical properties," *Journal of Materials Chemistry A*, vol. 3, no. 13, pp. 6819–6826, 2015.

[61] Y. Shi, Z. Long, B. Yu et al., "Tunable thermal, flame retardant and toxic effluent suppression properties of polystyrene based on alternating graphitic carbon nitride and multi-walled carbon nanotubes," *Journal of Materials Chemistry A*, vol. 3, no. 33, pp. 17064–17073, 2015.

[62] W. Hu, B. Yu, S. Jiang, L. Song, Y. Hu, and B. Wang, "Hyper-branched polymer grafting graphene oxide as an effective flame retardant and smoke suppressant for polystyrene," *Journal of Hazardous Materials*, vol. 300, pp. 58–66, 2015.

[63] H. Xie, X. Lai, H. Li, and X. Zeng, "Fabrication of ZrP nanosheet decorated macromolecular charring agent and its efficient synergism with ammonium polyphosphate in flame-retarding polypropylene," *Composites Part A: Applied Science and Manufacturing*, vol. 105, pp. 223–234, 2018.

[64] Y. Feng, X. Li, X. Zhao et al., "Synergetic improvement in thermal conductivity and flame retardancy of epoxy/silver nanowires composites by incorporating "branch-like" flame-retardant functionalized graphene," *ACS Applied Materials & Interfaces*, vol. 10, no. 25, pp. 21628–21641, 2018.

[65] X. Wang, E. N. Kalali, and D. Wang, "Renewable cardanol-based surfactant modified layered double hydroxide as a flame retardant for epoxy resin," *A. C. S. Sustain Chemistry & Engineering*, vol. 3, no. 12, pp. 3281–3290, 2015.

[66] W. Xu, B. Zhang, B. Xu, and A. Li, "The flame retardancy and smoke suppression effect of heptaheptamolybdate modified reduced graphene oxide/layered double hydroxide hybrids on polyurethane elastomer," *Composites Part A: Applied Science and Manufacturing*, vol. 91, no. Part 1, pp. 30–40, 2016.

[67] D. Yang, Y. Hu, H. Li, L. Song, H. Xu, and B. Li, "Synergistic flame retardant effect of α-zirconium phosphate in low-density polyethylene/ethylene–vinyl acetate/aluminum hydroxide hybrids," *Journal of Thermal Analysis and Calorimetry*, vol. 119, no. 1, pp. 619–624, 2015.

[68] X. Ren, Y. Mei, P. Lian et al., "Fabrication and application of black phosphorene/graphene composite material as a flame retardant," *Polymers-Basel*, vol. 11, no. 2, p. 193, 2019.

[69] K. Wenelska, K. Ma Lana, and E. Mijowska, "Study on the flammability, thermal stability and diffusivity of polyethylene nanocomposites containing few layered tungsten disulfide (WS 2) functionalized with metal oxides," *RSC Advances*, vol. 8, no. 23, pp. 12999–13007, 2018.

[70] A. Díez-Pascual and M. Naffakh, "Inorganic nanoparticle-modified poly(phenylene sulphide)/carbon fiber laminates: thermomechanical behaviour," *Materials*, vol. 6, no. 8, pp. 3171–3193, 2013.

[71] K. Wenelska and E. Mijowska, "Preparation, thermal conductivity, and thermal stability of flame retardant polyethylene with exfoliated MoS_2/M_xO_y," *New Journal of Chemistry*, vol. 41, no. 22, pp. 13287–13292, 2017.

[72] L. Yang, A. Mukhopadhyay, Y. Jiao et al., "Ultralight, highly thermally insulating and fire resistant aerogel by encapsulating cellulose nanofibers with two-dimensional MoS_2," *Nanoscale*, vol. 9, no. 32, pp. 11452–11462, 2017.

[73] X. Zhou, S. Qiu, W. Xing, C. S. R. Gangireddy, Z. Gui, and Y. Hu, "Hierarchical polyphosphazene@molybdenum disulfide hybrid structure for enhancing the flame retardancy and mechanical property of epoxy resins," *A. C. S. Applied Materials & Interfaces*, vol. 9, no. 34, pp. 29147–29156, 2017.

[74] D. Wang, P. Wen, J. Wang, L. Song, and Y. Hu, "The effect of defect-rich molybdenum disulfide nanosheets with phosphorus, nitrogen and silicon elements on mechanical, thermal, and fire behaviors of unsaturated polyester composites," *Chemical Engineering Journal*, vol. 313, pp. 238–249, 2017.

[75] K. Zhou, G. Tang, R. Gao, and H. Guo, "Constructing hierarchical polymer@MoS_2 core-shell structures for regulating thermal and fire safety properties of polystyrene nanocomposites," *Composites Part A: Applied Science and Manufacturing*, vol. 107, pp. 144–154, 2018.

[76] K. Zhou, R. Gao, Z. Gui, and Y. Hu, "The effective reinforcements of functionalized MoS_2 nanosheets in polymer hybrid composites by sol-gel technique," *Composites Part A: Applied Science and Manufacturing*, vol. 94, pp. 1–9, 2017.

[77] W. Cai, J. Zhan, X. Feng et al., "Facile construction of flame-retardant-wrapped molybdenum disulfide nanosheets for properties enhancement of thermoplastic polyurethane," *Industrial & Engineering Chemistry Research*, vol. 56, no. 25, pp. 7229–7238, 2017.

[78] K. Zhou, G. Tang, S. Jiang, Z. Gui, and Y. Hu, "Combination effect of MoS_2 with aluminum hypophosphite in flame retardant ethylene-vinyl acetate composites," *RSC Advances*, vol. 6, no. 44, pp. 37672–37680, 2016.

[79] X. Feng, B. Wang, X. Wang et al., "Molybdenum disulfide nanosheets as barrier enhancing nanofillers in thermal decomposition of polypropylene composites," *Chemical Engineering Journal*, vol. 295, pp. 278–287, 2016.

[80] X. Yang, N. Meng, Y. Zhu, Y. Zhou, W. Nie, and P. Chen, "Greatly improved mechanical and thermal properties of chitosan by carboxyl-functionalized MoS_2 nanosheets," *Journal of Materials Science*, vol. 51, no. 3, pp. 1344–1353, 2016.

[81] K. Zhou, Z. Gui, and Y. Hu, "Synthesis and characterization of Cu–MoS_2 hybrids and their influence on the thermal behavior of polyvinyl chloride composites," *RSC Advances*, vol. 6, no. 91, pp. 8877–88712, 2016.

[82] K. Zhou, J. Liu, W. Zeng, Y. Hu, and Z. Gui, "In situ synthesis, morphology, and fundamental properties of polymer/MoS_2 nanocomposites," *Composites Science and Technology*, vol. 107, pp. 120–128, 2015.

[83] Y. Zhong, M. Li, L. Zhang, X. Zhang, S. Zhu, and W. Wu, "Adding the combination of CNTs and MoS_2 into halogen-free flame retarding TPEE with enhanced the anti-dripping behavior and char forming properties," *Thermochimica Acta*, vol. 613, pp. 87–93, 2015.

[84] K. Zhou, Q. Zhang, J. Liu et al., "Synergetic effect of ferrocene and MoS_2 in polystyrene composites with enhanced thermal stability, flame retardant and smoke suppression properties," *RSC Advances*, vol. 4, no. 26, p. 13205, 2014.

[85] S. Jiang, G. Tang, Z. Bai, Y. Wang, Y. Hu, and L. Song, "Surface functionalization of MoS_2 with POSS for enhancing thermal, flame-retardant and mechanical properties in PVA composites," *RSC Advances*, vol. 4, no. 7, pp. 3253–3262, 2014.

[86] K. Zhou, R. Gao, and X. Qian, "Self-assembly of exfoliated molybdenum disulfide (MoS_2) nanosheets and layered double hydroxide (LDH): towards reducing fire hazards of epoxy," *Journal of Hazardous Materials*, vol. 338, pp. 343–355, 2017.

[87] K. Zhou, C. Liu, and R. Gao, "Polyaniline: a novel bridge to reduce the fire hazards of epoxy composites," *Composites Part A: Applied Science and Manufacturing*, vol. 112, pp. 432–443, 2018.

[88] S. Qiu, Y. Hu, Y. Shi et al., "In situ growth of polyphosphazene particles on molybdenum disulfide nanosheets for flame retardant and friction application," *Composites Part A: Applied Science and Manufacturing*, vol. 114, pp. 407–417, 2018.

[89] A. Li, W. Xu, G. Wang, and X. Wang, "Novel strategy for molybdenum disulfide nanosheets grown on titanate nanotubes for enhancing the flame retardancy and smoke suppression of epoxy resin," *Journal of Applied Polymer Science*, vol. 135, no. 15, p. 46064, 2018.

[90] H. Pan, Q. Shen, Z. Zhang, B. Yu, and Y. Lu, "MoS_2-filled coating on flexible polyurethane foam via layer-by-layer assembly technique: flame-retardant and smoke suppression properties," *Journal of Materials Science*, vol. 53, no. 12, pp. 9340–9349, 2018.

[91] X. Feng, X. Wang, W. Cai, N. Hong, Y. Hu, and K. M. Liew, "Integrated effect of supramolecular self-assembled sandwich-like melamine cyanurate/MoS_2 hybrid sheets on reducing fire hazards of polyamide 6 composites," *Journal of Hazardous Materials*, vol. 320, pp. 252–264, 2016.

[92] A. M. Díez-Pascual and M. Naffakh, "Mechanical and thermal behaviour of isotactic polypropylene reinforced with inorganic fullerene-like WS_2 nanoparticles: Effect of filler loading and temperature," *Materials Chemistry and Physics*, vol. 141, no. 2–3, pp. 979–989, 2013.

[93] D. Yang, Y. Hu, H. Li et al., "Flammability and carbonization of high-impact polystyrene/α-zirconium phosphate nanocomposites," *Iranian Polymer Journal*, vol. 24, no. 12, pp. 1069–1075, 2015.

[94] Y. Du, F. Deng, X. Jiang et al., "Preparation and performance of lipophilic α-zirconium phosphate with high thermal stability and its application in thermal-plastic polymers," *Progress in Natural Science–Materials International*, vol. 25, no. 5, pp. 503–511, 2015.

[95] Y. Pan, H. Pan, B. Yuan et al., "Construction of organic–inorganic hybrid nano-coatings containing α-zirconium phosphate with high efficiency for reducing fire hazards of flexible polyurethane foam," *Materials Chemistry and Physics*, vol. 163, pp. 107–115, 2015.

[96] Y. Zhang, X. Zeng, H. Li, X. Lai, Y. Guo, and R. Zheng, "Zirconium phosphate functionalized by hindered amine: a new strategy for effectively enhancing the flame retardancy of addition-cure liquid silicone rubber," *Materials Letters*, vol. 174, pp. 230–233, 2016.

[97] F. Fang, B. Tong, T. Du et al., "Unique nanobrick wall nanocoating for flame-retardant cotton fabric via layer-by-layer assembly technique," *Cellulose*, vol. 23, no. 5, pp. 3341–3354, 2016.

[98] C. Zhao, P. Li, D. He, Y. Li, F. Lei, and H. Sue, "Flame retardation behavior of polybenzoxazine/α-ZrP nanocomposites," *RSC Advances*, vol. 6, no. 77, pp. 73485–73495, 2016.

[99] L. C. Hatanaka, A. Diaz, Q. Wang, Z. Cheng, and M. S. Mannan, "Thermal stability of optically transparent alpha-zirconium phosphate/poly(methyl methacrylate) nanocomposites with high particle loading," *Polymers & Polymer Composites*, vol. 25, no. 4, pp. 267–272, 2017.

[100] Y. Xiao, J. Xu, S. Huang, and H. Deng, "Effects of α-ZrP on crystallinity and flame-retardant behaviors of PA6/MCA composites," *International Journal of Polymer Science*, vol. 2017, pp. 1–12, Article ID 6034741, 2017.

[101] L. Xu, C. Lei, R. Xu, X. Zhang, and F. Zhang, "Synergistic effect on flame retardancy and thermal behavior of polycarbonate filled with α-zirconium phosphate@gel-silica," *Journal of Applied Polymer Science*, vol. 134, no. 19, 2017.

[102] H. Xiang, L. Li, W. Chen, S. Yu, B. Sun, and M. Zhu, "Flame retardancy of polyamide 6 hybrid fibers: combined effects of α-zirconium phosphate and ammonium sulfamate," *Progress in Natural Science-Materials International*, vol. 27, no. 5, pp. 369–373, 2017.

[103] Y. Ding, Y. Luo, F. Xue, Z. Jia, and D. Jia, "Synthesis of phosphazene derivative modified α-zirconium phosphate and its effect on the flame retardancy and mechanical properties of silicone rubber in combination with ammonium polyphosphate," *Acta Polymer Sinica*, vol. 11, pp. 1796–1805, 2017.

[104] J. Yue, C. Zhao, Y. Dai, H. Li, and Y. Li, "Catalytic effect of exfoliated zirconium phosphate on the curing behavior of benzoxazine," *Thermochimica Acta*, vol. 650, pp. 18–25, 2017.

[105] K. Li, H. Lei, X. Zeng, H. Li, X. Lai, and S. Chai, "Preparation of a flame retardant phosphorus-containing polyacrylate/α-zirconium phosphate nanocomposite through in situ emulsion polymerization," *RSC Advances*, vol. 7, no. 78, pp. 49290–49298, 2017.

[106] H. Yan, L. Zhao, Z. Fang, and H. Wang, "Construction of multilayer coatings for flame retardancy of ramie fabric using layer-by-layer assembly," *Journal of Applied Polymer Science*, vol. 134, no. 48, p. 45556, 2017.

[107] Y. Zhang, X. Zeng, X. Lai, and H. Li, "Preparation of functionalized zirconium phosphate and its effect on the flame retardancy of silicone rubber," *RSC Advances*, vol. 8, no. 1, pp. 111–121, 2018.

[108] B. Xu, W. Xu, Y. Liu et al., "Surface modification of α-zirconium phosphate by zeolitic imidazolate frameworks-8 and its effect on improving the fire safety of polyurethane elastomer," *Polymers for Advanced Technologies*, vol. 29, no. 11, pp. 2816–2826, 2018.

[109] H. Xie, X. Lai, H. Li, and X. Zeng, "Remarkably improving the fire-safety of polypropylene by synergism of functionalized ZrP nanosheet and N-alkoxy hindered amine," *Applied Clay Science*, vol. 166, pp. 61–73, 2018.

[110] L. Xu, C. Lei, R. Xu, X. Zhang, and J. Xu, "Intumescent flame retardant of polypropylene system with enhanced thermal properties and flame retardancy based on α-zirconium phosphate composite particles," *Polymer Bulletin*, vol. 75, no. 6, pp. 2707–2727, 2018.

[111] S. Yu, H. Xiang, J. Zhou, Z. Zhou, and M. Zhu, "The synergistic effect of organic phosphorous/α-zirconium phosphate on flame-retardant poly(lactic acid) fiber," *Fibers and Polymers*, vol. 19, no. 4, pp. 812–820, 2018.

[112] N. Pérez, X. Qi, S. Nie, P. Acuña, M. Chen, and D. Wang, "Flame retardant polypropylene composites with low densities," *Materials*, vol. 12, no. 1, p. 152, 2019.

[113] L. Xu, C. Lei, R. Xu, X. Zhang, and F. Zhang, "Hybridization of α-zirconium phosphate with hexachlorocyclotriphosphazene and its application in the flame retardant poly(vinyl alcohol) composites," *Polymer Degradation and Stability*, vol. 133, pp. 378–388, 2016.

[114] X. Fu, X. Wang, W. Xing, P. Zhang, L. Song, and Y. Hu, "Two-dimensional cardanol-derived zirconium phosphate hybrid as flame retardant and smoke suppressant for epoxy resin," *Polymer Degradation and Stability*, vol. 151, pp. 172–180, 2018.

[115] S. Qiu, Y. Zhou, X. Zhou et al., "Air-stable polyphosphazene-functionalized few-layer black phosphorene for flame

retardancy of epoxy resins," *Small*, vol. 15, no. 10, Article ID 1805175, 2019.

[116] K. Zhou, Z. Gui, and Y. Hu, "Ultrathin 2D VOPO4 nanosheets: a novel reinforcing agent in polymeric composites," *RSC Advances*, vol. 6, no. 102, pp. 100344–100351, 2016.

[117] K. Zhou and R. Gao, "The influence of a novel two dimensional graphene-like nanomaterial on thermal stability and flammability of polystyrene," *Journal of Colloid and Interface Science*, vol. 500, pp. 164–171, 2017.

[118] X. Li, Y. Feng, C. Chen et al., "Highly thermally conductive flame retardant epoxy nanocomposites with multifunctional ionic liquid flame retardant-functionalized boron nitride nanosheets," *Journal of Materials Chemistry A*, vol. 6, no. 41, pp. 20500–20512, 2018.

[119] S. Qiu, Y. Hou, W. Xing et al., "Self-assembled supermolecular aggregate supported on boron nitride nanoplatelets for flame retardant and friction application," *Chemical Engineering Journal*, vol. 349, pp. 223–234, 2018.

[120] Y. Dong and G. Wang, "Influence of nano-boron nitride on fire protection of waterborne fire-resistive coatings," *Journal of Coatings Technology and Research*, vol. 11, no. 2, pp. 265–272, 2014.

[121] B. Yu, W. Xing, W. Guo et al., "Thermal exfoliation of hexagonal boron nitride for effective enhancements on thermal stability, flame retardancy and smoke suppression of epoxy resin nanocomposites via sol–gel process," *Journal of Materials Chemistry A*, vol. 4, no. 19, pp. 733–734, 2016.

[122] D. Liu, M. Zhang, L. He, Y. Chen, and W. Lei, "Layer-by-layer assembly fabrication of porous boron nitride coated multifunctional materials for water cleaning," *Advanced Materials Interfaces*, vol. 4, no. 16, Article ID 1700392, 2017.

[123] W. Cai, N. Hong, X. Feng et al., "A facile strategy to simultaneously exfoliate and functionalize boron nitride nanosheets via Lewis acid-base interaction," *Chemical Engineering Journal*, vol. 330, pp. 309–321, 2017.

[124] Y. Zhong, L. Zhang, A. Fischer, L. Wang, D. Drummer, and W. Wu, "The effect of hBN on the flame retardancy and thermal stability of P-N flame retardant PA6," *Journal of Macromolecular Science, Part A*, vol. 55, no. 1, pp. 17–23, 2018.

[125] W. Xu, A. Li, Y. Liu, R. Chen, and W. Li, "$CuMoO_4$ hexagonal boron nitride hybrid: an ecofriendly flame retardant for polyurethane elastomer," *Journal of Material Science*, vol. 53, no. 16, pp. 11265–11279, 2018.

[126] J. Wang, Y. Wu, Y. Xue et al., "Super-compatible functional boron nitride nanosheets/polymer films with excellent mechanical properties and ultra-high thermal conductivity for thermal management," *Journal of Materials Chemistry C*, vol. 6, no. 6, pp. 1363–1369, 2018.

[127] D. Wang, X. Mu, W. Cai, L. Song, C. Ma, and Y. Hu, "Constructing phosphorus, nitrogen, silicon-co-contained boron nitride nanosheets to reinforce flame retardant properties of unsaturated polyester resin," *Composites Part A: Applied Science and Manufacturing*, vol. 109, pp. 546–554, 2018.

[128] Z. Li, S. I. Montero Lira, L. Zhang, D. F. Expósito, V. B. Heeralal, and D. Wang, "Bio-inspired engineering of boron nitride with iron-derived nanocatalyst toward enhanced fire retardancy of epoxy resin," *Polymer Degradation and Stability*, vol. 157, pp. 119–130, 2018.

[129] L. Wang, L. Zhang, A. Fischer, Y. Zhong, D. Drummer, and W. Wu, "Enhanced thermal conductivity and flame retardancy of polyamide 6/flame retardant composites with hexagonal boron nitride," *Journal of Polymer Engineering*, vol. 38, no. 8, pp. 767–774, 2018.

[130] Q. Zhang, Z. Li, X. Li, L. Yu, and Z. Wu, "Boron nitride nanosheets decorated by bismuth ferrite particles: preparation, characterization, and effect on flame-retardant performance of epoxy resin," *Materials Research Express*, vol. 5, no. 9, p. 95019, 2018.

[131] W. Cai, X. Mu, Y. Pan et al., "Facile fabrication of organically modified boron nitride nanosheets and its effect on the thermal stability, flame retardant, and mechanical properties of thermoplastic polyurethane," *Polymers for Advanced Technologies*, vol. 29, no. 9, pp. 2545–2552, 2018.

[132] S. Chen, R. Xu, J. Liu et al., "Simultaneous production and functionalization of boron nitride nanosheets by sugar-assisted mechanochemical exfoliation," *Advanced Materials*, vol. 31, no. 10, Article ID 1804810, 2019.

[133] Q. Zhang, Z. Li, X. Li, L. Yu, Z. Zhang, and Z. Wu, "Zinc ferrite nanoparticle decorated boron nitride nanosheet: preparation, magnetic field arrangement, and flame retardancy," *Chemical Engineering Journal*, vol. 356, pp. 680–692, 2019.

[134] Y. Han, T. Li, B. Gao et al., "Synergistic effects of zinc oxide in montmorillonite flame-retardant polystyrene nanocomposites," *Journal of Applied Polymer Science*, vol. 133, p. 43047, 2016.

[135] D. Gao, R. Li, B. Lv, J. Ma, F. Tian, and J. Zhang, "Flammability, thermal and physical-mechanical properties of cationic polymer/montmorillonite composite on cotton fabric," *Composites Part B: Engineering*, vol. 77, pp. 329–337, 2015.

[136] F. Carosio, J. Kochumalayil, F. Cuttica, G. Camino, and L. Berglund, "Oriented clay nanopaper from biobased components—mechanisms for superior fire protection properties," *A. C. S. Applied Materials & Interfaces*, vol. 7, no. 10, pp. 5847–5856, 2015.

[137] P. Ming, Z. Song, S. Gong et al., "Nacre-inspired integrated nanocomposites with fire retardant properties by graphene oxide and montmorillonite," *Journal of Materials Chemistry A*, vol. 3, no. 42, pp. 21194–21200, 2015.

[138] K. Shang, W. Liao, J. Wang, Y. Wang, Y. Wang, and D. A. Schiraldi, "Nonflammable alginate nanocomposite aerogels prepared by a simple freeze-drying and post-cross-linking method," *A. C. S. Applied Materials & Interfaces*, vol. 8, no. 1, pp. 643–650, 2016.

[139] I. S. Zope, A. Dasari, F. Guan, and Z. Yu, "Influence of metal ions on thermo-oxidative stability and combustion response of polyamide 6/clay nanocomposites," *Polymer*, vol. 92, pp. 102–113, 2016.

[140] P. Scarfato, L. Incarnato, L. Di Maio, B. Dittrich, and B. Schartel, "Influence of a novel organo-silylated clay on the morphology, thermal and burning behavior of low density polyethylene composites," *Composites Part B: Engineering*, vol. 98, pp. 444–452, 2016.

[141] L. Zuo, W. Fan, Y. Zhang et al., "Graphene/montmorillonite hybrid synergistically reinforced polyimide composite aerogels with enhanced flame-retardant performance," *Composites Science and Technology*, vol. 139, pp. 57–63, 2017.

[142] S. Tang, V. Wachtendorf, P. Klack, L. Qian, Y. Dong, and B. Schartel, "Enhanced flame-retardant effect of a montmorillonite/phosphaphenanthrene compound in an epoxy thermoset," *RSC Advances*, vol. 7, no. 2, pp. 72–728, 2017.

[143] Q. Kong, T. Wu, H. Zhang et al., "Improving flame retardancy of IFR/PP composites through the synergistic effect of organic montmorillonite intercalation cobalt hydroxides modified by acidified chitosan," *Applied Clay Science*, vol. 146, pp. 230–237, 2017.

[144] G. Makhlouf, M. Hassan, M. Nour, Y. K. Abdel-Monem, and A. Abdelkhalik, "Evaluation of fire performance of linear low-density polyethylene containing novel intumescent flame retardant," *Journal of Thermal Analysis and Calorimetry*, vol. 130, no. 2, pp. 1031–1041, 2017.

[145] Q. Fu, L. Medina, Y. Li, F. Carosio, A. Hajian, and L. A. Berglund, "Nanostructured wood hybrids for fire-retardancy prepared by clay impregnation into the cell wall," *A. C. S. Applied Materials & Interfaces*, vol. 9, no. 41, pp. 36154–36163, 2017.

[146] S. Li, Z. Yang, J. Xu, J. Xie, and J. Sun, "Synthesis of exfoliated graphene–montmorillonite hybrids as the fillers for epoxy composites," *Journal of Composite Materials*, vol. 53, no. 3, pp. 315–326, 2018.

[147] F. Carosio, A. Di Pierro, J. Alongi, A. Fina, and G. Saracco, "Controlling the melt dripping of polyester fabrics by tuning the ionic strength of polyhedral oligomeric silsesquioxane and sodium montmorillonite coatings assembled through layer by layer," *Journal of Colloid and Interface Science*, vol. 510, pp. 142–151, 2018.

[148] L. Yan, Z. Xu, and X. Wang, "Synergistic effects of organically modified montmorillonite on the flame-retardant and smoke suppression properties of transparent intumescent fire-retardant coatings," *Progress in Organic Coatings*, vol. 122, pp. 107–118, 2018.

[149] L. Jia, W. Zhang, B. Tong, and R. Yang, "Crystallization, flame-retardant, and mechanical behaviors of poly(lactic acid)\9,10-dihydro-9-oxa-10-phosphaphenanthrene-10-oxide-calcium montmorillonite nanocomposite," *Journal of Applied Polymer Science*, vol. 136, no. 3, p. 46982, 2019.

[150] P. Chen, Y. Zhao, W. Wang, T. Zhang, and S. Song, "Correlation of montmorillonite sheet thickness and flame retardant behavior of a chitosan–montmorillonite nanosheet membrane assembled on flexible polyurethane foam," *Polymers-Basel*, vol. 11, no. 2, p. 213, 2019.

[151] H. Xie, X. Lai, Y. Wang, H. Li, and X. Zeng, "A green approach to fabricating nacre-inspired nanocoating for super-efficiently fire-safe polymers via one-step self-assembly," *Journal of Hazardous Materials*, vol. 365, pp. 125–136, 2019.

[152] J. Li, X. Li, Q. Wei et al., "Synergistic effect of organophosphate functionalized montmorillonite on properties and water resistance of intumescent flame-retarded SEBS," *Fire and Materials*, vol. 43, no. 1, pp. 74–83, 2019.

[153] K. Bocz, M. Domonkos, T. Igricz, Á. Kmetty, T. Bárány, and G. Marosi, "Flame retarded self-reinforced poly(lactic acid) composites of outstanding impact resistance," *Composites Part A: Applied Science and Manufacturing*, vol. 70, pp. 27–34, 2015.

[154] W. Xu, G. Wang, and X. Zheng, "Research on highly flame-retardant rigid PU foams by combination of nanostructured additives and phosphorus flame retardants," *Polymer Degradation and Stability*, vol. 111, pp. 142–150, 2015.

[155] Y. Ren, Y. Wang, L. Wang, and T. Liu, "Evaluation of intumescent fire retardants and synergistic agents for use in wood flour/recycled polypropylene composites," *Construction and Building Materials*, vol. 76, pp. 273–278, 2015.

[156] Y. Wang, S. Liao, K. Shang et al., "Efficient approach to improving the flame retardancy of poly(vinyl alcohol)/clay aerogels: incorporating piperazine-modified ammonium polyphosphate," *A. C. S. Applied Materials & Interfaces*, vol. 7, no. 3, pp. 1780–1786, 2015.

[157] L. Ye, J. Ren, S. Cai, Z. Wang, and J. Li, "Poly(lactic acid) nanocomposites with improved flame retardancy and impact strength by combining of phosphinates and organoclay," *Chinese Journal of Polymer Science*, vol. 34, no. 6, pp. 785–796, 2016.

[158] S. Deng, W. Liao, J. Yang, Z. Cao, and Y. Wang, "Flame-retardant and smoke-suppressed silicone foams with chitosan-based nanocoatings," *Industrial & Engineering Chemistry Research*, vol. 55, no. 27, pp. 7239–7248, 2016.

[159] M. Hassan, M. Nour, Y. Abdelmonem, G. Makhlouf, and A. Abdelkhalik, "Synergistic effect of chitosan-based flame retardant and modified clay on the flammability properties of LLDPE," *Polymer Degradation and Stability*, vol. 133, pp. 8–15, 2016.

[160] O. Köklükaya, F. Carosio, and L. Wågberg, "Superior flame-resistant cellulose nanofibril aerogels modified with hybrid layer-by-layer coatings," *A. C. S. Applied Materials & Interfaces*, vol. 9, no. 24, pp. 29082–29092, 2017.

[161] D. Vadas, T. Igricz, J. Sarazin, S. Bourbigot, G. Marosi, and K. Bocz, "Flame retardancy of microcellular poly(lactic acid) foams prepared by supercritical CO_2-assisted extrusion," *Polymer Degradation and Stability*, vol. 153, pp. 100–108, 2018.

[162] M. Jiang, Y. Zhang, Y. Yu et al., "Flame retardancy of unsaturated polyester composites with modified ammonium polyphosphate, montmorillonite, and zinc borate," *Journal of Applied Polymer Science*, vol. 136, no. 11, p. 47180, 2019.

[163] D. Zhang, B. L. Williams, E. M. Becher et al., "Flame retardant and hydrophobic cotton fabrics from intumescent coatings," *Advanced Composites and Hybrid Materials*, vol. 1, no. 1, pp. 177–184, 2018.

[164] M. Tomczak, J. Łopiński, K. Kowalczyk, B. Schmidt, and J. Rokicka, "Vinyl intumescent coatings modified with platelet-type nanofillers," *Progress in Organic Coatings*, vol. 126, pp. 97–105, 2019.

[165] F. Ronkay, B. Molnár, F. Szalay et al., "Development of flame-retarded nanocomposites from recycled pet bottles for the electronics industry," *Polymers-Basel*, vol. 11, no. 2, p. 233, 2019.

[166] Y. Li, C. Deng, X. Shi, B. Xu, H. Chen, and Y. Wang, "Simultaneously improved flame retardance and ceramifiable properties of polymer-based composites via the formed crystalline phase at high temperature," *A. C. S. Applied Materials & Interfaces*, vol. 11, no. 7, pp. 7459–7471, 2019.

[167] S. Zhang, Y. Yan, W. Wang et al., "Intercalation of phosphotungstic acid into layered double hydroxides by reconstruction method and its application in intumescent flame retardant poly (lactic acid) composites," *Polymer Degradation and Stability*, vol. 147, pp. 142–150, 2018.

[168] C. Li, J. Wan, E. N. Kalali, H. Fan, and D. Wang, "Synthesis and characterization of functional eugenol derivative based layered double hydroxide and its use as a nanoflame-retardant in epoxy resin," *Journal of Materials Chemistry A*, vol. 3, no. 7, pp. 3471–3479, 2015.

[169] P. Ding, B. Kang, J. Zhang et al., "Phosphorus-containing flame retardant modified layered double hydroxides and their applications on polylactide film with good transparency,"

Journal of Colloid and Interface Science, vol. 440, pp. 46–52, 2015.

[170] E. N. Kalali, S. De Juan, X. Wang, S. Nie, R. Wang, and D. Wang, "Comparative study on synergistic effect of LDH and zirconium phosphate with aluminum trihydroxide on flame retardancy of EVA composites," *Journal of Thermal Analysis and Calorimetry*, vol. 121, no. 2, pp. 619–626, 2015.

[171] Y. Qian, S. Zhou, and X. Chen, "Flammability and thermal degradation behavior of ethylene-vinyl acetate/layered double hydroxides/zinc borate composites," *Polymers for Advanced Technologies*, vol. 28, no. 3, pp. 353–361, 2017.

[172] Y. Shi, Z. Gui, B. Yu, R. K. K. Yuen, B. Wang, and Y. Hu, "Graphite-like carbon nitride and functionalized layered double hydroxide filled polypropylene-grafted maleic anhydride nanocomposites: comparison in flame retardancy, and thermal, mechanical and UV-shielding properties," *Composites Part B: Engineering*, vol. 79, pp. 277–284, 2015.

[173] K. Shang, W. Liao, J. Wang, Y. Wang, Y. Wang, and D. A. Schiraldi, "Nonflammable alginate nanocomposite aerogels prepared by a simple freeze-drying and post-cross-linking method," *A. C. S. Applied Materials & Interfaces*, vol. 8, no. 1, pp. 643–650, 2016.

[174] K. Zhou, Z. Gui, and Y. Hu, "Facile synthesis of LDH nanoplates as reinforcing agents in PVA nanocomposites," *Polymers for Advanced Technologies*, vol. 28, no. 3, pp. 386–392, 2017.

[175] S. Gómez-Fernández, M. Günther, B. Schartel, M. A. Corcuera, and A. Eceiza, "Impact of the combined use of layered double hydroxides, lignin and phosphorous polyol on the fire behavior of flexible polyurethane foams," *Industrial Crops and Products*, vol. 125, pp. 346–359, 2018.

[176] H. Wang, S. Tan, and R. Song, "Effect of trace chloride on the char formation and flame retardancy of the LLDPE filled with NiAl-layered double hydroxides," *Fire and Materials*, vol. 43, no. 1, pp. 110–120, 2019.

[177] K. Zhu, Y. Wang, D. Tang et al., "Flame-retardant mechanism of layered double hydroxides in asphalt binder," *Materials*, vol. 12, no. 5, p. 801, 2019.

[178] M. Hajibeygi, M. Shabanian, and H. A. Khonakdar, "Zn–AL LDH reinforced nanocomposites based on new polyamide containing imide group: From synthesis to properties," *Applied Clay Science*, vol. 114, pp. 256–264, 2015.

[179] E. N. Kalali, X. Wang, and D. Wang, "Synthesis of a Fe^3O^4 nanosphere@Mg–Al layered-double-hydroxide hybrid and application in the fabrication of multifunctional epoxy nanocomposites," *Industrial & Engineering Chemistry Research*, vol. 55, no. 23, pp. 6634–6642, 2016.

[180] E. N. Kalali, X. Wang, and D. Wang, "Multifunctional intercalation in layered double hydroxide: toward multifunctional nanohybrids for epoxy resin," *Journal of Materials Chemistry A*, vol. 4, no. 6, pp. 2147–2157, 2016.

[181] C. Li, J. Wan, Y. Pan, P. Zhao, H. Fan, and D. Wang, "Sustainable, biobased silicone with layered double hydroxide hybrid and their application in natural-fiber reinforced phenolic composites with enhanced performance," *A. C. S. Sustain Chemistry & Engineering*, vol. 4, no. 6, pp. 3113–3121, 2016.

[182] J. Cai, H. Heng, X. Hu, Q. Xu, and F. Miao, "A facile method for the preparation of novel fire-retardant layered double hydroxide and its application as nanofiller in UP," *Polymer Degradation and Stability*, vol. 126, pp. 47–57, 2016.

[183] M. Kumar, S. Chakraborty, P. Upadhyaya, and G. Pugazhenthi, "Morphological, mechanical, and thermal features of PMMA nanocomposites containing two-dimensional Co-Al layered double hydroxide," *Journal of Applied Polymer Science*, vol. 135, no. 5, p. 45774, 2018.

[184] X. Jin, X. Gu, C. Chen et al., "The fire performance of polylactic acid containing a novel intumescent flame retardant and intercalated layered double hydroxides," *Journal of Materials Science*, vol. 52, no. 20, pp. 12235–12250, 2017.

[185] J. Du, L. Jin, H. Zeng et al., "Facile preparation of an efficient flame retardant and its application in ethylene vinyl acetate," *Applied Clay Science*, vol. 168, pp. 96–105, 2019.

[186] K. Zhou, Y. Hu, J. Liu, Z. Gui, S. Jiang, and G. Tang, "Facile preparation of layered double hydroxide/MoS_2/poly(vinyl alcohol) composites," *Materials Chemisty and Physics*, vol. 178, pp. 1–5, 2016.

[187] A. Edenharter, P. Feicht, B. Diar-Bakerly, G. Beyer, and J. Breu, "Superior flame retardant by combining high aspect ratio layered double hydroxide and graphene oxide," *Polymer*, vol. 91, pp. 41–49, 2016.

[188] Y. Yan, H. Yao, L. Mao et al., "Micrometer-thick graphene oxide-layered double hydroxide nacre-inspired coatings and their properties," *Small*, vol. 12, no. 6, pp. 745–755, 2016.

[189] K. Zhou, R. Gao, and X. Qian, "Self-assembly of exfoliated molybdenum disulfide (MoS_2) nanosheets and layered double hydroxide (LDH): towards reducing fire hazards of epoxy," *Journal of Hazardous Materials*, vol. 338, pp. 343–355, 2017.

[190] B. Guo, Y. Liu, Q. Zhang et al., "Efficient flame-retardant and smoke-suppression properties of Mg–Al-layered double-hydroxide nanostructures on wood substrate," *A. C. S. Sustain Chemistry & Engineering*, vol. 9, no. 27, pp. 23039–23047, 2017.

[191] W. Xu, B. Zhang, X. Wang, G. Wang, and D. Ding, "The flame retardancy and smoke suppression effect of a hybrid containing $CuMoO_4$ modified reduced graphene oxide/layered double hydroxide on epoxy resin," *Journal of Hazardous Materials*, vol. 343, pp. 364–375, 2018.

[192] Y. Hou, S. Qiu, Y. Hu, C. K. Kundu, Z. Gui, and W. Hu, "Construction of bimetallic ZIF-derived Co–Ni ldhs on the surfaces of go or cnts with a recyclable method: toward reduced toxicity of gaseous thermal decomposition products of unsaturated polyester resin," *ACS Applied Materials & Interfaces*, vol. 10, no. 21, pp. 18359–18371, 2018.

[193] Z. Li, J. Zhang, F. Dufossea, and D. Wang, "Ultrafine nickel nanocatalyst-engineering of an organic layered double hydroxide towards a super-efficient fire-safe epoxy resin via interfacial catalysis," *Journal of Materials Chemistry A*, vol. 6, no. 18, pp. 8488–8498, 2018.

[194] S. Xu, M. Zhang, S. Li et al., "Surface modification of phosphorus-containing hydrotalcite using rare-earth coupling agent and its application in polypropylene," *Powder Technology*, vol. 342, pp. 555–561, 2019.

[195] F. Carosio, L. Maddalena, J. Gomez, G. Saracco, and A. Fina, "Graphene oxide exoskeleton to produce self-extinguishing, nonignitable, and flame resistant flexible foams: a mechanically tough alternative to inorganic aerogels," *Advanced Materials and Interfaces*, vol. 5, no. 23, Article ID 1801288, 2018.

[196] B. Wicklein, A. Kocjan, G. Salazar-Alvarez et al., "Thermally insulating and fire-retardant lightweight anisotropic foams based on nanocellulose and graphene oxide," *Nature Nanotechnology*, vol. 10, no. 3, pp. 277–283, 2015.

[197] C. Hu, J. Xue, L. Dong et al., "Scalable preparation of multifunctional fire-retardant ultralight graphene foams," *ACS Nano*, vol. 10, no. 1, pp. 1325–1332, 2016.

[198] L. Zhang, H. Li, X. Lai, X. Su, T. Liang, and X. Zeng, "Thiolated graphene-based superhydrophobic sponges for oil-water separation," *Chemical Engineering Journal*, vol. 316, pp. 736–743, 2017.

[199] Y. Yan, H. Yao, L. Mao et al., "Micrometer-thick graphene oxide-layered double hydroxide nacre-inspired coatings and their properties," *Small*, vol. 12, no. 6, pp. 745–755, 2016.

[200] L. Dong, C. Hu, L. Song, X. Huang, N. Chen, and L. Qu, "A large-area, flexible, and flame-retardant graphene paper," *Advanced Functional Materials*, vol. 26, no. 9, pp. 1470–1476, 2016.

[201] B. Yuan, H. Sheng, X. Mu et al., "Enhanced flame retardancy of polypropylene by melamine-modified graphene oxide," *Journal of Materials Science*, vol. 50, no. 16, pp. 5389–5401, 2015.

[202] B. Yu, Y. Shi, B. Yuan et al., "Enhanced thermal and flame retardant properties of flame-retardant-wrapped graphene/epoxy resin nanocomposites," *Journal of Materials Chemistry A*, vol. 3, no. 15, pp. 8034-8044, 2015.

[203] J. Gu, C. Liang, X. Zhao et al., "Highly thermally conductive flame-retardant epoxy nanocomposites with reduced ignitability and excellent electrical conductivities," *Composites Science and Technology*, vol. 139, pp. 83–89, 2017.

[204] B. Yuan, A. Fan, M. Yang et al., "The effects of graphene on the flammability and fire behavior of intumescent flame retardant polypropylene composites at different flame scenarios," *Polymers Degradation Stability*, vol. 143, pp. 42–56, 2017.

[205] W. Cai, X. Feng, B. Wang et al., "A novel strategy to simultaneously electrochemically prepare and functionalize graphene with a multifunctional flame retardant," *Chemical Engineering Journal*, vol. 316, pp. 514–524, 2017.

[206] W. Yan, M. Zhang, J. Yu, S. Nie, D. Zhang, and S. Qin, "Synergistic flame-retardant effect of epoxy resin combined with phenethyl-bridged DOPO derivative and graphene nanosheets," *Chinese Journal of Polymer Science*, vol. 37, no. 1, pp. 79–88, 2019.

[207] B. Yuan, Y. Sun, X. Chen, Y. Shi, H. Dai, and S. He, "Dual modification of graphene by polymeric flame retardant and $Ni(OH)_2$ nanosheets for improving flame retardancy of polypropylene," *Composites Part A: Applied Science and Manufacturing*, vol. 109, pp. 345–354, 2018.

[208] B. Wu, Y. Liu, Y. Shu, L. Ye, and X. Zhao, "Intrinsic flame-retardant urea formaldehyde/graphene nanocomposite foam: structure and reinforcing mechanism," *Polymer Composites*, vol. 40, no. S1, pp. E811–E820, 2019.

[209] W. Cai, J. Wang, X. Wang et al., "Mussel-inspired functionalization of electrochemically exfoliated graphene: based on self-polymerization of dopamine and its suppression effect on the fire hazards and smoke toxicity of thermoplastic polyurethane," *Journal of Hazardous Materials*, vol. 352, pp. 57–69, 2018.

[210] J. Long, S. Li, J. Liang, Z. Wang, and B. Liang, "Preparation and characterization of graphene oxide and it application as a reinforcement in polypropylene composites," *Polymer Composites*, vol. 40, no. 2, pp. 723–729, 2019.

[211] G. Yuan, B. Yang, Y. Chen, and Y. Jia, "Synthesis of a novel multi-structure synergistic POSS-GO-DOPO ternary graft flame retardant and its application in polypropylene," *Composites Part A: Applied Science and Manufacturing*, vol. 117, pp. 345–356, 2019.

[212] B. Yu, Y. Shi, B. Yuan et al., "Enhanced thermal and flame retardant properties of flame-retardant-wrapped graphene/epoxy resin nanocomposites," *Journal of Materials Chemistry A*, vol. 3, no. 15, pp. 8034–8044, 2015.

[213] J. Jing, Y. Zhang, X. Tang, X. Li, M. Peng, and Z. Fang, "Combination of a bio-based polyphosphonate and modified graphene oxide toward superior flame retardant polylactic acid," *RSC Advances*, vol. 8, pp. 4304–4313, 2018.

[214] Y. Feng, C. He, Y. Wen et al., "Superior flame retardancy and smoke suppression of epoxy-based composites with phosphorus/nitrogen co-doped graphene," *Journal of Hazardous Materials*, vol. 346, pp. 140–151, 2018.

[215] D. A. Pethsangave, R. V. Khose, P. H. Wadekar, and S. Some, "Novel approach toward the synthesis of a phosphorus-functionalized polymer-based graphene composite as an efficient flame retardant," *A. C. S. Sustainable Chemistry & Engineering*, vol. 7, no. 13, pp. 11745–11753, 2019.

[216] M. Li, H. Zhang, W. Wu et al., "A novel POSS-based copolymer functionalized graphene: an effective flame retardant for reducing the flammability of epoxy resin," *Polymers-Basel*, vol. 11, no. 2, p. 241, 2019.

[217] K. Zhou, Z. Gui, Y. Hu, S. Jiang, and G. Tang, "The influence of cobalt oxide–graphene hybrids on thermal degradation, fire hazards and mechanical properties of thermoplastic polyurethane composites," *Composites Part A: Applied Science and Manufacturing*, vol. 88, pp. 10–18, 2016.

[218] S. Wang, R. Gao, and K. Zhou, "The influence of cerium dioxide functionalized reduced graphene oxide on reducing fire hazards of thermoplastic polyurethane nanocomposites," *Journal of Colloid and Interface Science*, vol. 536, pp. 127–134, 2019.

[219] H. Sheng, Y. Zhang, C. Ma et al., "Influence of zinc stannate and graphene hybrids on reducing the toxic gases and fire hazards during epoxy resin combustion," *Polymers Advanced Technologies*, vol. 30, no. 3, pp. 666–674, 2019.

[220] B. Yuan, Y. Hu, X. Chen et al., "Dual modification of graphene by polymeric flame retardant and $Ni(OH)_2$ nanosheets for improving flame retardancy of polypropylene," *Composites Part A: Applied Science and Manufacturing*, vol. 100, pp. 106–117, 2017.

[221] L. Wang, J. Wang, L. Zheng, Z. Li, L. Wu, and X. Wang, "Superelastic, anticorrosive, and flame-resistant nitrogen-containing resorcinol formaldehyde/graphene oxide composite aerogels," *A. C. S. Sustainable Chemistry & Engineering*, vol. 7, no. 12, pp. 10873–10879, 2019.

[222] F. L. Guan, C. X. Gui, H. B. Zhang, Z. G. Jiang, Y. Jiang, and Z. Z. Yu, "Enhanced thermal conductivity and satisfactory flame retardancy of epoxy/alumina composites by combination with graphene nanoplatelets and magnesium hydroxide," *Composites Part B: Engineering*, vol. 98, pp. 134–140, 2016.

[223] W. Xu, X. Wang, Y. Wu, W. Li, and C. Chen, "Functionalized graphene with Co-ZIF adsorbed borate ions as an effective flame retardant and smoke suppression agent for epoxy resin," *Journal of Hazardous Materials*, vol. 363, pp. 138–151, 2019.

[224] W. Xu, X. Wang, G. Wang, A. Li, and B. Xu, "A novel graphene hybrid for reducing fire hazard of epoxy resin," *Polymers Advanced Technologies*, vol. 29, no. 4, pp. 1194–1205, 2018.

[225] P. Ming, Z. Song, S. Gong et al., "Nacre-inspired integrated nanocomposites with fire retardant properties by graphene oxide and montmorillonite," *Journals of Materials Chemistry A*, vol. 3, no. 42, pp. 21194–21200, 2015.

[226] F.-F. Chen, Y.-J. Zhu, F. Chen, L.-Y. Dong, R.-L. Yang, and Z.-C. Xiong, "Fire alarm wallpaper based on fire-resistant hydroxyapatite nanowire inorganic paper and graphene oxide thermosensitive sensor," *ACS Nano*, vol. 12, no. 4, pp. 3159–3171, 2018.

[227] L. Zuo, W. Fan, Y. Zhang et al., "Graphene/montmorillonite hybrid synergistically reinforced polyimide composite aerogels with enhanced flame-retardant performance," *Composites Science and Technology*, vol. 139, pp. 57–63, 2017.

[228] Y. Guo, Y. Xue, X. Zuo et al., "Capitalizing on the molybdenum disulfide/graphene synergy to produce mechanical enhanced flame retardant ethylene-vinyl acetate composites with low aluminum hydroxide loading," *Polymer Degradation and Stability*, vol. 144, pp. 155–166, 2017.

[229] W. Lin, W. Hong, L. Sun, D. Yu, D. Yu, and X. Chen, "Bioinspired mesoporous chiral nematic graphitic carbon nitride photocatalysts modulated by polarized light," *ChemSusChem.*, vol. 11, no. 1, pp. 114–119, 2018.

[230] L. Sun, M. Yang, J. Huang, D. Yu, W. Hong, and X. Chen, "Freestanding graphitic carbon nitride photonic crystals for enhanced photocatalysis," *Advanced Functional Materials*, vol. 26, no. 27, pp. 4943–4950, 2016.

[231] Y. Q. Shi, Z. Gui, B. Yu, R. K. K. Yuen, B. Wang, and Y. Hu, "Graphite-like carbon nitride and functionalized layered double hydroxide filled polypropylene-grafted maleic anhydride nanocomposites: Comparison in flame retardancy, and thermal, mechanical and UV-shielding properties," *Journal/Composites Part B: Engineering*, vol. 79, pp. 277–284, 2015.

[232] Y. Q. Shi, W. Y. Xing, B. B. Wang et al., "Synergistic effect of graphitic carbon nitride and ammonium polyphosphate for enhanced thermal and flame retardant properties of polystyrene," *Materials Chemistry and Physics*, vol. 177, pp. 283–292, 2016.

[233] Y. Zhu, Y. Shi, Z. Huang, L. Duan, Q. Tai, and Y. Hu, "Novel graphite-like carbon nitride/organic aluminum diethylhypophosphites nanohybrid: preparation and enhancement on thermal stability and flame retardancy of polystyrene," *Composites Part A: Applied Science and Manufacturing*, vol. 99, pp. 149–156, 2017.

[234] Y. Shi, B. Yu, K. Zhou et al., "Novel $CuCo_2O_4$/graphitic carbon nitride nanohybrids: Highly effective catalysts for reducing CO generation and fire hazards of thermoplastic polyurethane nanocomposites," *Journal of Hazardous Materials*, vol. 293, pp. 87–96, 2015.

[235] Y. Shi, B. Yu, L. Duan et al., "Graphitic carbon nitride/phosphorus-rich aluminum phosphinates hybrids as smoke suppressants and flame retardants for polystyrene," *Journal of Hazardous Materials*, vol. 332, pp. 87–96, 2017.

[236] Y. Shi, L. Wang, L. Fu et al., "Sodium alginate-templated synthesis of g-C_3N_4/carbon spheres/Cu ternary nanohybrids for fire safety application," *Journal of Colloid and Interface Science*, vol. 539, pp. 1–10, 2019.

[237] Y. Hou, W. Hu, Z. Gui, and Y. Hu, "Preparation of metal–organic frameworks and their application as flame retardants for polystyrene," *Industrial & Engineering Chemistry Research*, vol. 56, no. 8, pp. 2036–2045, 2017.

[238] Y. Hou, L. Liu, S. Qiu, X. Zhou, Z. Gui, and Y. Hu, "DOPO-modified two-dimensional Co-based metal–organic framework: preparation and application for enhancing fire safety of poly(lactic acid)," *A. C. S. Applied Materials & Interfaces*, vol. 10, no. 9, pp. 8274–8286, 2018.

[239] X. Mu, J. Zhan, C. Ma et al., "Integrated effect of flame retardant wrapped macromolecular covalent organic nanosheet on reduction of fire hazards of epoxy resin," *Composites Part A: Applied Science and Manufacturing*, vol. 117, pp. 23–33, 2019.